UNIVERSITY OF MANITOBA

# THE MICROSTRUCTURAL CHARACTERISTICS AND TEMPERATURE EFFECTS ON THE WEAR BEHAVIORS OF THE ELECTROLESS NICKEL-PHOSPHORUS COATINGS

YUGANG LIU

A THESIS SUBMITTED TO THE FACULTY OF GRADUATE STUDIES IN PARTIAL FULFILLMENT OF THE REQUIREMENTS FOR THE DEGREE OF

MASTER OF SCIENCE

Metallurgical Sciences Laboratory.
Department of Mechanical & Industrial Engineering
Winnipeg, Manitoba

ISBN 0-612-16196-X

Name _____

*Dissertation Abstracts International* and *Masters Abstracts International* are arranged by broad, general subject categories. Please select the one subject which most nearly describes the content of your dissertation or thesis. Enter the corresponding four-digit code in the spaces provided.

SUBJECT TERM

Materials Science

0794 UMI

SUBJECT CODE

## Subject Categories

# THE HUMANITIES AND SOCIAL SCIENCES

### COMMUNICATIONS AND THE ARTS
- Architecture 0729
- Art History 0377
- Cinema 0900
- Dance 0378
- Design and Decorative Arts 0389
- Fine Arts 0357
- Information Science 0723
- Journalism 0391
- Landscape Architecture 0390
- Library Science 0399
- Mass Communications 0708
- Music 0413
- Speech Communication 0459
- Theater 0465

### EDUCATION
- General 0515
- Administration 0514
- Adult and Continuing 0516
- Agricultural 0517
- Art 0273
- Bilingual and Multicultural 0282
- Business 0688
- Community College 0275
- Curriculum and Instruction 0727
- Early Childhood 0518
- Elementary 0524
- Educational Psychology 0525
- Finance 0277
- Guidance and Counseling 0519
- Health 0680
- Higher 0745
- History of 0520
- Home Economics 0278
- Industrial 0521
- Language and Literature 0279
- Mathematics 0280
- Music 0522
- Philosophy of 0998
- Physical 0523
- Reading 0535
- Religious 0527
- Sciences 0714
- Secondary 0533
- Social Sciences 0534
- Sociology of 0340
- Special 0529
- Teacher Training 0530
- Technology 0710
- Tests and Measurements 0288
- Vocational 0747

### LANGUAGE, LITERATURE AND LINGUISTICS
- Language
  - General 0679
  - Ancient 0289
  - Linguistics 0290
  - Modern 0291
  - Rhetoric and Composition 0681
- Literature
  - General 0401
  - Classical 0294
  - Comparative 0295
  - Medieval 0297
  - Modern 0298
  - African 0316
  - American 0591
  - Asian 0305
  - Canadian (English) 0352
  - Canadian (French) 0355
  - Caribbean 0360
  - English 0593
  - Germanic 0311
  - Latin American 0312
  - Middle Eastern 0315
  - Romance 0313
  - Slavic and East European 0314

### PHILOSOPHY, RELIGION AND THEOLOGY
- Philosophy 0422
- Religion
  - General 0318
  - Biblical Studies 0321
  - Clergy 0319
  - History of 0320
  - Philosophy of 0322
- Theology 0469

### SOCIAL SCIENCES
- American Studies 0323
- Anthropology
  - Archaeology 0324
  - Cultural 0326
  - Physical 0327
- Business Administration
  - General 0310
  - Accounting 0272
  - Banking 0770
  - Management 0454
  - Marketing 0338
- Canadian Studies 0385
- Economics
  - General 0501
  - Agricultural 0503
  - Commerce-Business 0505
  - Finance 0508
  - History 0509
  - Labor 0510
  - Theory 0511
- Folklore 0358
- Geography 0366
- Gerontology 0351
- History
  - General 0578
  - Ancient 0579
  - Medieval 0581
  - Modern 0582
  - Church 0330
  - Black 0328
  - African 0331
  - Asia, Australia and Oceania 0332
  - Canadian 0334
  - European 0335
  - Latin American 0336
  - Middle Eastern 0333
  - United States 0337
- History of Science 0585
- Law 0398
- Political Science
  - General 0615
  - International Law and Relations 0616
  - Public Administration 0617
- Recreation 0814
- Social Work 0452
- Sociology
  - General 0626
  - Criminology and Penology 0627
  - Demography 0938
  - Ethnic and Racial Studies 0631
  - Individual and Family Studies 0628
  - Industrial and Labor Relations 0629
  - Public and Social Welfare 0630
  - Social Structure and Development 0700
  - Theory and Methods 0344
- Transportation 0709
- Urban and Regional Planning 0999
- Women's Studies 0453

# THE SCIENCES AND ENGINEERING

### BIOLOGICAL SCIENCES
- Agriculture
  - General 0473
  - Agronomy 0285
  - Animal Culture and Nutrition 0475
  - Animal Pathology 0476
  - Fisheries and Aquaculture 0792
  - Food Science and Technology 0359
  - Forestry and Wildlife 0478
  - Plant Culture 0479
  - Plant Pathology 0480
  - Range Management 0777
  - Soil Science 0481
  - Wood Technology 0746
- Biology
  - General 0306
  - Anatomy 0287
  - Animal Physiology 0433
  - Biostatistics 0308
  - Botany 0309
  - Cell 0379
  - Ecology 0329
  - Entomology 0353
  - Genetics 0369
  - Limnology 0793
  - Microbiology 0410
  - Molecular 0307
  - Neuroscience 0317
  - Oceanography 0416
  - Plant Physiology 0817
  - Veterinary Science 0778
  - Zoology 0472
- Biophysics
  - General 0786
  - Medical 0760

### EARTH SCIENCES
- Biogeochemistry 0425
- Geochemistry 0996
- Geodesy 0370
- Geology 0372
- Geophysics 0373
- Hydrology 0388
- Mineralogy 0411
- Paleobotany 0345
- Paleoecology 0426
- Paleontology 0418
- Paleozoology 0985
- Palynology 0427
- Physical Geography 0368
- Physical Oceanography 0415

### HEALTH AND ENVIRONMENTAL SCIENCES
- Environmental Sciences 0768
- Health Sciences
  - General 0566
  - Audiology 0300
  - Dentistry 0567
  - Education 0350
  - Administration, Health Care 0769
  - Human Development 0758
  - Immunology 0982
  - Medicine and Surgery 0564
  - Mental Health 0347
  - Nursing 0569
  - Nutrition 0570
  - Obstetrics and Gynecology 0380
  - Occupational Health and Safety 0354
  - Oncology 0992
  - Ophthalmology 0381
  - Pathology 0571
  - Pharmacology 0419
  - Pharmacy 0572
  - Public Health 0573
  - Radiology 0574
  - Recreation 0575
  - Rehabilitaion and Therapy 0382
  - Speech Pathology 0460
  - Toxicology 0383
- Home Economics 0386

### PHYSICAL SCIENCES

#### Pure Sciences
- Chemistry
  - General 0485
  - Agricultural 0749
  - Analytical 0486
  - Biochemistry 0487
  - Inorganic 0488
  - Nuclear 0738
  - Organic 0490
  - Pharmaceutical 0491
  - Physical 0494
  - Polymer 0495
  - Radiation 0754
- Mathematics 0405
- Physics
  - General 0605
  - Acoustics 0986
  - Astronomy and Astrophysics 0606
  - Atmospheric Science 0608
  - Atomic 0748
  - Condensed Matter 0611
  - Electricity and Magnetism 0607
  - Elementary Particles and High Energy 0798
  - Fluid and Plasma 0759
  - Molecular 0609
  - Nuclear 0610
  - Optics 0752
  - Radiation 0756
- Statistics 0463

#### Applied Sciences
- Applied Mechanics 0346
- Computer Science 0984
- Engineering
  - General 0537
  - Aerospace 0538
  - Agricultural 0539
  - Automotive 0540
  - Biomedical 0541
  - Chemical 0542
  - Civil 0543
  - Electronics and Electrical 0544
  - Environmental 0775
  - Industrial 0546
  - Marine and Ocean 0547
  - Materials Science 0794
  - Mechanical 0548
  - Metallurgy 0743
  - Mining 0551
  - Nuclear 0552
  - Packaging 0549
  - Petroleum 0765
  - Sanitary and Municipal 0554
  - System Science 0790
- Geotechnology 0428
- Operations Research 0796
- Plastics Technology 0795
- Textile Technology 0994

### PSYCHOLOGY
- General 0621
- Behavioral 0384
- Clinical 0622
- Cognitive 0633
- Developmental 0620
- Experimental 0623
- Industrial 0624
- Personality 0625
- Physiological 0989
- Psychobiology 0349
- Psychometrics 0632
- Social 0451

THE UNIVERSITY OF MANITOBA

FACULTY OF GRADUATE STUDIES

COPYRIGHT PERMISSION

# THE MICROSTRUCTURAL CHARACTERISTICS AND TEMPERATURE EFFECTS ON THE WEAR BEHAVIORS OF THE ELCTROLESS NICKEL-PHOSPHORUS COATINGS

BY

YUGANG LIU

A Thesis/Practicum submitted to the Faculty of Graduate Studies of the University of Manitoba in partial fulfillment of the requirements for the degree of

MASTER OF SCIENCE

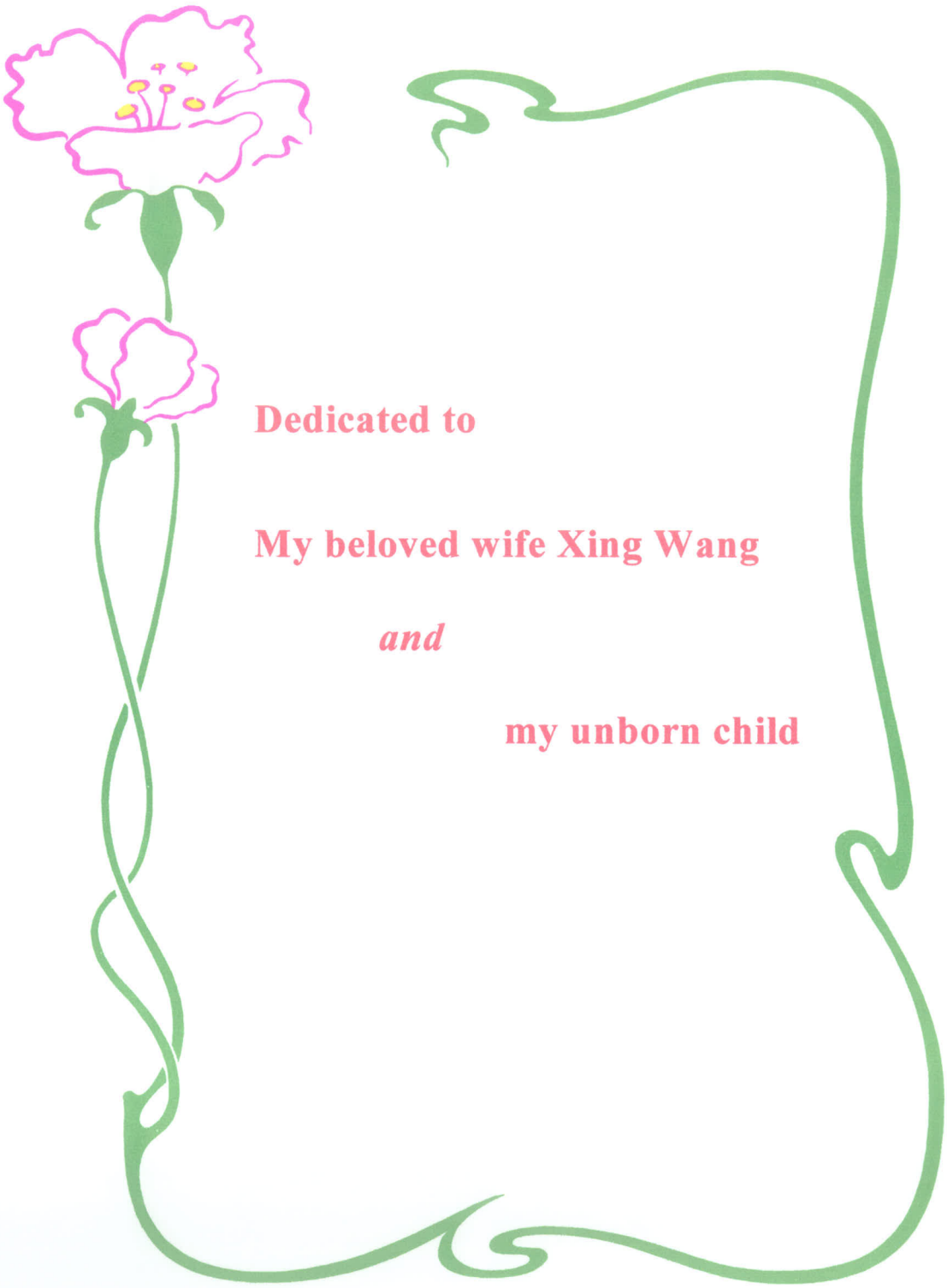

Dedicated to

My beloved wife Xing Wang

*and*

my unborn child

# ACKNOWLEDGMENTS

I gratefully acknowledge Dr. K.N. Tandon for providing me with the opportunity to work on this project. His consistent support, guidance and the financial support during my study period are very appreciated.

I sincerely thank Dr. J. R. Cahoon and J. I. Glanville for being my advisory committee and reviewing my thesis.

I am more grateful than I can express for the loving and encouraging contributions of my wife, Xing Wang, to my studies and to my endeavors during the whole period of my graduate studies.

I acknowledge the dedicated assistance from the technicians I have worked with in Metallurgical Science Lab, Mr. Don Mardis and John Vandorp; they made my research contributions possible.

I am grateful for the support of colleagues at the Metallurgical Science Lab., especially Mr. Xianyao Li who gave me valuable discussions and suggestions; and Ms. Bev Dobran who helped with proofreading the thesis.

# ABSTRACT

Electroless nickel coatings, especially Ni-P coatings, are useful in many areas such as the chemical process industry and the aerospace, nuclear and automotive industries. As applied, electroless nickel-phosphorus coatings are uniform, hard and highly wear and corrosion resistant. The hardness of the coating can be increased through heat treatment. It becomes an alternative coating for locomotive diesel engine liners where hard chrome is a conventional coating material.

The present thesis reports the experimental results and findings on the microstructural characteristics and temperature effects on the wear behaviors of the Electroless Nickel-Phosphorus coatings by using Transmission Electron Microscopy (TEM), Scanning Electron Microscopy (SEM), X-ray diffractometery and an Energy Dispersed Spetrometry (EDS). The microstructure of as-deposited nickel phosphorus coating with 10-12 wt% phosphorus is found to be an amorphous phase with tiny nickel crystallites present in it. After 400°C/1hr and 600° C/1hr heat treatment the microstructure is composed of nickel crystallites and nickel phosphides $Ni_3P$ and other nickel-phosphides, which may be $Ni_5P_2$ and $Ni_2P$. The structure of Ni crystallites and $Ni_3P$ is clearly revealed by TEM.

The hardness of the coating changes with the heat treatment, and is determined by the size of nickel crystallites and nickel-phosphides. It is also observed that the coating on a mild steel substrate builds up a clear diffusion layer after 600°C heat treatment.

It is found that the temperature has a significant effect on the lubricated reciprocating sliding wear of the electroless nickel-phosphorus coatings. A temperature rise from 25°C to 100°C reduces the lubricated wear of as-deposited electroless nickel-phosphorus coatings, especially under a high load condition. Increasing temperature also reduces the lubricated wear of 400°C and 600°C heat treated coatings.

Wear track surface characteristics were studied using a SEM. For as-deposited coatings under lubricating condition, the wear mechanism changes from mainly delamination at room temperature testing to the polishing at 100°C testing for 4kg load condition. The wear mechanism changes from delamination/spalling and abrasive wear at room temperature testing to polishing wear at 100°C testing for 8kg load condition. Delamination wear dominates the wear of the coatings after 400°C and 600°C heat treatments at room temperature and polishing wear mechanism dominates the wear at 100°C test.

It was also observed that there is a change in Ni, P content on the wear track after the 100°C test. Ni content decreases and P content increases. S is also present on the wear track after the 100°C test. It is believed that the P and S compounds films are formed on the wear track during the high temperature test, which reduces the wear of the coatings

The temperature effects on the dry wear (without lubrication) of the coatings are also investigated. The morphology of the wear track and the wear mechanisms are revealed and discussed in the thesis. Adhesive and abrasive wear dominates the reciprocating sliding of the Ni-P coating at the room temperature test under dry wear condition. Polishing wear is the main wear mechanism for the tests at 100°C.

# TABLE OF CONTENTS

# LIST OF FIGURES

# LIST OF TABLES

# CHAPTER 1

# INTRODUCTION

Electroless nickel (EN) coatings have been used for decades to protect materials from corrosion, erosion and wear. Electroless nickel coatings, especially Ni-P coatings, are useful in many areas such as the chemical process industry and the aerospace, nuclear and automotive industries. The advantages of the electroless nickel coating include excellent uniformity and good resistance to corrosion and wear. As applied, nickel-phosphorus coatings are uniform, hard, relatively brittle, lubricious, easily solderable and highly corrosion resistant. The as-plated hardness of the coating is around 500HV and this can be increased to over 1000HV after heat treatment, due to the precipitation of $Ni_3P$ phases.

The microstructure of the electroless nickel-phosphorus coatings depends on the formulation of the coating solution which gives different phosphorus content in the coating, and the coating structure varies with the phosphorus content. High phosphorus coatings are mainly amorphous while the low phosphorus ones are mainly composed of the nickel crystallites. The microstructure of the coatings also varies with the heat treatment. The hardness of the coating changes as the heat treatment temperature changes, which determines the wear properties of the coating.

Wear, a gradual damage caused when two materials in contact moving relative to each other, is not only a mechanical process depending upon such factors as the materials properties, applied load and sliding speed, but wear process is also affected by several environmental factors such as humidity, temperature and atmospheres, though wear is usually thought of as a mechanical process. Wear must be considered as a conjoint chemico-mechanical process, like corrosion-fatigue or stress-corrosion-cracking. High temperature wear is common in many industrial and

commercial applications. Chemical interactions with metal surfaces tend to speed up as the temperature is increased and may drastically alter wear properties. In addition, physical properties of the metals themselves are often quite different at elevated temperatures, and this may affect the wear processes.

Several investigations in the past have dealt with the wear resistance of electroless nickel-phosphorus coatings. There seems, however, to be little research conducted to date on how the environmental temperature affects the wear of the electroless nickel coatings. Since these coatings may be considered as an alternative coating for locomotive diesel engine liners where hard chrome is a conventional coating material, it is important to study the effect of temperature on the wear characteristics of the EN coatings under lubricated conditions. The effect of environmental temperature on the wear process for different materials has been noted and studied mainly to determine how high temperature oxidation influences the wearing of metal surfaces. Some recent studies have also shown that in a certain range of temperature, the wear of steel and copper-graphite composites decreases as temperature increases.

In this research, temperature effects on the wear characteristics of the electroless Ni-P coatings applied on mild steel are investigated, mainly under lubricated reciprocating sliding conditions. The entire experiment was conducted using the ball-on-block testing method carried out on the custom designed test rig. The coated blocks were received in as-deposited state. Three states of the Ni-P coatings were evaluated: as-deposited, as-deposited + 400°C/1hr heat treatment and as-deposited + 600°C/1hr heat treatment. A motor oil Nugold 10W30 was selected as a lubricant. The wear was evaluated by the weight loss method, and a balance with 0.1mg readability was used to measure the weight loss. Scanning Electron Microscopy (SEM) and Energy Dispersed Spectrometry (EDS) as well as X-ray mapping were used to characterize the wear tracks and to investigate the wear mechanisms. The microstructure of the coatings was analyzed by using a Transmission Electron Microscope (TEM) and an X-ray Diffractometer. The structure of the

nickel phosphides formed in the heat-treated coatings were indexed. Meanwhile, dry wear was tested on two kinds of coatings: as-deposited and as-deposited + 600°C/1hr heat treatment. The wear tracks were examined by SEM, SEM/EDS and X-ray mapping as well, and the possible wear mechanisms are discussed in the thesis.

# CHAPTER 2

# LITERATURE REVIEW

Recently, interest in the environmental effect on wear of materials has grown rapidly. It has been noted that the temperature and humidity play important roles in the wear process of materials [1]. Due to these factors, wear mechanisms get altered or changed significantly. Few investigations in the past were paid attention to how temperature affects the wear of electroless nickel-phosphorus coatings. The wear mechanism of the electroless nickel coatings at different temperatures is not quite clear. In this chapter, a general concept of the wear process, main wear mechanisms and the newly developed wear mechanisms, various studies of the temperature effect on wear, and lubrication theories are briefly summarized. The electroless nickel coatings, the microstructure and properties of nickel-phosphorus coatings, and the wear of nickel-phosphorus coatings are reviewed in this chapter as well.

## 2.1 WEAR

### 2.1.1 WEAR OF MATERIALS

Wear is one of three main aspects of tribology. Tribology is the science and technology of interacting surfaces in relative motion and of related subjects and practices [2]. It includes many aspects of solids in contact. The field of tribology is concerned with the phenomena that take place when surfaces in contact are moving relative to each other. Tribology includes many important effects, the nature of friction, wear at the interface, the chemical and physical effects of lubricants, and adhesion taking place at the tribological interface, and is crucial to virtually all areas of manufacturing [2-3].

### 2.1.2 DEFINITION OF WEAR

Wear is defined as "damage to a solid surface, most of the time in the form of gradual material removal from a surface, by the action of relative motion with a contacting substance or substances" [2-4]. This definition, according to Rigney [5], can immediately be divided into two categories. In the first, materials may be displaced so that a given object is changed in shape and /or properties, but little or no material is actually lost. In the second, there is a net change of mass or volume from at least one of the interacting components, and loose wear debris may be observed. He stated that these distinctions are important because even if there is no volume or mass change during the wear test, the damage due to material displacement may be pronounced. Rigney's interpretation is very important in understanding the damage caused by wear in the view of material science, as the dislocation concept has been used in explaining the phenomenon of wear [6].

### 2.1.3 TYPES OF WEAR

Wear is a complex process and has been categorized in various ways. The phenomenological approach is based on a macroscopic description of the appearance of worn surfaces (for example, scuffed, rubbed and fretted). This system is limited, because it does not focus on mechanisms of wear. The common method to categorize wear is on the basis of the fundamental mechanism that is operating. This approach, according to Tucker [7], is complicated by the fact that more than one mechanism may be operating at a time and by the lack of sufficient information. Both approaches have been described and summarized in several publications [1-5, 7-8]. Most mechanisms involve some type of fracture of material from a surface. Budinski [4] summarized the wear processes into four main wear mechanisms which have been widely accepted (Fig.2-1). Though these are universally accepted wear mechanisms, the terminology of wear is still unsettled and basic definitions have not yet been standardized. For example, surface fatigue, now more

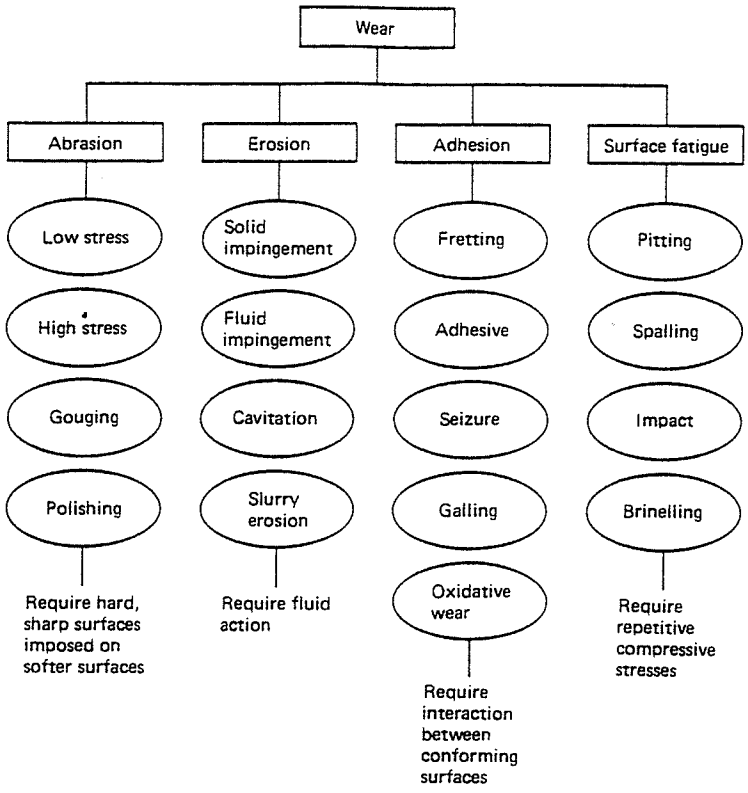


Fig. 2-1 The Basic categories of wear and modes of wear [4]

generally called fatigue, involves the crack nucleation at subsurface instead of surface and crack propagation under the surface as well. The adhesive wear has been criticized on several aspects. Delamination as a wear mechanism in sliding wear has been developed [9]. A different approach is generated which involves describing sliding wear mechanisms on the basis of the shape and size of the wear debris particles [10]. The simplest classification of wear is defined as mild wear and severe wear which is based on the load used in the wear process [2]. The following section describes some main wear mechanisms.

### 2.1.3.1 Mild wear and severe wear

"Mild wear" is generally associated with low loads where metallic interactions are somewhat inhibited and the wear debris consists of fine particles and is usually in the form of oxides. This

does not imply that metallic contacts have never occurred at all, since the resulting metallic debris would tend to become oxidized at the high local temperatures at the interface. Nevertheless, the nature of the surface-asperity interaction is relatively gentle, resulting in characteristically mild wear and a smoothing of the surfaces. At a high applied load, a much coarser wear process occurs. The wear debris is of a much larger particle-size, and the worn surfaces are much rougher and the increase in volume wear rate changes by several orders of magnitude. This means wear transferred into "severe wear". There is a rapid transition from one mode to the other as the load is increased between these two wear regimes (Fig. 2-2). This trend is also shown in the dry wear of composites [11]. With some materials at higher loads, the increasing temperatures cause metallurgical changes in the materials, such as a decrease in the hardness. Therefore, these effects lead to a second transition from the "severe wear" back to the "mild wear" regime [2].

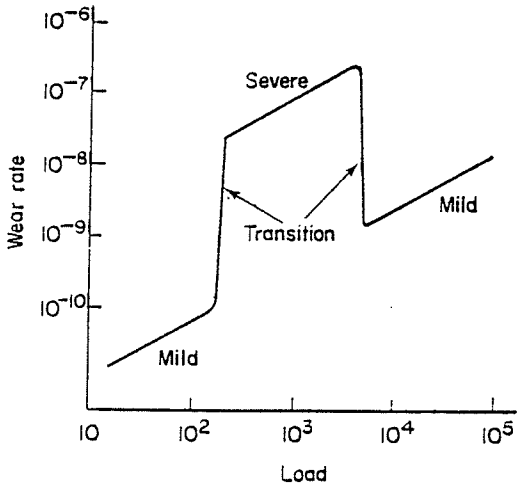


Fig. 2-2 The transition phenomena in wear [2]

### 2.1.3.2 Adhesive wear

Adhesive wear is identified by such terms as scoring, galling, seizing, and scuffing. It was defined as "Wear by transference of material from one surface to another during relative motion due to a process of solid-phase welding; particles that are removed from one surface are either permanently or temporarily attached to the other surface" [7].

Naturally, the solid surfaces consists of asperities of various shapes. When two such surfaces contact each other under a load normal to the general planes of the surfaces, the asperities come into contact and elastically or plastically deform until the real area of contact is sufficient to carry the load. A "cold welding" may occur between the two surfaces, which is stronger than the intrinsic strength of the weaker of the two solids in contact. When relative motion between the two surfaces occurs, the weaker of the two materials fails, and material is transferred to the contacting surface. If one assumes that the wear particles are geometrically similar, the wear volume would be expected to be proportional to the real areas of contact at which adhesion occurs, and also to the distance of sliding. Adhesive wear can be described by the following formulae:

$$V = \frac{kWL}{3H} \qquad \text{or} \qquad V = \frac{kWL}{H}$$

where V is the volume of wear, W is the load, L is the distance of sliding , H is the hardness of the material and k is often called the adhesive wear coefficient or the Archard constant. "k" is also interpreted as a probability factor that a given area contact will fracture within the weaker material rather than at the original interface. The k value is determined experimentally. It is found that k values range from about $10^{-3}$ to $10^{-8}$ [2]. As mentioned above, the adhesive wear

mechanism is now challenged in several aspects and the delamination wear mechanism has been developed which is described later in this chapter [9].

### 2.1.3.3 Abrasive wear

Abrasive wear is defined as wear by displacement of material caused by hard particles or protuberances. Abrasive wear is usually covered by such diverse terms as scratching, scoring, grooving, polishing, grinding, gouging and erosion. All of these processes probably involve a good measure of the basic abrasive cutting mechanism, but it is possible, in some cases, that other basic mechanisms are also involved [2, 3].

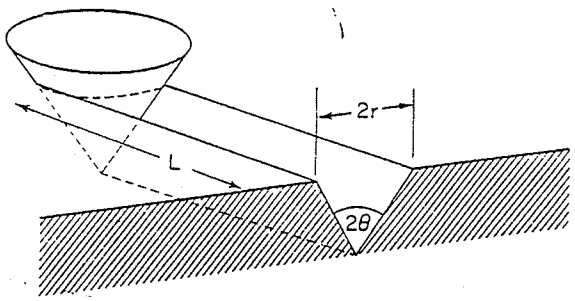


Fig. 2-3 Wear due to a single conical asperity [2]

If supposing the asperity has the conical geometry of Fig.2-3, the following formulae can thus be derived to describe abrasive wear:

$$V = \frac{6\cot\theta}{\pi}\frac{W}{H}L = K_a\frac{W}{H}L$$

where θ is the conical angle, W is the load, H is the hardness and L is the sliding distance. One can see that this equation is similar to the adhesive one, but the k value is different. For abrasive wear, $K_{\alpha}$ has a much higher value than the K in the adhesive wear mechanism [2].

### 2.1.3.4 Fatigue wear

Fatigue wear, as Kimura states [12], has an increased importance in recent work on wear processes as adhesive wear mechanism gets re-examined. This type of failure can occur after a large number of loading cycles, even though the load is less than that we would normally expect to produce failure in a single load application. Fatigue failure often occurs below the surface in the rolling contact as the highest stress position of rolling contact is below the surface. Cracks are produced by fatigue and the propagation of cracks leads to the removal of large pieces of metal. If the contacted surfaces are separated by a lubricant film, adhesive and abrasive wear are virtually eliminated. The applied load, however, is still transmitted to the solid surfaces through a lubricant film and can still cause stresses in the surface, so that fatigue-type wear can still occur [2].

### 2.1.3.5 Corrosive wear

Corrosive wear is due to the removal of loose contaminant films on the surface of metals such as rust films on steel. Rubbing removes the films leaving exposed clean metal, which immediately reacts with its environment to provide new surface films, which are again removed during rubbing. As a result, the wear occurs.

Corrosive effects are not entirely deleterious. Sometimes the presence of oxide films in preventing metal-to-metal contact greatly reduces the coefficient of friction. So does the decrease in wear. The films with low shear strength give a low coefficient of friction and thus decrease the adhesion between the two contacting surfaces. Sometimes so-called E.P.(extreme pressure) additives to

lubricating oil produce surface films such as chlorides and sulphides and provide protective surface layers[3, 4].

### 2.1.3.6 Polishing wear

Polishing wear is unintentional progressive removal of material from a surface by the action of rubbing from other solids. The materials are removed without visible scratching, fracture, or plastic deformation of the surface. Usually, polishing wear gives a very smooth or bright surface. Polishing wear is categorized as "abrasive wear", but this is not always the case [4].

### 2.1.3.7 Spalling wear

In spalling wear, particles fracture from a surface in the form of flakes. Spalling is the result of surface fatigue, and it occurs in the same types of systems. The coating surfaces are easy to spall under rolling contact and cyclic sliding conditions. Under rolling contact, the highest stress point is located under the surface; cracks are easy produced by fatigue. If the surface coating is very hard, the crack will propagate quickly to the surface and this will give the spalling [4].

### 2.1.3.8 Delamination wear

Adhesive wear mechanism, though widely accepted, has been criticized in two aspects [12]. First, the adhesion theory fails to explain the presence of the loose wear particles as a logical consequence. If the welding occurring at a junction is not strong enough to prevent separation along the original interface, neither metal transfer nor a loose particle results. On the other hand, if it is strong enough, there would be transfer but no loose wear particles.

Second, the analysis of wear particles has shown that particles seldom belong in the adhesive wear category. Instead, it has turned out that the most frequently-observed particles appear as thin flakes of metal. Samuels et al [10] raised the same questions about the adhesive wear particles.

Suh and co-workers [9] have raised questions about the adhesion theory in friction which is the basis of the adhesive wear mechanism. They have proposed and developed a new theory to describe the wear of surfaces in sliding contact: the delamination theory of wear. According to this theory, wear takes place by the deformation of the surface layer, nucleation of cracks at the subsurface, and the propagation of those cracks nearly parallel to the surface. Eventually, loose sheet-like wear particles are generated. The cracks may initiate at second phases or at particulate inclusions. The nucleation in a homogeneous material is not well understood. The depth of nucleation and distance of the propagation are a function of the material's properties as well as the load and frictional characteristics of the surface. Crack nucleation can be expected to be controlling in materials that deform plastically at low stress levels or have rapid crack-propagation rates.

They have also proposed a new theory for the genesis of friction, based on the following postulate:

> The coefficient of friction between the sliding surfaces is due to the various combined effects of asperity deformation, $\mu_d$, plowing by wear particles and hard surface asperities, $\mu_p$, and adhesion between the flat surfaces, $\mu_a$. The relative contributions of these components depend on the condition of the sliding interface, which is affected by the history of sliding, the specific materials used, the surface topography and the environment.

Based on this theory, instead of the traditional adhesion theory, a friction space was generated and is shown in Fig.2-4.

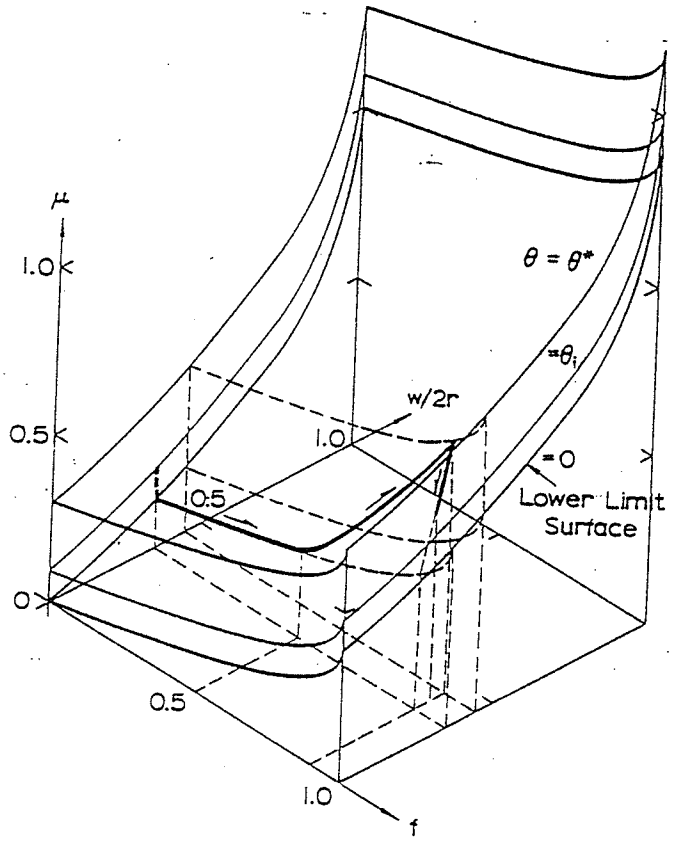


NOTE: $f=\tau_s/k$, ,where $\tau_s$ is the shear stress at the interface and k is the shear flow strength of the soft metal; θ=the slope of asperities; w/2r=width of asperity penetration/diameter of the spherical particle.

Fig. 2-4 "Friction space" showing the coefficient of friction as a function of adhesion between flat contacts, wear particle penetration, and surface roughness [9]

### 2.1.4 WEAR-MECHANISM MAPS

Lim and Ashby [13], based upon the analysis of plenty of work about wear, have developed wear-mechanism maps. Fig.2-5 is the empirical wear-mechanism map for steel using the pin-on-disc

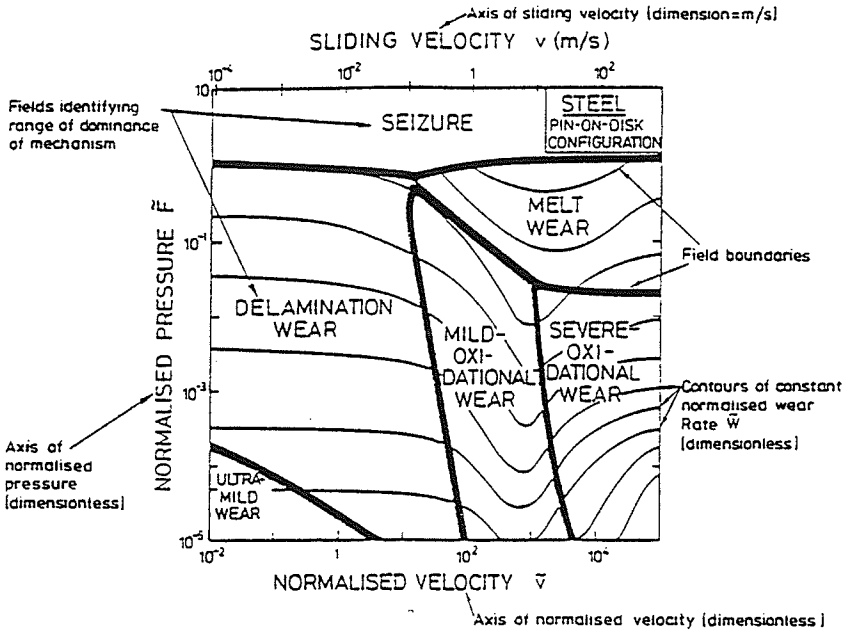


Fig.2-5 The empirical wear-mechanism map for steel using the pin-on-disk configuration [13]

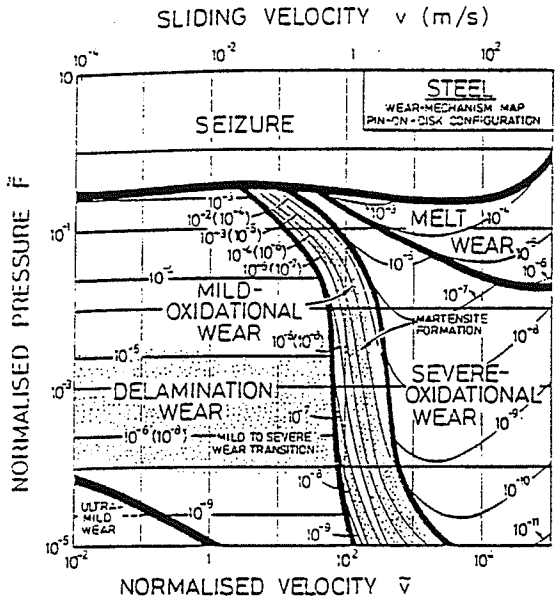


Fig.2-6 The wear-mechanism map for a steel sliding pair using the pin-on-disk configuration. Contours of constant normalized wear rates are superimposed on fields showing the regimes of dominances of different wear mechanisms. There are discontinuities in the contours when they cross the field boundaries into the regimes of severe-oxidational wear and melt wear. The wear rates given in parentheses are the values when mild wear takes place. The shaded regions indicate a transition between mild and severe wear [13].

configuration, and Fig.2-6 is the one generated based on physical modeling. The wear mechanisms are thereby classed into four groups according to their study: 1) Seizure, 2) Melt-dominated wear, 3) Oxidation-dominated wear (mild and severe-oxidational wear) and 4) Plasticity-dominated wear (including delamination wear). The description of these four wear mechanism has been summarized in [8] and therefore will not be presented here.

### 2.1.5 FACTORS AFFECTING WEAR BEHAVIOR OF MATERIALS

Several factors will affect the wear of materials [2]. These factors include the properties of materials (hardness, crystal structure), the operation parameters (load and speed of sliding or rolling) and the environmental factors (temperature, humidity and oxidizing atmospheres) [1]. Under lubrication conditions, wear can be reduced significantly. Actually, most tribology systems are under lubrication conditions.

#### 2.1.5.1 Hardness

According to the adhesive wear equation, V=kWL/H, increasing hardness of the material will decrease the wear. Since the hardness of a material depends on temperature, the ability of the material to hold its hardness into higher temperatures (the so-called "hot hardness" characteristics of a material) is particularly significant. Fig.2-7 and Fig.2-8 give the effect of hardness on the abrasive wear resistance.

#### 2.1.5.2 Load and sliding speed

As mentioned above, the change of load leads the wear change from "mild" to "severe" wear and, for some materials, back to the "mild" wear again. High sliding speed generally results in severe wear because it will induce a high temperature on the sliding surface. High temperature

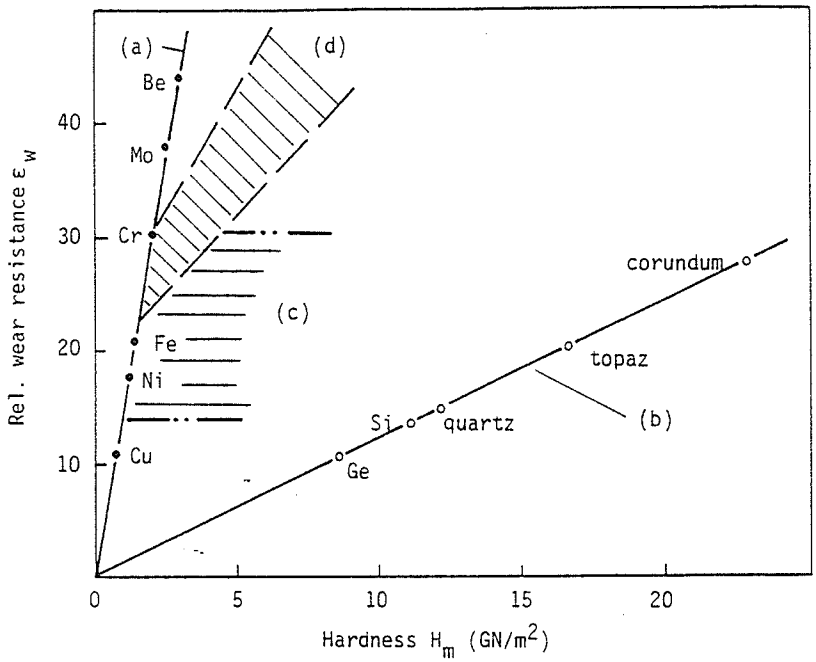


Fig.2-7 Khrushov diagram: wear resistance as a function of the hardness of materials [3]

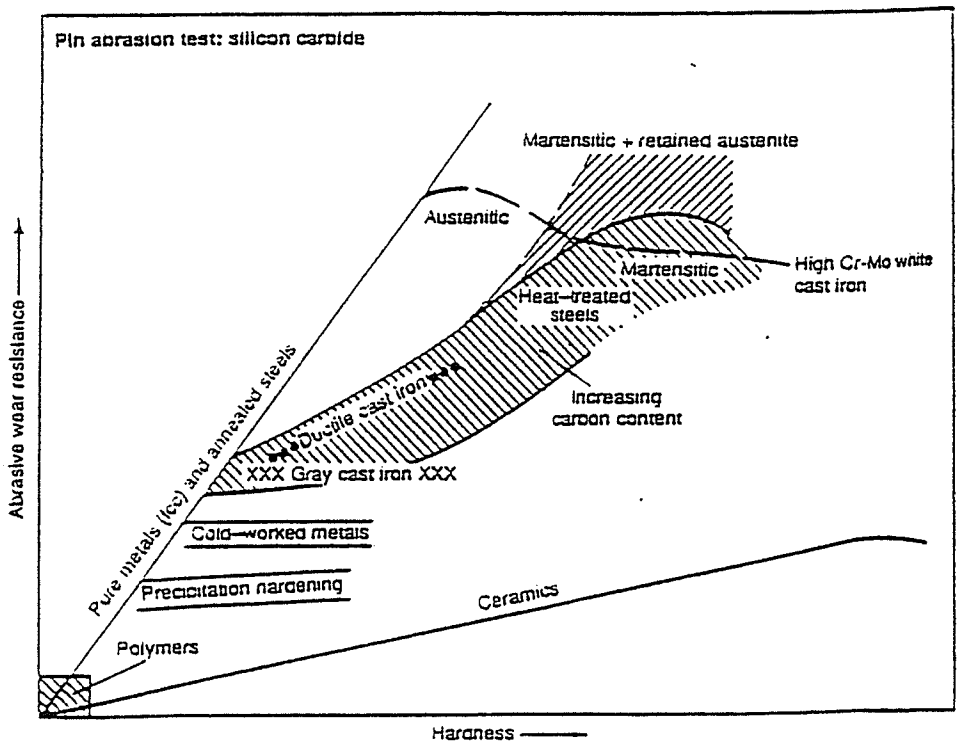


Fig.2-8 Two-body abrasion resistance (1/volume wear rate) for various materials plotted against bulk hardness [51]

affects the hardness of a material (softening or hardening the surface of the material) and oxidizes the surface of material. If the work-hardening effect occurs and the oxidation film has a good bonding strength with the matrix and a low shear strength, the wear rate will be decreased as sliding speed increases. Thus, the sliding speed exhibits the same trend as load. Fig.2-9 shows the effects of load and sliding speed on the dry wear of steel [14]. However, depending on different materials, load and sliding speed may play different roles in the wear process.

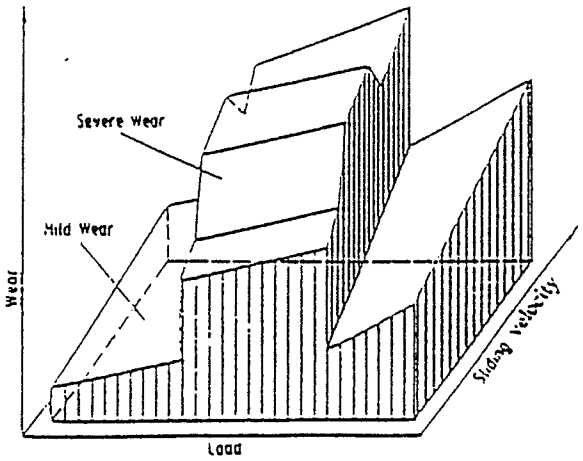


Fig.2-9 Wear intensity of steels in dry sliding as a function of load and sliding velocity (logarithmic scales) [14]

### 2.1.5.3 Effect of lubrication

One important means of reducing wear is lubrication. Lubrication not only reduces the power required to overcome friction but also protects rolling and sliding contact surfaces from excessive wear. Wear, however, still occurs under the lubrication condition.

The wear process is usually mild, and generates fine debris on lubricated surfaces. Abrasive wear, or delamination wear, predominates under the lubricated condition. The fine debris generated by abrasion becomes suspended in the oil or grease.

There are several basic modes of lubrication. In all modes, contact surfaces are separated by a lubricating medium. This medium may be a solid, a semisolid, a pressurized liquid or gaseous film. Generally, lubrication falls into these modes: 1) hydrodynamic lubrication, 2) Hydrostatic lubrication, 3) elastohydrodynamic lubrication, 4) boundary lubrication. Lubricants can be either liquid or solid. One of the functions of a lubricant is to carry away the heat generated by two surfaces sliding under contact pressure. Liquid lubricants can dissipate heat better than solid or semifluid lubricants, but in all types, the shear properties of the lubricant (viscosity for liquid) are important to its performance. For boundary lubrication, wear is completely governed by any film that happens to be on the surface, either planned or unplanned [15].

#### 2.1.5.4 Effect of humidity on wear

The humidity effect on wear depends on the details of the experiment. Moisture can have a pronounced effect on the fracture mechanisms of some steel and aluminum alloys with or without oxygen present. Moist air increases the crack propagation rate about 10 times over dry air for 4340 steel [16]. Tsuji and Ando [17-18] have studied the humidity effect on wear of carbon steels and cast irons and concluded that the atmospheric humidity effect on wear behavior was more pronounced on cast irons than on carbon steels. At relative humidities over 50% the wear rates of the cast irons decreased in air temperatures at ranging from 15°C to 25°C. The recent study by Tuan et. al [19] on steel C1045 concluded that at a given temperature, the wear rate increased rapidly with the humidity. Humidity has no consistent effect on the size of the wear scar, showing that wear rates and friction coefficients are not always related linearly [1].

### 2.1.6 EFFECT OF TEMPERATURE ON WEAR

High temperature wear is a problem in many industrial and commercial applications. Chemical interactions with metal surfaces tend to speed up as the temperature is increased and may drastically alter wear properties. Physical properties of the metals are often quite different at elevated or depressed temperatures, and this may affect the wear process. Tsuji et. at [17] concluded that the maximum wear rate on both carbon steels increased with an increase in air temperature from 15 to 25°C. This behavior had been explained by an adhesive wear mechanism. In their further work, Tsuji and Ando [18] concluded that the maximum wear rates of the carbon steels increased with air temperature from 15-25°C. Wear rates decreased at 30°C with the same relative humidity. The wear rates of the cast irons were maximum at 30°C.

By reviewing the research studies that have been conducted, the effects of temperature on wear can be classified into the following aspects: 1) temperature effect on the formation of the oxidation films; 2) temperature effect on the lubricated wear; 3) temperature effect on the wear of coatings.

#### 2.1.6.1 Temperature effect on the formation of oxidation film

Peterson and Florek [20], after studying the coefficient of friction of pure metals, indicated that, as temperature increases, a large increase in friction and surface damage occurs as the material softens. This condition persists until a particular temperature is reached, at which an oxide film is continually reformed at the sliding surface. At this particular temperature, the sliding characteristics are markedly improved. Extremely high friction, surface damage, and greater wear take place with the metals sliding against themselves at a temperature where the material softens appreciably, if no protective oxide is formed. If an oxide is formed, the galling tendency is reduced and effective sliding results as long as the oxide film adheres to the surface. They also

indicated that the soft oxide is good for preventing surface damage, but too much oxide increases the wear rate. If hard oxide is removed from the surface, abrasive wear occurs. The same results were obtained by Scott and Wood [21] on nickel base alloys. All the nickel alloys, under test conditions and air temperatures of 20 to 800°C, show a transition temperature. Above this temperature, low wear and a low coefficient of friction during sliding are observed after a time; below this temperature, these parameters remain relatively high throughout. Such changes can be closely correlated to the formation of a stable, adherent, thermally-softened oxide layer, or glaze on the load-bearing areas during the sliding. Once the glaze is established, very little further wear takes place.

The results obtained by Chaudhuri and Slifka [22] show that an increase in temperature increases the wear rate during self-mated sliding of 440C steel. High contact temperatures are generated during the sliding friction, causing rapid oxidation and localized surface melting. A combination of fatigue, delamination, and loss of hardness due to tempering of the martensitic structure is responsible for the high wear rate. Slifka et. al [23] generated wear mechanism maps of 440C martensitic stainless steel and indicated that the low wear area at all speeds, above 600°C, is a rapid oxidation regime, where an apparently wear-resistant oxide prevents wear and also provides for a relatively low coefficient of friction. The film formation due to the high temperature or generated high temperature by sliding is also used in the interpretation of wear of silicon nitrides and high speed steels [24-25].

### 2.1.6.2 Effect of temperature on lubricated wear of materials

It is well-known that the viscosity of most oils decreases with temperature. This is an important effect in tribology. The changes in temperature are due to the environment and the heat generated during the shearing of lubricant films. The increased temperature reduces the shear rate of the lubrication film and the film thickness during the hydrostatic lubrication, so that the solid surfaces

approach each other. When the thickness of the lubricant film approaches the dimensions of surface roughness, asperity contact begins, and evidence of wear can be detected. Surface temperature has the greatest influence on the effectiveness of boundary lubrication. Under extreme pressure (EP) lubrication, chemical additives in the lubricant react with metal surfaces to form soft, solid reaction products, which are presumably the agents that prevent metal adhesion and surface damage. Because heat increases the reaction rate during the sliding, at asperity contacts, where the load surface temperatures are highest, the reaction rate is greatest, and a solid lubricant is provided in the spots where the potential for adhesion is greatest. Thus, by chemical attack, modified by the localized surface temperature, the occurrence of severe wear is prevented by substitution of mild corrosion [7, 26]. When oil is heated in the presence of air, oxidation occurs, which increases the viscosity and organic acid concentration of mineral oils with the result that varnish and lacquer deposits may form on hot metal surfaces. Under severe conditions, the deposits may be converted to hard carbonaceous substances, which would increase the abrasive wear [7]. When sliding under lubrication conditions, sulfur in anti-wear aditives undergoes a change in chemical nature during wear testing of the steel surface. Surface sulphide is associated with boundary lubrication [27].

#### 2.1.6.3 Effect of temperature on the wear of coatings

This section reviews some research on the wear or friction of hard coatings at elevated temperature. It is found that the friction and wear behavior of ceramic coatings, such as fatigue spalling, plastic deformation and adhesive transfer of the ceramic coatings are similar to those of metals [28]. Under high temperature (450°C), the dry friction coefficients of the ceramic coatings are much higher than the lubricated friction coefficients. The high local temperature softens contacts and plastic deformation happens easily. Therefore, adhesive transfer occurs easily under dry friction conditions [28]. Jeng and Yan [29] have further observed that the surface polishing and abrasive wear mechanisms are dominant at lower temperatures. At higher temperatures,

delamination fatigue, tribochemical and adhesive wear mechanisms are active, and material transfer is an additional mechanism of sliding pairs. It increases with increasing temperature during the sliding wear of alumina.

Bell and Delargy [30] confirmed that the conventional chrome platings for piston rings are susceptible to excessive wear at temperatures of 300°C and over. The alumina coating at the higher temperature caused a substantial increase in the wear of the cast iron counterface. It also failed to provide any improvement in wear resistance against Mg-PSZ at 300°C, in contrast with the improvement at 200°C. This appears to arise from adverse thermal conditions and poor lubricant surface film formation. The study on the wear behavior of Ti-coating at elevated temperatures indicated that the wear on the Ti6Al4V-Co+Cr2O3 pair was very low, especially in the higher temperature range of 250-400°C [31].

Coatings are widely used in tribological applications, either being placed there intentionally to reduce wear, to avoid surface damage, or to modify frictional behavior; or formed in situ during the sliding process as discussed above. The use of coatings is to increase the base materials' resistance to wear or corrosion. Since wear- and corrosion-resistant alloys are usually more expensive than low alloy structural alloys, this approach usually offers economical advantages. Furthermore, replacing the coating during rework or repair is usually less expensive than part replacement.

In the following section in this literature review, the science and technology of nickel-phosphorus coatings are described. The literature review also includes their microstructures and ability for wear-resistance.

## 2.2 ELECTROLESS NICKEL COATINGS

### 2.2.1 INTRODUCTION

Electroless nickel (EN) coatings have been widely used to protect materials from corrosion, erosion, and wear [32-35]. It was invented in 1946 by A. Brenner and G. Riddell [34]. The traditional galvanic (electro-plating) nickel plating has some disadvantages in certain applications. For example, the coatings for components subjected to significant wear are not sufficiently hard. The unevenness in the thickness causes some difficulties in nickel plating of parts of complex shape. Electroless nickel plating complements galvanic nickel plating, and closes the gap between the mechanical properties of the electro-chemical nickel and the hard-chrome coatings. Various chemical processes of the electroless nickel plating are nowadays used for repair purposes as well as protection against corrosion and wear of new parts of machines and apparatus. They offer particular advantages for coating of inner surfaces of vessels, pipes, bored holes, etc. where galvanic processes can only be used at great expense or where they fail completely. Chemical plating also has its place in the metallisation of various insulators (plastics, glass, ceramics) as well as of semi-conductors (germanium, silicon, etc.).

Electroless nickel coatings can eliminate the need for expensive high-alloy materials in corrosive environments, prolong the life of wear components by factors of four or more, improve release properties of molds and improve the appearance of metal components [33].

There are several types of EN coatings: Ni-P, Ni-B and composite coatings. The variety of coatings available within these categories allows the designer to optimize an important property. Among them, Ni-P coatings offer the best corrosion resistance and are the most widely used [33]. Because of these advantages, the electroless nickel coatings have become an alternative in many applications to the hard chromium platings in industries [36].

Unlike the electroplating, the EN plating does not require electrical current to sustain the deposition. EN coatings are produced by the autocatalytic chemical reduction of nickel ions from an aqueous solution. As a result, the part is not susceptible to differences in deposit thickness due to the current density variations. Once a layer of nickel has formed on the substrate, that layer becomes the catalyst for nucleation of nickel and phosphorus that causes deposition to continue. This unique property of EN coatings makes it possible to coat internal surfaces of pipes, valves, threads on nuts and bolts, and other complex parts that are very difficult or impossible to be coated and protected by any other means.

The electroless nickel solutions are generally a mixture of different chemicals, each performing an important function. They contain:

1. A source of nickel, usually nickel sulfate.
2. A reducing agent to supply electrons for the reduction of nickel
3. Energy (heat)
4. Complexing agents (chelators) to control the free nickel available to the reaction
5. Buffering agents to resist the pH changes caused by the hydrogen released during deposition
6. Accelerators (exultants) to help increase the speed of the reaction
7. Accelerators (extrutants) to help increase the speed of the reaction
8. Inhibitors (stabilizers) to help control reduction
9. Reaction by-products [32]

The typical widely-accepted mechanisms for the chemical reactions are listed by the equations

$$(H_2PO_2)^- + H_2O \xrightarrow{\text{Catalyst heat}} H^+ + (HPO_3)^= + 2H_{abs} \quad \text{(Eq. 1)}$$

$$Ni^{++} + 2H_{abs} \rightarrow Ni + 2H^+ \quad \text{(Eq. 2)}$$

$$(H_2PO_2)^- + H_{abs} \rightarrow H_2O + OH^- + P \quad \text{(Eq. 3)}$$

$$(H_2PO_2)^- + H_2O \rightarrow H^+ + (HPO_3)^= + H_2 \quad \text{(Eq. 4)}$$

In the presence of a catalytic surface and sufficient energy, the hypophosphite ions are oxidized to orthophosphite ions. The hydrogen atoms which are given off during this reaction are partly absorbed on the surface of the catalyst (Eq. 1). The nickel ions are then reduced to metallic nickel by active hydrogen atoms whereby they are oxidized to hydrogen ions (Eq. 2). Simultaneously, some of the absorbed hydrogen reduces a small amount of the hypophosphite at the catalytic surface to water, hydroxyl ions, and phosphorus (Eq. 3). The speed of the reaction is an inverse function of the pH value. A part of the hypophosphite ions is oxidized catalytically to orthophosphite ions whereby gaseous, molecular hydrogen is given off (Eq. 4). Usually 5 kg (10lb) of sodium hypophosphite is required to reduce 1 kg (2lb) of nickel, for an average efficiency of 37% [32].

### 2.2.2 THE STRUCTURE OF THE NI-P COATINGS

Depending on the formulation of the plating solution, commercial coatings may contain 6 to 12 wt% phosphorus dissolved in nickel, and as much as 0.25 wt% of other elements. As applied, most of these coatings are amorphous; they have no crystal or phase structure. Coatings with lower phosphorus content, especially those applied from baths stabilized with heavy metals or sulfur compounds, are often porous. Coatings containing more than 10 wt% phosphorus and less than 0.05 wt% impurities are typically continuous [32-35].

The structure of the electroless nickel-phosphorus coatings undergoes important changes because of heat-treatment. As the electroless nickel-phosphorus is heated to temperatures above 220 to 260°C, structural changes begin to occur from amorphous. First coherent and then distinct particles of the nickel phosphite ($Ni_3P$) form within the alloy. At temperatures above 320°C, the deposit begins to crystallize and lose its amorphous character. With continued heating, nickel phosphite particles conglomerate and a two-phase alloy forms. With coatings containing more than 8 wt% phosphorus, a matrix of nickel phosphite forms, whereas almost pure nickel is the predominant phase in the deposits with lower phosphorus content [32-35, 37-38]].

E. Vafaei-Makhsoos and co-workers in 1978 [39] analyzed in-situ crystallization of the electroless Ni-P plating by TEM. They summarized that, in low P content (<12 at% P) Ni-P films, the as-deposited Ni-P consists of a single FCC supersaturated Ni phase. The grain size in the as-deposited films decreases with increasing P content. Heating the FCC supersaturated Ni grains causes the transformation to Ni and $Ni_3P$. Nucleation and growth of the $Ni_3P$ grains occurs with Ni grain coarsening. In high P content (>12 at% up to 22.5 at%), the films contain regions of microcrystallinity when viewed in a high resolution dark field. This result has not been found in X-ray studies. Crystallization of the microcrystalline regions results in the formation of Ni and $Ni_3P$; crystallization of the amorphous regions results in the formation of $Ni_xP_y$ and Ni. The transformation from the amorphous to crystalline involves complex morphologies:

$$\text{amorphous}(\text{Ni}-\text{P}) \rightarrow \text{Ni}_x\text{P}_y + \text{Ni}(\text{random})$$

E. Vafaei-Makhsoos and co-workers also observed two types of $Ni_xP_y$ grains. In one type, the individual grains are heavily striated with the striations being perpendicular to the transformation front. In the other type, the grains are not striated. $Ni_xP_y$ is a metastable phase, and further electron beam heating causes it to transform to $Ni_3P$. E. Vafaei-Makhsoos and co-workers' further studies [40-41] were involved in identification of the metastable phases during the

transformation of the Ni-P deposit from amorphous to $Ni_3P$. Unfortunately, they concluded that the crystallization of the amorphous Ni-P films was more complex than expected, and it must depend on a number of factors, including rates of electron beam heating, temperature gradients, and the homogeneity of the as-deposited sample.

D. N. Lee et al [42] in 1988 published their study about the microstructure and phase transformation of the electroless nickel deposits containing 7.4 to 10 wt% P. They concluded that the microstructure was a phosphorus-supersaturated nickel solid solution, whose grain size was thought to be 4 to 5 nm. They stated that the phase transformation temperature increases linearly with the heating rate and was independent of the phosphorus content. The stable phases of the deposits after the phase transformation are FCC nickel and BCT $Ni_3P$ with a=0.835nm and c=0.439nm.

Lee and Hur et al in 1990 [43] studied the microstructures and crystallization of the electroless Ni-P deposits by TEM and X-ray diffraction. They investigated five different phosphorus content films from 6.3 wt% to 13.6 wt%. They concluded that the electroless Ni-P deposit containing a low phosphorus content of 11.3 at% is a phosphorus-supersaturated crystalline nickel solid solution, whose grain size is thought to be 5 to 10 nm. The deposit was decomposed into $Ni_3P$ and phosphorus-depleted nickel crystallites. Subsequent coarsening of the nickel grains occurred when annealed. The electroless Ni-P deposit containing high phosphorus content has an amorphous structure. The amorphous deposits containing up to 21 at% P crystallized into the spherulitic $Ni_3$(P, Ni) phase preceded by the precrystallized nickel after heating. The amorphous deposits containing phosphorus higher than 21 at% were polymorphically crystallized into metastable phases of BCT $Ni_3$(P, Ni) or hexagonal $Ni_5$(P, $Ni)_2$, which was subsequently decomposed into stable phases of FCC nickel and BCT $Ni_3P$.

### 2.2.3 PROPERTIES OF THE ELECTROLESS NICKEL-PHOSPHORUS COATINGS

The properties of the electroless nickel coatings vary depending on the compositions of the coatings and on the materials of the carriers (substrates). The properties of the coatings are also determined by the structure of the coatings.

In general, the electroless nickel coatings are in appearance similar to bright steels with a more matt, or metallic silver color. They have high strength, limited ductility, and a high modulus of elasticity. The ultimate tensile strength of commercial coatings exceeds 700 MPa and allows the coatings to withstand a considerable amount of abuse without damage. Different content of P will affect the strength of the coatings (Fig.2-10). The ductility of electroless nickel coatings varies with composition as well. High phosphorus, high purity coatings have a ductility of about 1 to 1.5% (as elongation). In lower phosphorus deposits, or deposits containing metallic or sulfur impurities, the ductility is greatly reduced and may approach zero.

The internal stress in electroless nickel coatings varies with the composition. With lower phosphorus deposits, tensile stresses developed because of the difference in the thermal expansion between the deposits and the substrates. High level of stress in these coatings promotes cracking and porosity. The internal stress is neutral or compressive when P content is more than 10 wt%. The uniformity of the electroless nickel is very impressive. The thickness of coatings can be controlled to suit the applications. The solderability of electroless nickel coatings is excellent. The coatings can be easily soldered. The adhesion of electroless nickel coatings to most metals is also excellent. With proper pretreatment and activation, the bond strength of the coatings usually exceeds 140 MPa.

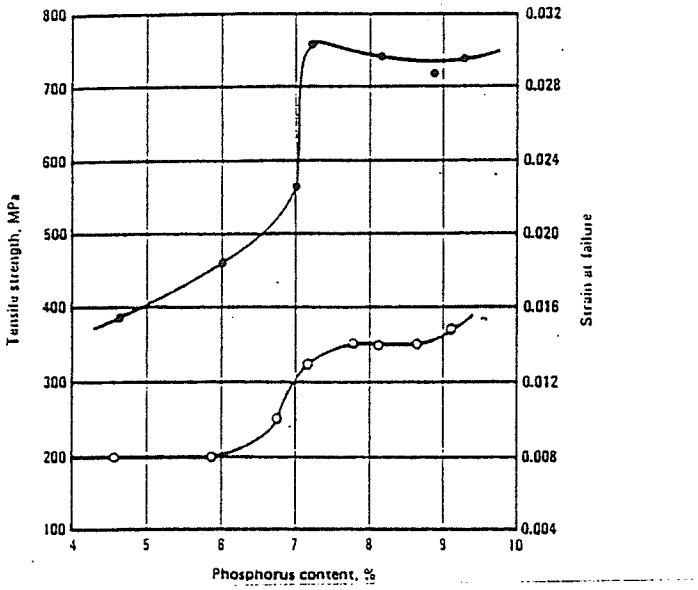


Fig.2-10 Effect of phosphorus content on strength and strain at fracture [32]

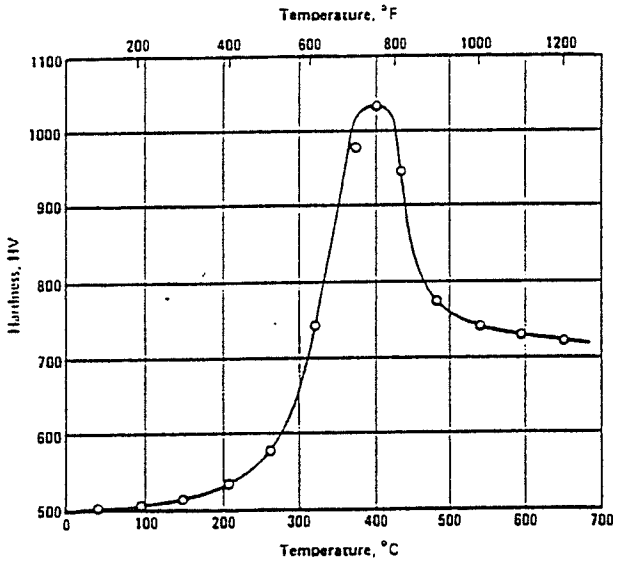


Fig.2-11 Effect of heat treatment at different temperatures on the hardness of 10.5% phosphorus electroless nickel coating [32]

One of the important advantages using electroless nickel coatings is their corrosion-resistance. Because of its amorphous nature and passivity, the corrosion resistance of the coating is excellent and , in many environments, superior to that of pure nickel or chromium alloys. Most deposits are naturally passive and very resistant to attack in most environments. Their degree of the passivity and corrosion resistance, however, is greatly affected by their phosphorus content. Alloys containing more than 10% phosphorus are more resistant to attack than those with lower phosphorous contents. As the nickel-phosphorus deposits are heated to temperatures above 220° C, the nickel phosphide particles begin to form, reducing the phosphorus content of the remaining material. This reduces the corrosion-resistance of the coatings. The particles also create small active/passive corrosion cells, further contributing to the destruction of the deposits. The deposits also shrink as they harden, which can crack the coatings and expose the substrate to attack.

Hardness and wear resistance are also important advantages of using the electroless nickel coatings. As deposited, the microhardness of the electroless nickel coatings is about 500 to 600 HV, around 48-52 HRC. Heat treatment causes these alloys to age-harden and can produce hardness values as high as 1100 HV, which are equal to that of most commercial hard chromium coatings (Fig.2-11). Because of their high hardness, electroless nickel coatings have excellent resistance to wear and abrasion, both in the as-deposited and hardened conditions. The hardness of EN coatings is due primarily to the precipitation of nickel phosphite particles within the alloy. At temperatures above 246°C, coherent and then distinct $Ni_3P$ particles begin to form, and at temperatures of 329°C to 346°C the glass begins to crystallize. Maximum hardening is obtained through treatments at 385°C [35]. Table 2-1 lists the typical properties of the electroless nickel deposits.

**Table 2-1 Typical properties of Functional Electroless Nickel Deposits [33]**

| | |
|---|---|
| Material | 10 to 13 phosphorus dissolved in Nickel |
| Structure | Amorphous; no crystal or phase structure, lamination or segregation |
| Density | 7.70 to 7.75 gmicc |
| Melting point | 875 to 890 C |
| Electrical resistivity | 75 to 90 μΩ-cm |
| Thermal conductivity | 0.01 cal/cm.sec.C |
| Magnetic coercity | Non-magnetic |
| Tensile strength | Greater than 100,000 psi |
| Ductility | 4 to 6% elongation |
| Modulus of Elasticity | 25 to 28 x $10^6$ psi |
| Adhesion strength | 40 to 60,000 psi |
| Hardness | 45 to 48 RCH as deposited heat treatable to 69 RCH |
| Wear resistance | 10 to 20 mg/1000 cycles TWI, as deposited; 2 to 3 mg/1000 cycles after heat treatment |
| Corrosion resistance | Resists attack by most organic and inorganic environments |

### 2.2.4 THE WEAR CHARACTERISTICS OF THE ELECTROLESS NI-P COATINGS

The Taber Wear Index (1000 gm CS10) of deposited coatings is about 15-20mg/1000 cycles. This is significantly better than conventional metals like steel or aluminum. After heat treatment, wear can be reduced to 2-3 mg/1000 cycles, which is similar to the results obtained with hard chrome. Both heat-treated and non-heat treated coatings are thus commonly used to minimize the effect of erosion abrasion and wear [35].

Under dry wear conditions, heating up of low friction surfaces is minimized. As a result, these coating surfaces are less subject to scoring, galling, or scuffing. Because of its high phosphorus content, the electroless nickel deposits have a low coefficient of friction, typically 0.13 to 0.14.

The wear of the electroless nickel-phosphorus coatings before 1980 has been summarized by Gawrilov in his book **Chemical (electroless) Nickel-Plating** [34]. Campbell's work [44] has shown the results that a coating of 25μm thickness is removed completely in the course of 9.0hr

with an average speed of wear of 2.8 μm/h. This is lower than observed with low carbon steel and carbon steel alloyed with nickel.

Gostin [45] reported information about the resistance to wear of nickel-phosphorus layers obtained by tests under the conditions of dry friction and use of a pin (hardness 60 RC)-on-disc method. The results gave the resistance to wear of the nickel-phosphorus coating as equivalent to that of hardened steel, and 10 times better than that of unhardened steel.

Randin and Hintermann [46] examined the influence of phosphorus contents in the coating on the wear value at dry friction. The greatest wear was established in the state of deposition at a phosphorus content of about 7%. With increasing hardening temperature, the wear lessened at this phosphorus content. At hardening around 400°C and above, wear lessened with increasing phosphorus content, while at lower temperatures wear at first increased with increasing phosphorus content, and then, above 7%, it decreased again.

Wiegand and co-workers [47] indicated that a connection between hardness and abrasion cannot be established for conditions of wear by furrowing or by lapping. This is also obtained by Parker [37], who investigated the heat treatment effect on properties of the electroless nickel deposits. Parker stated that hardness and wear resistance are not synonymous and sometimes a softer coating will provide longer wear life. With metal-to-metal contact, the hardness of the contacting metals must be taken into consideration when the deposit is heat treated. Nickel coatings containing 11.5 percent P and heat treated to 750 VHN (5 Hr at 600°C) had better wear resistance under a rotating steel ball (RC 62) than deposits with a lower phosphorus content.

Parker indicated that heating electroless nickel deposits above 200°C produces structural changes. Between 300 and 375°C, a crystalline mixture of nickel and nickel phosphide ($Ni_3P$) is formed. At a phosphorus content of 11 percent, there exists a eutectic mixture of Ni and $Ni_3P$ phases with a

melting point of 880°C. Above 400°C, re-crystallization and grain growth occur. As the crystals increase in size, the hardness of the deposit decreases gradually. When heated at more than 600°C when deposit plated on steel, the nickel diffuses into the steel substrate and the iron into the nickel coating. The intermetallic Ni-Fe diffusion zone thickens slowly with annealing time.

The abrasion resistance (dry friction), as measured using a Teledyne Taber Abraser with CS-10 wheels, increases with the temperature of heat treatment. Under a relatively light load, the abrasion resistance increases with the size of the nickel grains. The deposit will tolerate high loads, but not point or shock loading. The friction coefficient of electroless nickel vs. quenched, annealed steel varies only slightly with the phosphorus content or heat treatment temperature. The cavitation resistance of autocatalytic nickel deposits is best after a 200°C heat treatment or after a 525 to 650°C heat treatment to less than 900 VHN.

The strongest bond on steel is attained by annealing at 600 to 700°C to produce an intermetallic diffusion layer. The high temperature also improves the corrosion resistance of the deposit. On stainless steel, heat treating at 200°C is mandatory to increase the adhesion of the deposit.

Ma and Gawne [48], using the Falex apparatus, studied the effect of counter face materials on the wear of electroless nickel-phosphorus coatings. The coated pin was run against the two V-blocks for a 30-second running-in period with a 13.5 kg load; the load was then increased to 22.5kg for the remainder of the test. The wear behavior of the electroless nickel against itself, plain carbon steel, stainless steel and electrodeposited chromium under dry, sliding contact has been investigated. They concluded that the wear of electroless nickel in metal-metal sliding contact is dependent upon the nature of the counterface material. Catastrophic adhesive wear was incurred when electroless nickel in the as-deposited state was against all the counterfaces, with the exception of electrodeposited chromium. But the chromium counterface still gave rise to significant adhesive transfer and intermediate wear rate. Adhesive transfer of nickel to the

chromium counterface was evident from the SEM observations. Heat treatment eliminated catastrophic adhesive wear of electroless nickel against all counterfaces except stainless steel, which consistently gave rise to the most severe wear. This severe to mild wear-transition on heat treatment has been attributed to the formation of nickel phosphide and crystalline nickel, which are expected to exhibit high interfacial free energies and correspondingly less adhesive wear, relative to the amorphous nickel in the as-deposited coating. The lowest wear rates were obtained when both contacting surfaces were heat treated electroless nickel.

Yu and Zhang [49], studied the friction and wear behavior of the electroless Ni-P coatings by using pin-on-block reciprocating movement under dry condition. They also studied the heat treatment effect on the wear of electroless Ni-P coatings. They reported that the bonding strength of the coatings with 14.4 wt% P was higher than that of the corresponding coatings with 9.4 wt% P. Bonding strength reaches the maximum value when the heat treatment temperature reached 600°C. At this temperature, the microhardness of the coatings is not the highest. This may be due to stronger diffusion between the coating and the substrate and may form an interface diffusion layer, consequently increasing the bonding strength of the coatings considerably. The hardness is not the sole factor affecting the wear behavior of the coating, especially after the coating has undergone heat treatment at a higher temperature (above 400°C). The microstructure, the bonding strength and the brittleness of the coatings may become the dominant factors determining the friction and wear behavior of the coatings. The brittleness of the electroless Ni-P coating is obviously increased by heat treatment at higher temperatures (above 400°C). Severe adhesion and scuffing occurred on the worn surface of the bare substrate. The adhesion and scuffing apparently abated on the worn surfaces of the coated specimens, especially on those of the coated specimens heat treated above 400°C. After being heat treated at 400°C, more vertical fractures appeared on the worn surfaces of the coating containing 9.4 wt%P. The hardness of the coating reaches its highest value. The brittleness of the coatings also increases to its maximum hardness point. After 600°C, the hardness of the coatings is obviously not at its highest value, but the brittleness of the

coating is also not at its highest value. Heat treatment at a temperature higher than 400°C results in an interface diffusion between the coating and the substrate, and increases the bonding strength of the coatings. Consequently it improves the wear behavior of the coatings. Heat treatment has little effect on the frictional coefficient.

The resistance against wear of the electroless nickel-phosphorus coatings can be explained not only by their high values of hardness, but also by the fact that the phosphides present in the coating material decrease the coefficient of sliding friction [34].

Li and Tandon [50] evaluated the wear performance and mechanisms of heat-treated electroless nickel-phosphorus coating under reciprocating sliding conditions using the pin-on-block testing method. The results show that the weight loss of the coating increased with the load and sliding cycles during the dry wear tests. Under the lubricated conditions, wear of the coatings was drastically reduced and the weight loss of coating reached a stable stage after a certain number of sliding cycles. The mechanisms of wear of the coating follow the sequence of abrasive wear, adhesive wear, redeposition/redetachment of debris. Adhesion has been eliminated under the lubrication condition.

### 2.2.5 THE APPLICATIONS OF ELECTROLESS NICKEL-PHOSPHORUS COATINGS

Electroless nickel-phosphorus coatings are being used in many industries. The purposes of using electroless nickel coatings can be due to (1) corrosion resistance, (2) wear resistance (c) lubricity, (4) solderability or (5) buildup of worn or over-machined surfaces. Table 2 summarizes the most applications in different industries.

**Table 2-2 Applications of Functional Electroless Nickel Deposits[33]**

| | |
|---|---|
| Chemical Process industry | Vales, tanks, mixing equipment, turbines, heat exchange equipment, screens, pumps, extruders, compressor blades, pellitizers |
| Medical Industry | Scissors, suture needles, clamps, forceps, hypodermic needle hubs |
| Pharmaceutical Industry | extruders, sizing screens, pill sorters, filling equipment |
| Aerospace Industry | engine components, airframe and landing gear pieces, refueling systems, hydraulic cylinders and servos, fuel tanks, mirrors |
| Textile Industry | cylinders and rolls, thread guides, fiber feeds, fabric knives, bobbins, shuttles, rapiers, ratchets, knitting needles and picks |
| Printing Industry | cylinders and rolls, shafts, bearing blocks |
| Electronics Industry | Headers, coaxial connectors, housings and cases, heat sinks, diode cans, wave guides |
| Computer Industry | clutches and drives, shutters, interlocks, memory discs and drums |
| Food Industry | packaging and handling equipment, canning machinery, molds and grills, bun warmers, baking pans, friers |
| Petroleum Industry | valves, chokes, pipe swivels, downhole tools, packers, bridges, BOP's, mandrels, brake reels, hydraulic components, mud pumps, downhole pumps |
| Salvage Industry | buildup and repair of worn or mismachined components |
| Molding Industry | molds and dies for plastics, zinc die casting, glass and some rubbers |

## 2.3 THE SCOPE OF THE PRESENT RESEARCH

Although a significant amount of research work has been done on the wear characteristics of electroless Ni-P coatings and the effect of environmental temperature on the wear of materials has also been studied on several materials, there seems to be little research on how the environmental temperature affects the wear of the electroless nickel coatings. As mentioned before, the environmental temperature will promote chemical interactions between mating surfaces, and thus may alter the wear mechanisms. Since this coating is considered to be an alternative coating for locomotive diesel engine liners where hard chrome is a conventional coating material, it is important to study the effect of temperature on the wear characteristics of the EN coating under lubricated conditions.

The objective of the present research is, at first, to characterize the microstructure of the electroless nickel-phosphorus coatings on mild steel substrates. X-ray diffractometer, Transmission Electron Microscopy (TEM) and Scanning Electron Microanalyser (SEM) are to be used to analyze the microstructure of the as-deposited nickel-phosphorus coating and the coatings after different heat treatment conditions. Second, this research is to investigate how temperature affects the wear characteristics of electroless Ni-P coatings applied on a mild steel substrate under lubricated and dry reciprocating sliding conditions. Focus is on the lubricated sliding wear condition. In order to evaluate temperature effects on the wear characteristics of the nickel-phosphorus coatings at different load situations, two load conditions (low load at 4.0kg and high load at 8.0kg) is used. Reciprocating sliding frequency is fixed and total cycles is set at a constant value so that the effect of sliding frequency is eliminated in present study. A common motor engine oil is chosen as a lubricant. The wear mechanisms of the coatings under different temperatures with different load conditions, is investigated and analyzed using SEM and SEM/EDS in the present research.

# CHAPTER 3

# EXPERIMENTAL DETAILS

## 3.1 MATERIALS

The electroless nickel-phosphorus coatings were deposited on mild steel blocks by using a Shipley formula NIPOSIT Electroless Nickel NL-63. Specimens were supplied by Cadorath Plating Ltd. in Winnipeg. The as-received blocks with coatings had dimensions of 51x25.4x6.4 mm. The coating thickness measured was around 65μm on both sides of the mild steel block. The coating layer was very uniform. The phosphorus content analyzed by SEM/EDS was around 10-12 wt%. All coatings were deposited in the same bath. Table 3-1 gives the composition of coating and mild steel substrate obtained by SEM/EDS:

Table 3-1 The composition of coated blocks

| | Coating | | Mild steel | | |
|---|---|---|---|---|---|
| | Ni | P | Fe | Mn | Si |
| wt% | 88-90 | 10-12 | 98.62 | 0.99 | 0.39 |
| at% | 80-83 | 17-20 | 98.23 | 1.01 | 0.77 |

A bearing steel ball of 52100 with a diameter of 10mm was chosen as the counterface material in the tests. The structure of this bearing ball was tempered martensite. The hardness of the bearing steel ball was around HRC60.

## 3.2 SPECIMEN PREPARATION

The coatings on the mild steel blocks were in the as-deposited condition without any heat treatment. In order to obtain different coating conditions, heat treatments were performed on

some coated blocks. Specimens needing heat-treatment were vacuum-sealed in glass tubes and put into a furnace for heat treatment. Two heat treatment conditions were chosen: 400°C/1hr and 600°C/1hr. Table 3-2 lists the three conditions specimens were subjected to and used in this research project.

Table 3-2 Three different coating conditions

| | |
|---|---|
| 1 | As-deposited |
| 2 | As-deposited + 400°C, 1 hour air cool |
| 3 | As-deposited + 600°C , 1 hour air cool |

For the microhardness test of the coatings and the micrographic examination of coating condition on the mild steel, a small cross-section from samples of each coating conditions was cut off and mounted in bakelite. In order to reveal the structure of the coating layer, an 100% nitric acid was used as etchant to etch the specimens.

Thin foil specimens of the coatings for transmission electron microscope examination were cut using a spark cutting machine from the coating surface with thickness of 300μm. The cut foils were then mechanically polished on the cutting side, approaching to the coating surface. This ensured that the thin foils would be the Ni-P coating. The thin foils were mechanically polished to 150-200μm thickness, and punched into 3mm diameter disks. With the help of the disk-polishing tool, the 3mm disks were further polished on the #600 sand paper to 70~100μm, which was ready for twin-jet electrolyte polishing. The electrolytic for twin jet polishing consisted of 10% perchloric acid, 10% glycerol and 80% methanol and cooled to -40°C. Fig. 3-1 gives the schematic steps how the thin foil specimens were prepared.

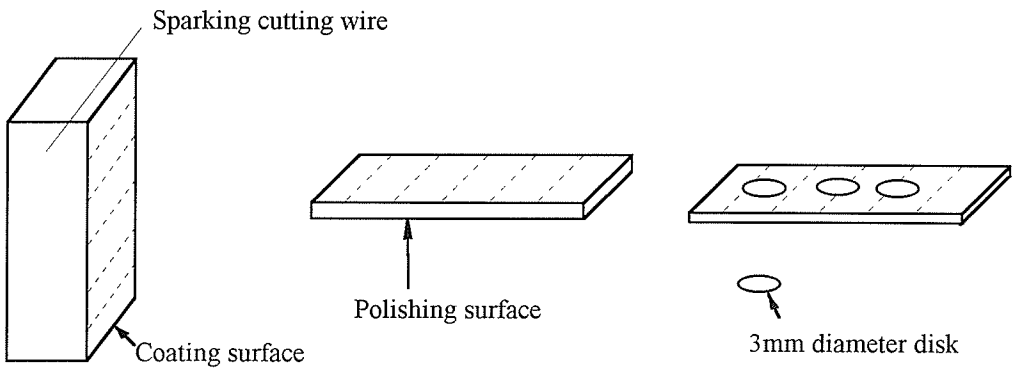


Fig. 3-1 Schematic description of thin foil preparation steps

## 3.3 MICROHARDNESS TEST

A Leitze microhardness tester was used to determine the hardness of the coatings. The load chosen was 200g. Tests were done on the etched cross-section samples and each coating conditions was tested at least three times to obtain an average hardness value.

## 3.4 X-RAY DIFFRACTION

An X-ray diffractometer was used to analyze the structure of the coatings on the mild steel in different heat treatment conditions. After a slight modification of the clamp in the Rigaku D/Max-2200 X-ray diffractometer, big block specimens could be clamped on the sample stage directly. The x-ray diffraction data were directly collected and analyzed by the computer.

## 3.5 WEAR TEST

All wear tests were conducted using a ball-on-block reciprocating configuration, schematically shown in Fig.3-2. The wear test rig was a custom-fabricated to perform the reciprocating sliding,

and schematically shown in Fig.3-3 [8]. In this test rig, the stage was designed to be electrically-heated so that the specimens can be heated. In order to control the temperature of specimens, a thermocouple was placed in a small hole in the block. The temperature was controlled within a range of ± 5°C. The parameters used in the entire lubricated wear tests are listed in Table 3-3. All specimens and the balls were ultrasonically cleaned in ethanol/methanol before the wear test. Specimens were cleaned again after tests in an oil detergent and ultrasonic cleaning for the weight loss measurement and for scanning electron microscopy examination.

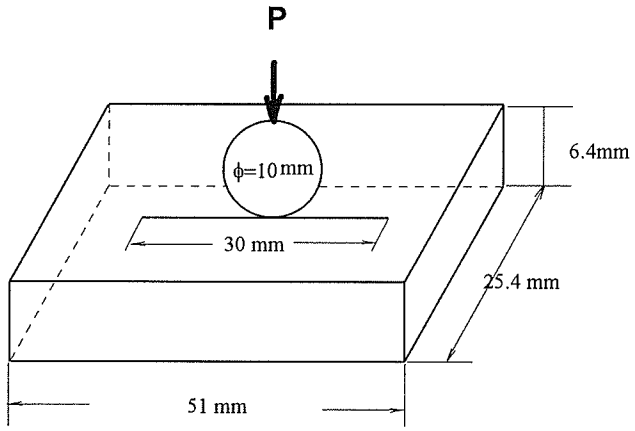


**Fig.3-2 Schematic diagram of the reciprocating ball-on-block wear test**

Table 3-3 Wear testing parameters

| Test parameters | Value |
|---|---|
| Temperature | room temperature (25°C), 50°C, 100°C |
| Load | 4kg, 8 kg |
| Lubrication | Nugold 10W30, supplied at a rate of 5ml/1hr |
| Reciprocating frequency | 160/min |
| Total cycles | 100,000 |
| Length of track | 30 mm |
| Humidity | 45% |
| Atmosphere | Laboratory air |

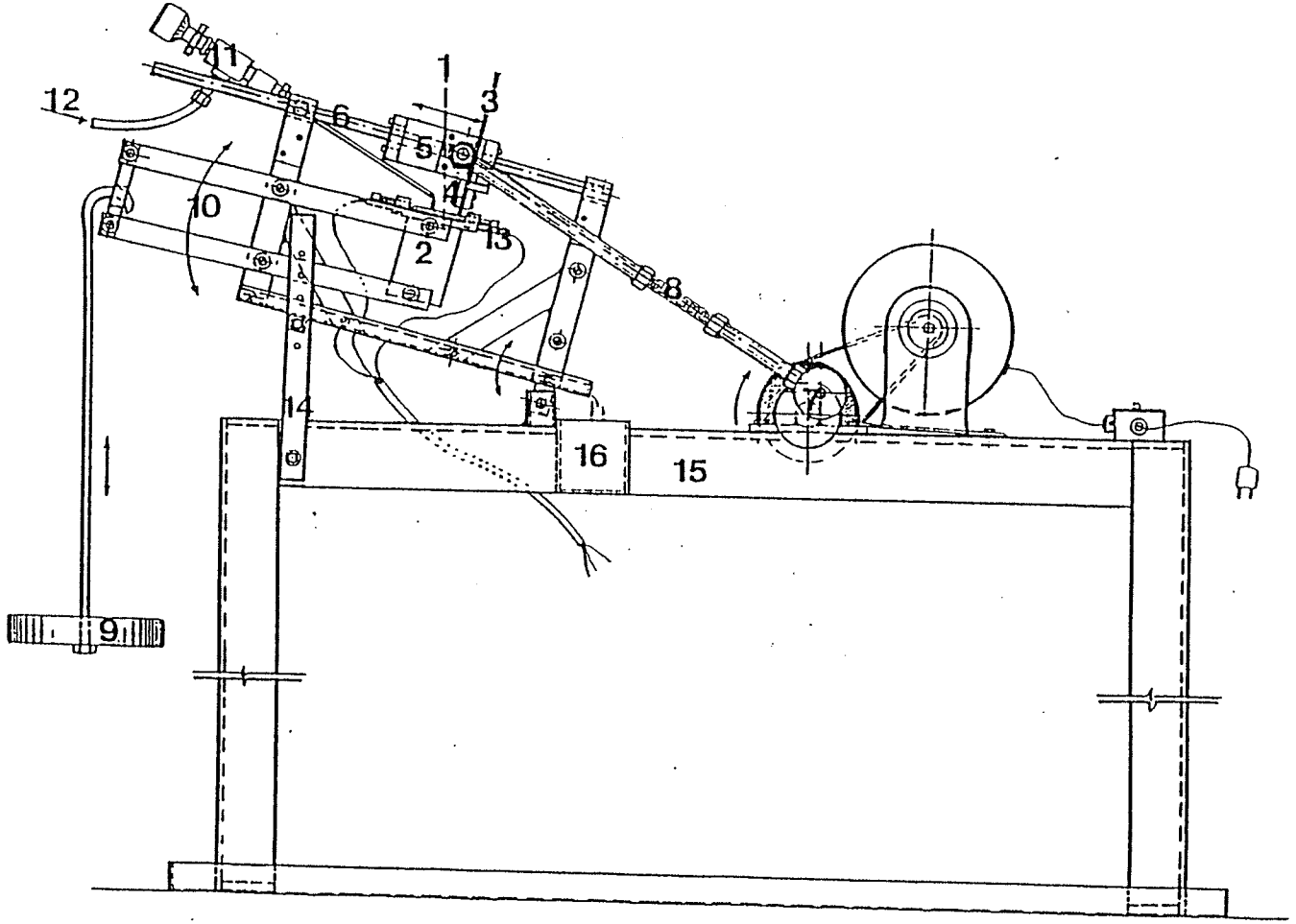


Fig. 3-3 Wear test rig [8]

The dry wear tests were conducted on two kinds of coatings: as-deposited and as-deposited with 600°C/1hr heat treatment. The parameters for the dry wear tests are listed in Table 3-4 as reference.

Table 3-4 Dry wear testing parameters

| Test parameters | Value |
|---|---|
| Temperature | room temperature (25°C), 50°C, 100°C |
| Load | 4kg |
| Reciprocating frequency | 160/min |
| Total cycles | 500 |
| Length of track | 30 mm |
| Humidity | 45% |
| Atmosphere | Laboratory air |

## 3.6 WEIGHT LOSS MEASUREMENT

Weight loss method was used in this research to quantitatively determine the wear under different testing conditions. The specimens were cleaned before and after the wear test and weighed on an electronic scale (Fisher Meter H18) with readability of 0.1mg.

## 3.7 TEM, SEM AND SEM/EDS ANALYSIS

The microstructure of the coatings was analyzed by using transmission electron microscopy. High magnification image and the crystal structure of the coatings can be determined by using TEM. The model of the TEM used in this research was JEOX JEM-2000FX electron microscope.

Wear track morphology was analyzed using a JEOX JXA-840 scanning electron microanalyzer. Scanning electron microscopy gives a very clear surface image so that the wear mechanisms can

be determined by observing the morphology of the wear track. SEM can also reveal the failure mode of the coatings after the sliding wear.

Energy dispersive spectrometry X-ray analysis was used to investigate material transfer from the coating to the mating ball or from the ball to the coating. The element distribution on the wear track was determined by using X-ray mapping.

# CHAPTER 4

# EXPERIMENTAL RESULTS

## 4.1 MICROSTRUCTURAL CHARACTERISTICS OF THE ELECTRO-LESS NICKEL-PHOSPHORUS COATINGS

### 4.1.1 SEM MORPHOLOGY OF THE NI-P COATINGS.

The as-deposited electroless nickel-phosphorus coating as seen in a SEM on the mild steel was very uniform. The surface roughness measured by a roughness meter was around Ra=1.5μm (Fig.4-1). The cross-section of the coating on the mild steel before and after heat-treatments is shown in Fig.4-2a, b, c. The as-deposited coating shows the layer structure with vertical grooves (Fig.4-2a). The coating after 400°C/1h heat treatment shows very uniform structure without those vertical grooves (Fig.4-2b). The coating layer can still be seen from the Fig.4-2b. The coating after 600°C/1h heat treatment shows a diffusion layer between the coating and substrate (Fig.4-2c). The structure of the coating is composed of the very tiny precipitates of nickel phosphides and Ni crystallites. SEM, however, cannot display the microstructure of the coatings due to the very small size of precipitates of nickel phosphides and Ni crystallites. Therefore, the transmission electron microscope was used to analyze the microstructure of the coatings.

### 4.1.2 TEM MORPHOLOGY OF THE NI-P COATINGS

The previous studies indicated that the microstructure of the electroless Ni-P coatings varied with the content of the phosphorus. The amorphous structure appears when the phosphorus content is higher than 10 wt%. TEM analysis of the Ni-P coatings on the mild structure has been carried out to characterize the structure of the electroless Ni-P coatings in this study.

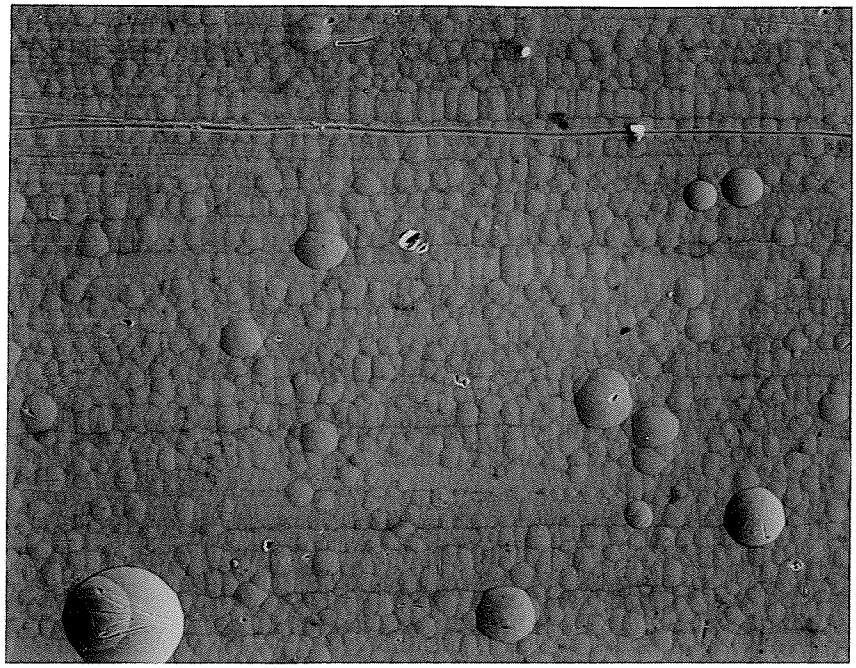


Fig.4-1 SEM morphology of the coating surface

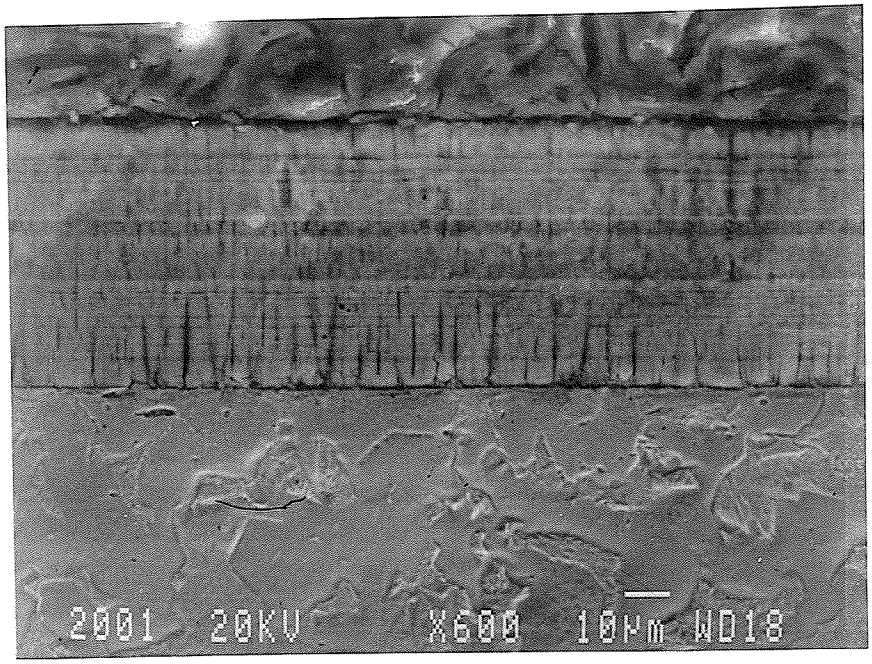


Fig.4-2a The cross-section of the as-deposited electroless nickel coating on the mild steel

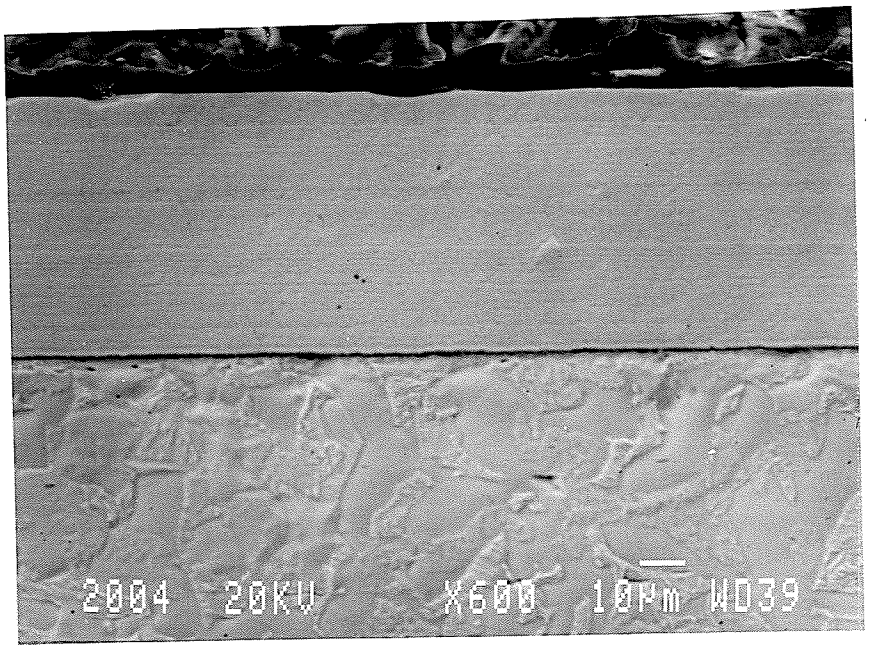


Fig.4-2b The cross-section of the electroless nickel-phosphorus coating with 400°C/1hr heat treatment

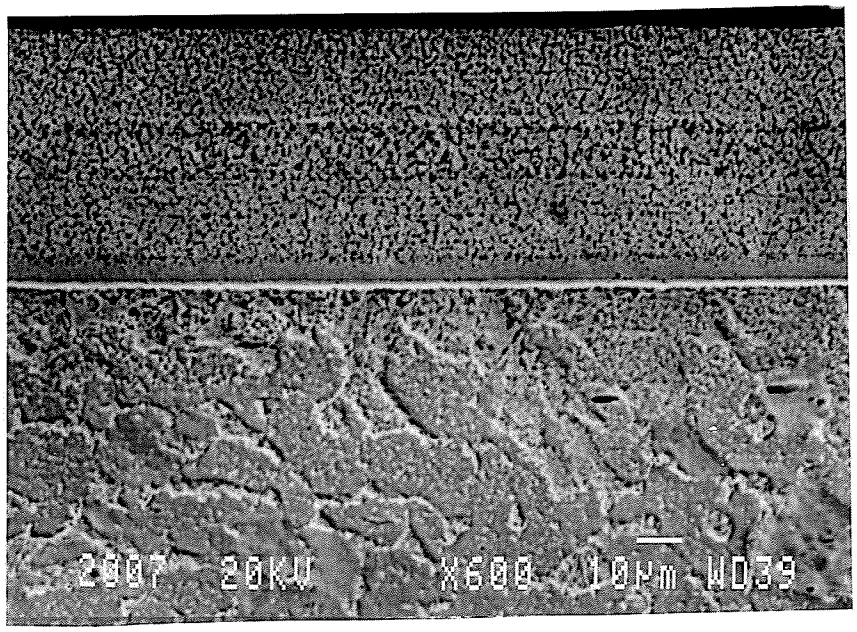


Fig.4-2c The cross-section of the electroless nickel-phosphorus coating with 600°C/1hr heat treatment

Fig. 4-3 shows the TEM morphology of as-deposited Ni-P coating. The coating is composed of very small nickel crystallites included in the amorphous structure. The nickel crystallite size is less than 25nm. Selected area diffraction pattern (SADP) of the coating gives the amorphous ring pattern with nickel ring form (Fig.4-4a), indicating the major part of the coating is an amorphous phase. The SADP from the place with more nickel particles gives the nickel crystallites ring pattern (Fig.4-4b).

The coating after 400°C/1h heat treatment, is subjected to a phase transformation. The amorphous phase in as-deposited coating crystallizes into $Ni_3P$ precipitates, and the nickel crystallites grow in size (Fig.4-5). It should be noted that the particles in Fig.4-5 are those of nickel crystallites (A). The $Ni_3P$ precipitates are those in the background of the picture (B). The SADP in Fig.4-6 gives continuous spot rings originating from fine nickel particles and the spot pattern which have streaks from the $Ni_3P$ precipitates.

Table 4-1 gives the calculated ring radius and correspondent d values for Ni crystallites. The standard d values and reflecting planes of the nickel crystal is also list in Table 4-1 for comparison. The calculated lattice parameter "a" for Ni in this coating is 3.49Å. This value is very close to the standard one of 3.5238Å.

Table 4-1 The experimental and calculated data of the nickel ring pattern

| Radius | d value (calculated) | d value (standard) | Reflecting plane | a (calculated) | a (average) |
|---|---|---|---|---|---|
| 0.61 | 2.049 | 2.034 | 1 1 1 | 3.55 | |
| 0.7 | 1.786 | 1.762 | 2 0 0 | 3.57 | |
| 1.0 | 1.250 | 1.246 | 2 2 0 | 3.54 | 3.49 |
| 1.175 | 1.064 | 1.062 | 3 1 1 | 3.53 | |
| 1.25 | 1.000 | 1.017 | 2 2 2 | 3.46 | |
| 1.5 | 0.833 | 0.881 | 4 0 0 | 3.33 | |
| 1.575 | 0.794 | 0.808 | 3 3 1 | 3.46 | |

*$\lambda$=0.025Å at V=200KV and camera length is 50cm

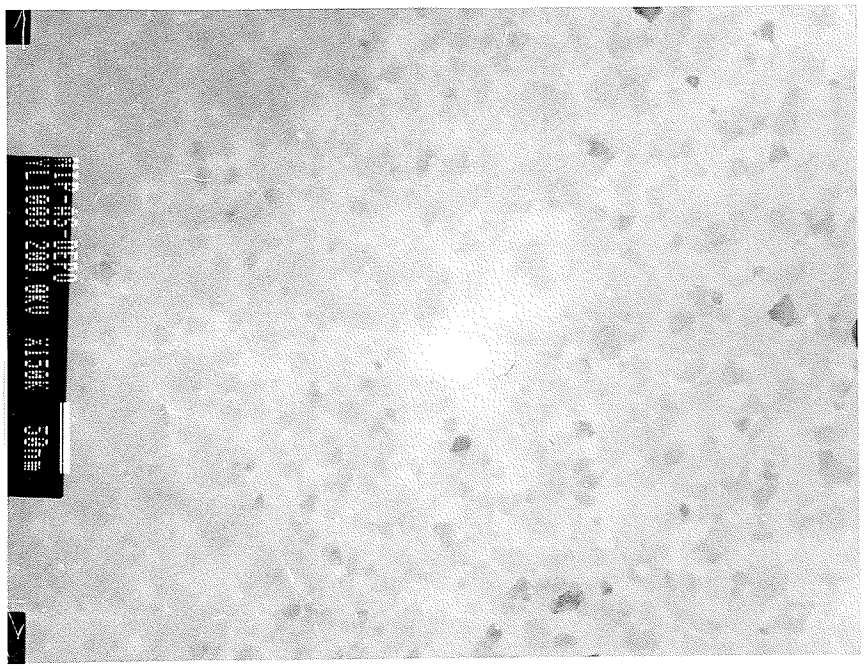

Fig.4-3 TEM bright field image of the as-deposited electroless Ni-P coating

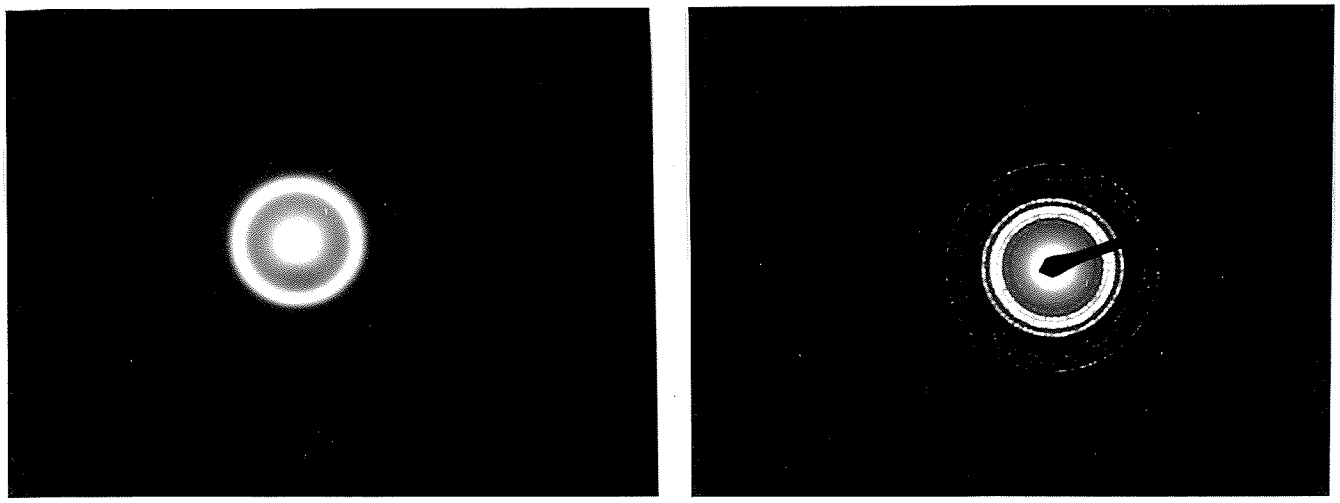

Fig.4-4 Selected area diffraction pattern of the as-deposited Ni-P coating
a. area with amorphous; b. area with nickel crystallites

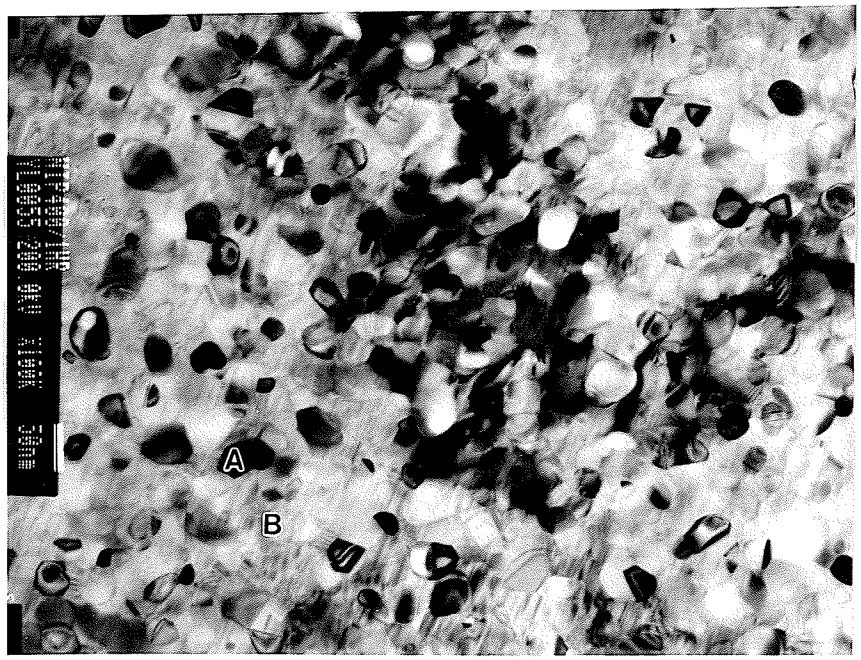


Fig.4-5 TEM bright field image of the 400°C/1hr
heat treated electroless Ni-P coating

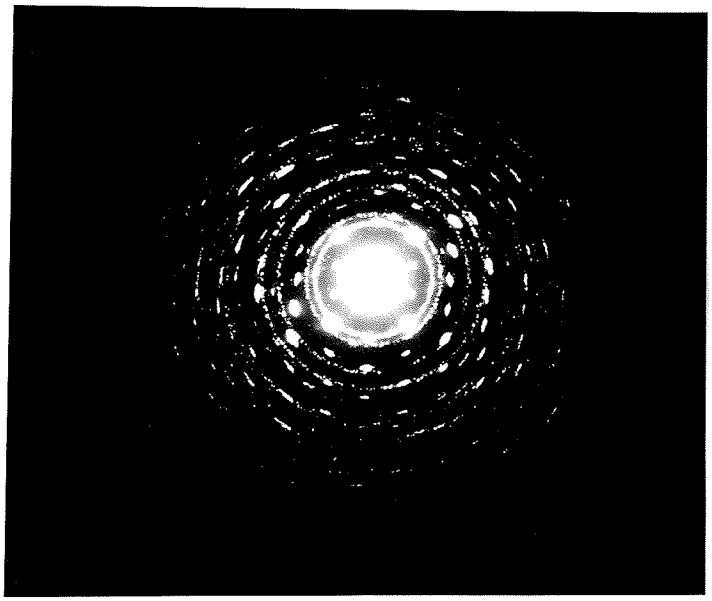

Fig.4-6 Selected area diffraction pattern from the 400°C/1hr heated treated coating

Fig.4-7 shows the microstructure of Ni-P coating after a 600°C/1hr heat treatment. The nickel crystallites have grown after this high temperature heat treatment. The $Ni_3P$ precipitates also grew in size. The $Ni_3P$ precipitates have various shapes and sizes but most of them are irregular (A). The nickel crystallites, on the other hand, are more regularly shaped (B) with distinguished corners. It is noted that there are plenty of twin boundaries in the nickel crystallites as the arrow C indicates in the picture. It is also seen from Fig.4-7 that the boundary between the $Ni_3P$ particles is not smooth like the one between the nickel particles. Dislocations or some precipitates may exist in these grain boundaries.

The SADF pattern obtained from the dark area (A) in Fig.4-7 is given in Fig.4-8. This gives the tetragonal $Ni_3P$ structure at zone axis of [011]. The index of the Ni and $Ni_3P$ from the 600°C/1h heat treated coating are given in Fig.4-9 and Fig.4-10.

## 4.2 X-RAY DIFFRACTION OF THE NICKEL-PHOSPHORUS COATINGS

The x-ray diffraction pattern of as-deposited Ni-P coating is given in Fig.4-11. It shows the typical amorphous diffraction with strong FCC nickel (111) preferred orientation reflection. The x-ray diffraction of the coating after 400°C/1hr heat treatment gives the obvious crystalline peaks (Fig.4-12). The same XRD was obtained from 600°C/1hr heat treated coating (Fig.4-13) except the intensity of the peaks is stronger than that in 400°C/1hr heat treated coating. The x-ray diffractions give the strong nickel and $Ni_3P$ crystal diffraction peaks. It is noted that the intensity of the nickel peaks is stronger than those from $Ni_3P$ in both heat treated situations. The intensity of the $Ni_3P$ peaks does not increase too much while the intensity of nickel peaks increases significantly as the heat treatment temperature increases (Fig.4-14). This may indicate that there are more nickel crystallites than nickel phosphides in the coatings after crystallization. It has been observed from the TEM images that the size of nickel crystallites is much larger compared with

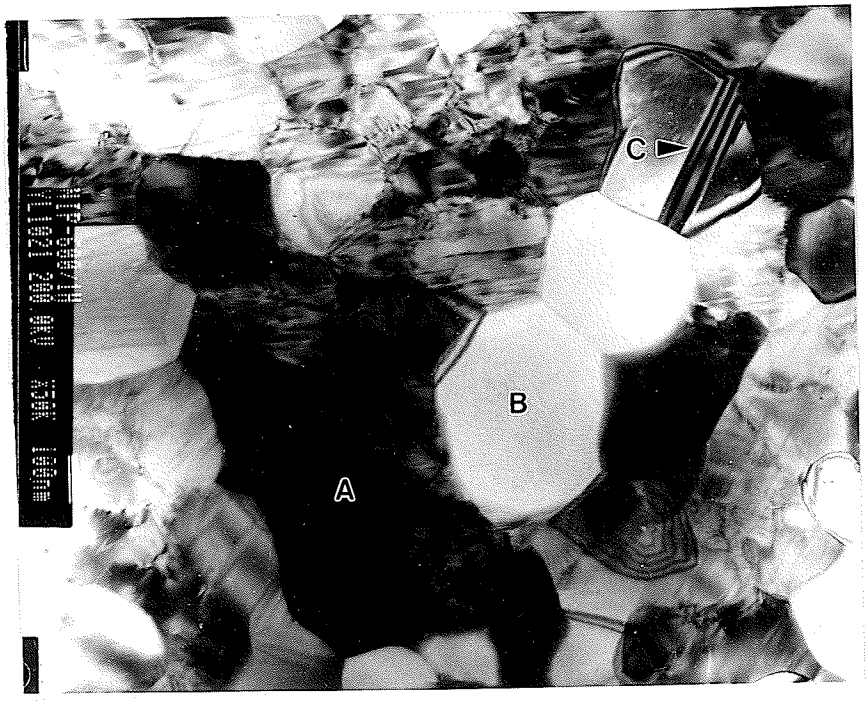


Fig.4-7 TEM bright field image of 600°C/1hr heat treated electroless Ni-P coating

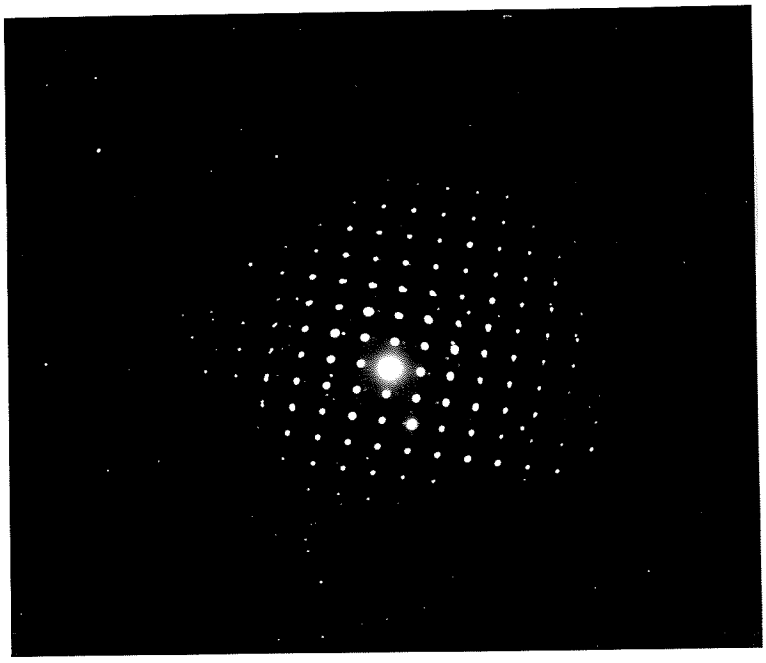

Fig.4-8 Selected area diffraction pattern from the 600°C/1hr heated treated coating

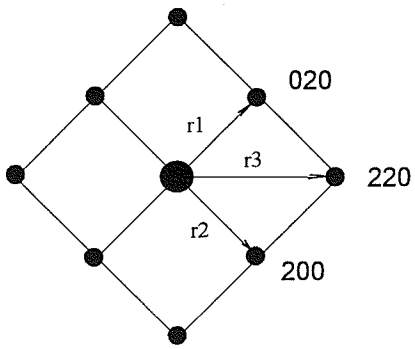


r1=r2
r3/r1=1.429
[001]

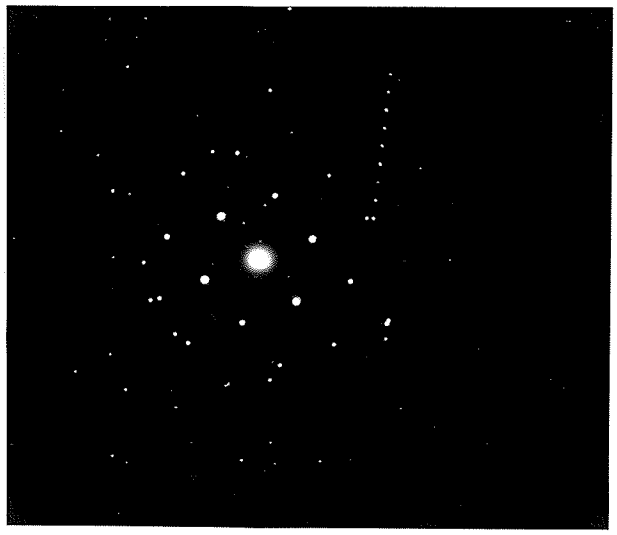

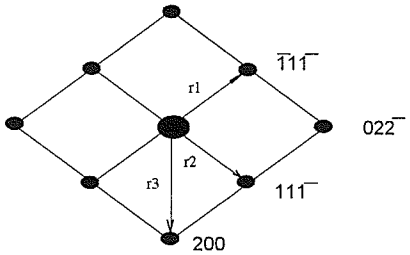


r1=r2
r3/r1=1.147
[011]

Fig.4-9 SADP of two zone axis from a nickel crystalline in 600°C/1hr HT Ni-P coating

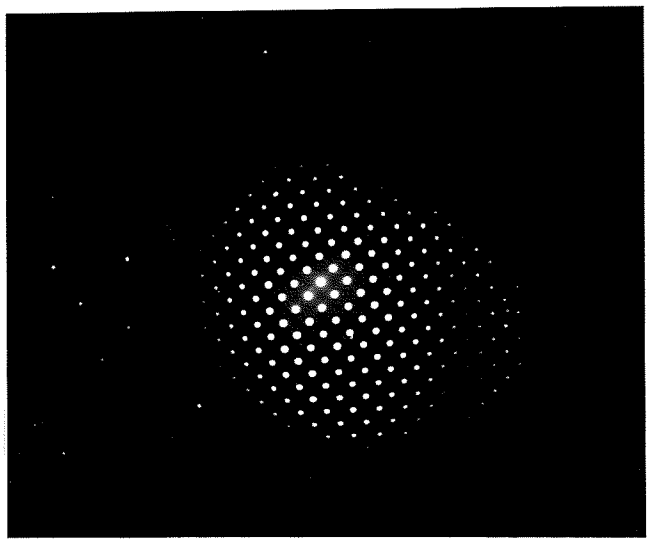

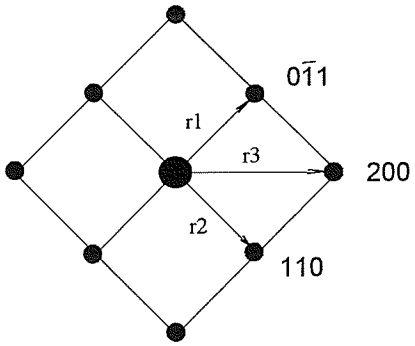


r1=r2
r3/r1=1.4

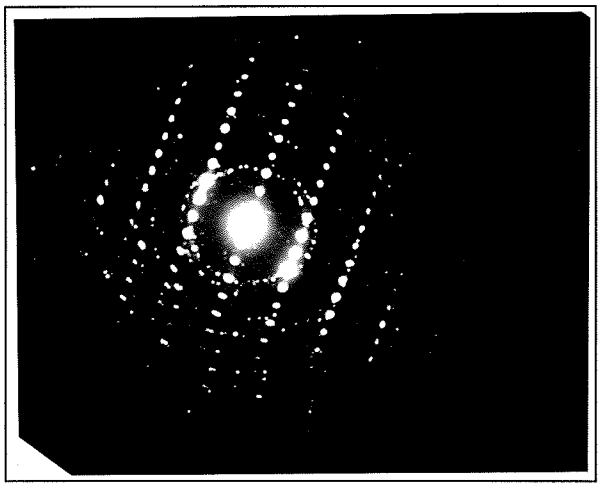

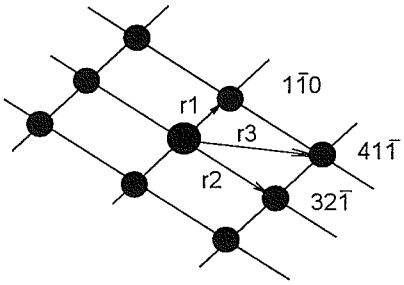


r2/r1=2.935
r2^r1=80 ‘’
[115]

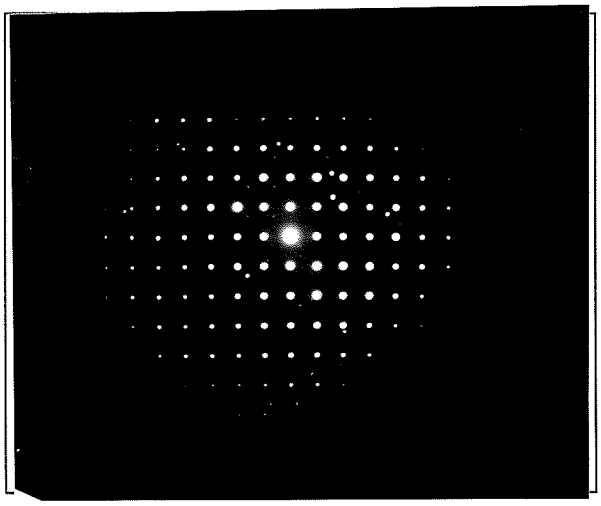

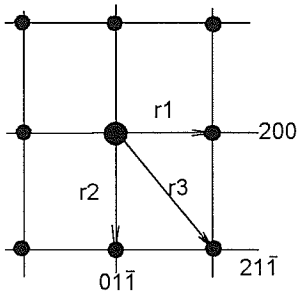


r2/r1=1.125
r3/r1=2.113
[011]

Fig.4-10 SADP of three zone axises from $Ni_3P$ precipitate in 600°C/1hr HT Ni-P coating

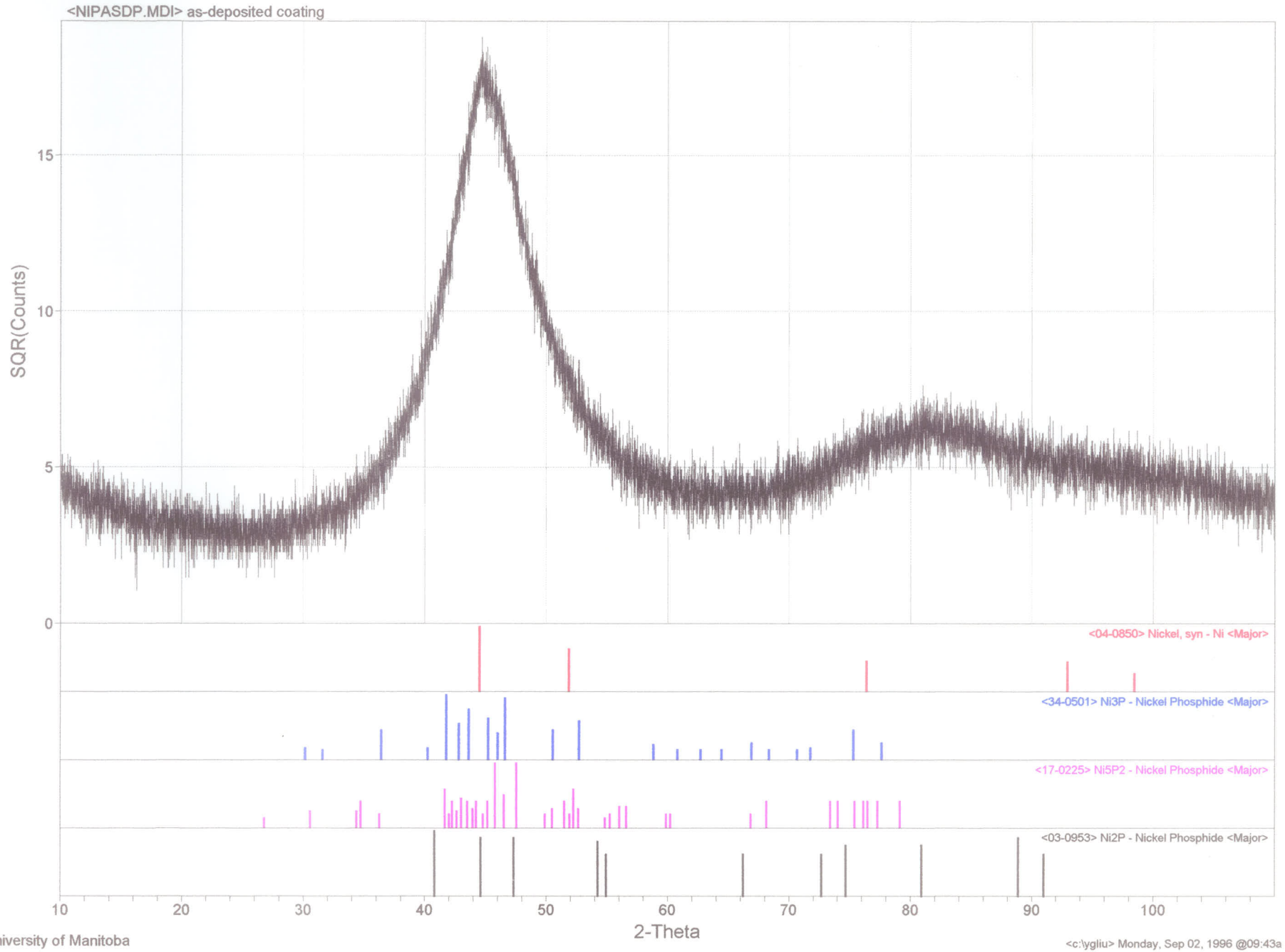
<NIPASDP.MDI> as-deposited coating
SQR(Counts)
15
10
5
0
<04-0850> Nickel, syn - Ni <Major>
<34-0501> Ni3P - Nickel Phosphide <Major>
<17-0225> Ni5P2 - Nickel Phosphide <Major>
<03-0953> Ni2P - Nickel Phosphide <Major>
10
20
30
40
50
60
70
80
90
100
2-Theta
University of Manitoba
<c:\ygliu> Monday, Sep 02, 1996 @09:43a

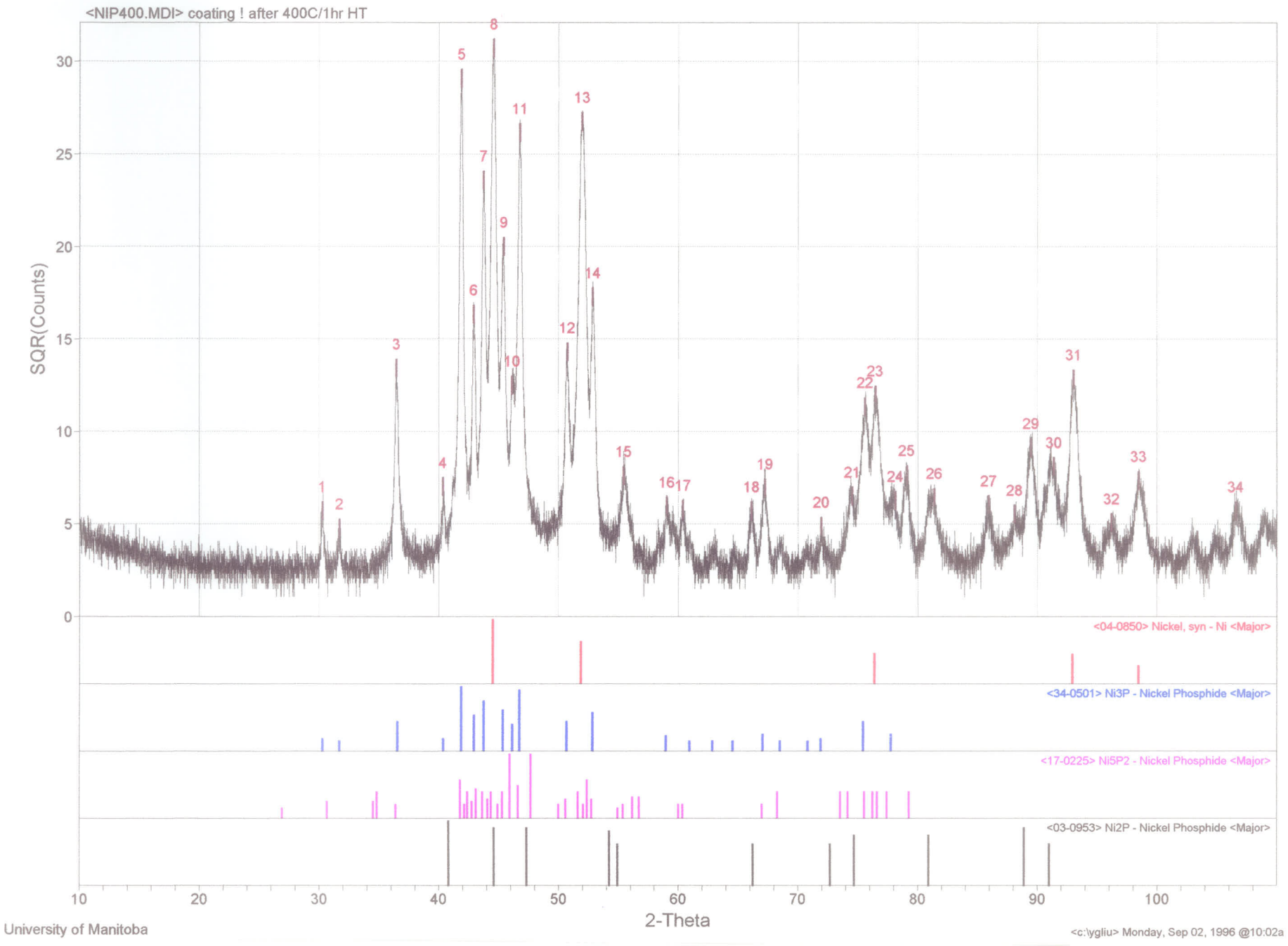


Fig. 4-12 X-ray diffraction of Ni-P coating after 400°C/1hr heat treatment

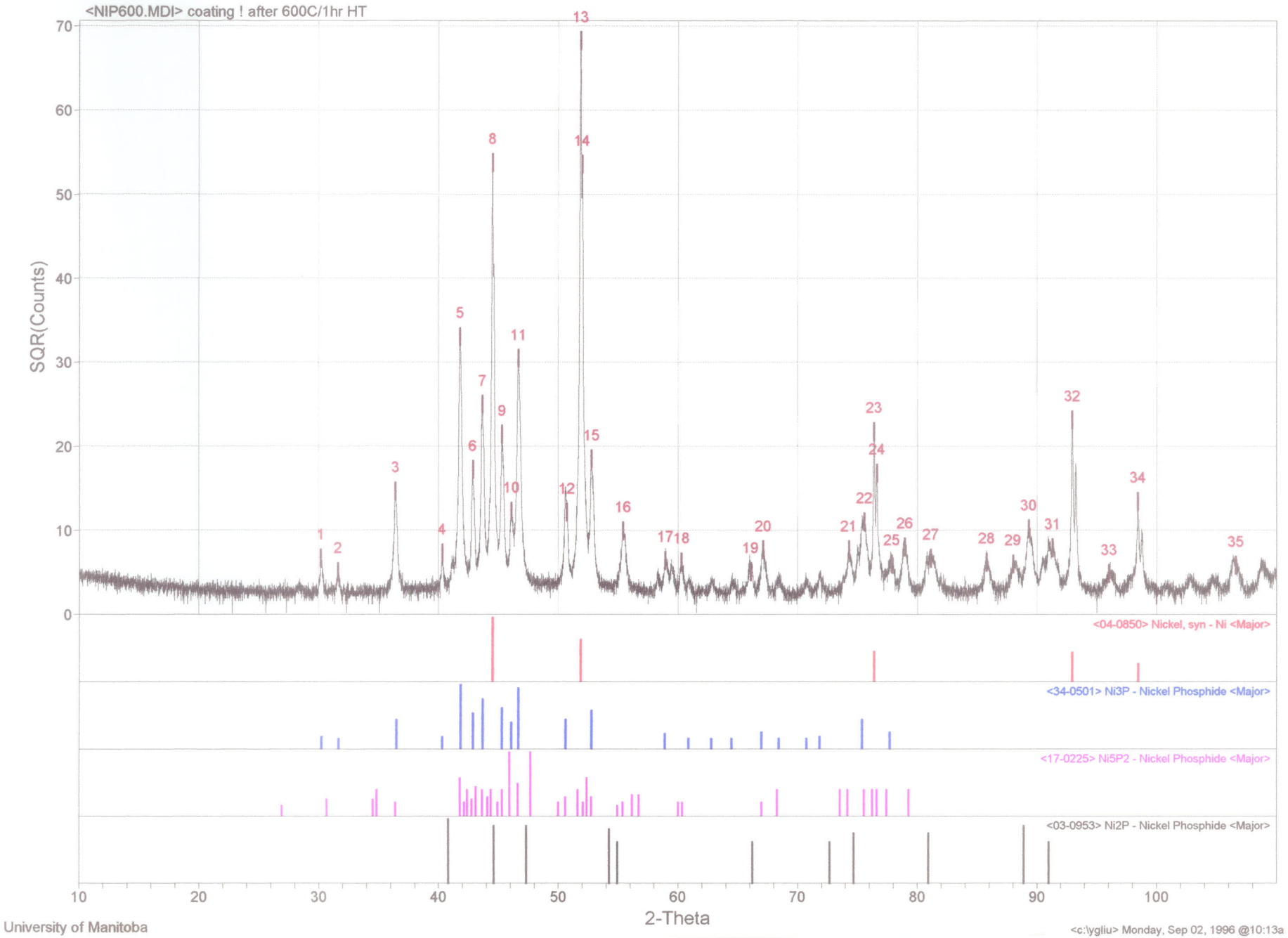


Fig. 4-13 X-ray diffraction of Ni-P coating after 600°C/1hr heat treatment

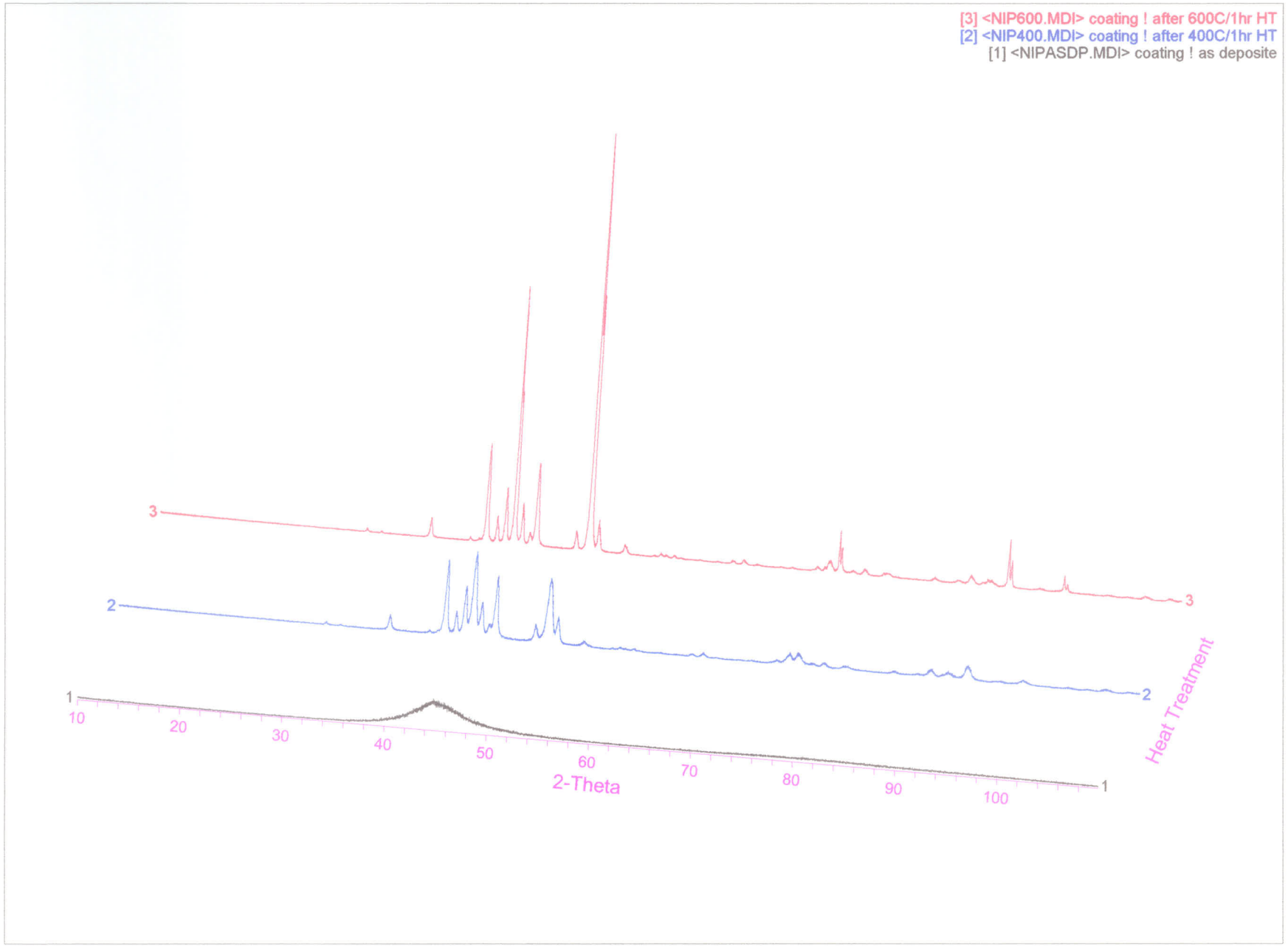


University of Manitoba

Fig. 4-14 X-ray diffraction patterns of three Ni-P coatings

<c:\ygliu> Monday, Sep 02, 1996 @10:34a

# Table 4-2 X-ray diffraction data of Ni-P coating after 400°C/1hr heat treatment

<NIP400.MDI> coating ! after 400C/1hr HT [JADE 3.0 - Peak ID Report]

Scan Parameters: Range = 10.0-109.99/0.01, Dwell = 0.12(sec), Max-I = 981, Anode = CU Date: 02-20-96@11:45

Search Parameters: Filter = 7(pts), Threshold = 0.5(esd), Peak-Cutoff = 4.0%, 2-Theta Zero Offset = 0.0(deg)

Note: Intensity data from raw counts, Centroid peak location, Wavelength for computing d-spacing = 1.540562<CU, K-alpha1>

| # | 2-Theta | d(A) | BG | Int | I% | Area | A% | FWHM | | Phase-ID | d(A) | I% | h | k | l | 2-Theta | Delta-2T | # |
|---|---|---|---|---|---|---|---|---|---|---|---|---|---|---|---|---|---|---|
| 1 | 30.274 | 2.9498 | 5 | 29 | 3.5 | 7 | 2.0 | 0.217 | <> | Ni3P | 2.9600 | 3 | 1 | 2 | 1 | 30.167 | -0.107 | 1 |
| 2 | 31.689 | 2.8213 | 5 | 19 | 2.3 | 3 | 0.9 | 0.142 | <> | Ni3P | 2.8300 | 2 | 1 | 3 | 0 | 31.589 | -0.100 | 2 |
| 3 | 36.450 | 2.4629 | 9 | 175 | 20.9 | 57 | 16.7 | 0.293 | <> | Ni3P | 2.4650 | 20 | 0 | 3 | 1 | 36.418 | -0.032 | 3 |
| 4 | 40.332 | 2.2344 | 15 | 36 | 4.3 | 1 | 0.3 | 0.025 | <> | Ni3P | 2.2390 | 3 | 0 | 4 | 0 | 40.245 | -0.087 | 4 |
| 5 | 41.880 | 2.1553 | 23 | 837 | 100.0 | 289 | 84.5 | 0.311 | <> | Ni5P2 | 2.1600 | 35 | 4 | 2 | 0 | 41.784 | -0.095 | 5 |
| 6 | 42.911 | 2.1059 | 61 | 212 | 25.3 | 53 | 15.5 | 0.225 | <> | Ni3P | 2.1100 | 30 | 3 | 3 | 0 | 42.823 | -0.089 | 6 |
| 7 | 43.711 | 2.0692 | 68 | 499 | 59.6 | 163 | 47.7 | 0.294 | <> | Ni3P | 2.0730 | 60 | 1 | 1 | 2 | 43.626 | -0.085 | 7 |
| 8 | 44.570 | 2.0313 | 167 | 791 | 94.5 | 308 | 90.1 | 0.350 | <> | Ni2P | 2.0300 | 80 | 2 | 0 | 1 | 44.599 | 0.029 | 8 |
| 9 | 45.407 | 1.9958 | 75 | 333 | 39.8 | 101 | 29.5 | 0.273 | <> | Ni5P2 | 2.0010 | 16 | 5 | 0 | 6 | 45.281 | -0.126 | 9 |
| 10 | 46.104 | 1.9672 | 108 | 52 | 6.2 | 8 | 2.3 | 0.138 | <> | Ni3P | 1.9710 | 16 | 2 | 0 | 2 | 46.009 | -0.095 | 10 |
| 11 | 46.759 | 1.9411 | 31 | 665 | 79.5 | 280 | 81.9 | 0.379 | <> | Ni5P2 | 1.9470 | 25 | 3 | 1 | 10 | 46.610 | -0.149 | 11 |
| 12 | 50.718 | 1.7985 | 21 | 188 | 22.5 | 82 | 24.0 | 0.393 | <> | Ni5P2 | 1.8030 | 8 | 4 | 3 | 4 | 50.583 | -0.136 | 12 |
| 13 | 51.940 | 1.7590 | 111 | 617 | 73.7 | 342 | 100.0 | 0.499 | <> | Nickel, syn | 1.7620 | 42 | 2 | 0 | 0 | 51.846 | -0.094 | 13 |
| 14 | 52.841 | 1.7311 | 21 | 284 | 33.9 | 122 | 35.7 | 0.387 | <> | Ni5P2 | 1.7340 | 8 | 2 | 1 | 13 | 52.747 | -0.094 | 14 |
| 15 | 55.440 | 1.6560 | 14 | 46 | 5.5 | 24 | 7.0 | 0.470 | <> | Ni5P2 | 1.6580 | 4 | 4 | 3 | 7 | 55.367 | -0.073 | 15 |
| 16 | 59.009 | 1.5640 | 11 | 26 | 3.1 | 8 | 2.3 | 0.277 | <> | Ni3P | 1.5680 | 5 | 0 | 4 | 2 | 58.846 | -0.163 | 16 |
| 17 | 60.378 | 1.5318 | 11 | 24 | 2.9 | 4 | 1.2 | 0.150 | <> | Ni5P2 | 1.5330 | 4 | 4 | 4 | 6 | 60.327 | -0.052 | 17 |
| 18 | 66.101 | 1.4124 | 8 | 26 | 3.1 | 10 | 2.9 | 0.346 | <> | Ni2P | 1.4100 | 40 | 3 | 1 | 0 | 66.227 | 0.126 | 18 |
| 19 | 67.238 | 1.3912 | 7 | 43 | 5.1 | 19 | 5.6 | 0.398 | <> | Ni5P2 | 1.3960 | 4 | 7 | 2 | 1 | 66.978 | -0.260 | 19 |
| 20 | 71.919 | 1.3118 | 8 | 17 | 2.0 | 2 | 0.6 | 0.106 | <> | Ni3P | 1.3140 | 3 | 0 | 3 | 3 | 71.777 | -0.142 | 20 |
| 21 | 74.518 | 1.2723 | 11 | 33 | 3.9 | 27 | 7.9 | 0.736 | <> | Ni2P | 1.2700 | 60 | 4 | 0 | 0 | 74.677 | 0.158 | 21 |
| 22 | 75.601 | 1.2568 | 28 | 104 | 12.4 | 68 | 19.9 | 0.588 | <> | Ni5P2 | 1.2580 | 16 | 5 | 5 | 6 | 75.513 | -0.088 | 22 |
| 23 | 76.449 | 1.2449 | 32 | 115 | 13.7 | 79 | 23.1 | 0.618 | <> | Nickel, syn | 1.2460 | 21 | 2 | 2 | 0 | 76.370 | -0.079 | 23 |
| 24 | 78.118 | 1.2224 | 29 | 12 | 1.4 | 1 | 0.3 | 0.075 | <> | | | | | | | | | 24 |
| 25 | 79.078 | 1.2100 | 13 | 48 | 5.7 | 25 | 7.3 | 0.469 | <> | Ni5P2 | 1.2080 | 16 | 6 | 4 | 8 | 79.234 | 0.156 | 25 |
| 26 | 81.370 | 1.1816 | 11 | 32 | 3.8 | 23 | 6.7 | 0.647 | <> | | | | | | | | | 26 |
| 27 | 85.915 | 1.1303 | 10 | 28 | 3.3 | 7 | 2.0 | 0.225 | <> | | | | | | | | | 27 |
| 28 | 88.080 | 1.1081 | 17 | 15 | 1.8 | 1 | 0.3 | 0.060 | <> | | | | | | | | | 28 |
| 29 | 89.469 | 1.0944 | 20 | 66 | 7.9 | 40 | 11.7 | 0.545 | <> | | | | | | | | | 29 |
| 30 | 91.376 | 1.0765 | 26 | 42 | 5.0 | 16 | 4.7 | 0.343 | <> | | | | | | | | | 30 |
| 31 | 93.010 | 1.0618 | 24 | 145 | 17.3 | 70 | 20.5 | 0.434 | <> | Nickel, syn | 1.0624 | 20 | 3 | 1 | 1 | 92.944 | -0.066 | 31 |
| 32 | 96.192 | 1.0350 | 7 | 20 | 2.4 | 13 | 3.8 | 0.585 | <> | | | | | | | | | 32 |
| 33 | 98.443 | 1.0172 | 13 | 43 | 5.1 | 30 | 8.8 | 0.628 | <> | Nickel, syn | 1.0172 | 7 | 2 | 2 | 2 | 98.446 | 0.003 | 33 |
| 34 | 106.552 | 0.9610 | 12 | 22 | 2.6 | 12 | 3.5 | 0.491 | <> | | | | | | | | | 34 |

@ End-of-List Average Delta 2-Theta = 0.103

> PDF#04-0850 ———— Nickel, syn - Ni

> PDF#34-0501 ———— Ni3P - Nickel Phosphide

> PDF#17-0225 ———— Ni5P2 - Nickel Phosphide

> PDF#03-0953 ———— Ni2P - Nickel Phosphide

# Table 4-3 X-ray diffraction data of Ni-P coating after 600°C/1hr heat treatment

<NIP600.MDI> coating ! after 600C/1hr HT [JADE 3.0 - Peak ID Report]

Scan Parameters: Range = 10.0-109.99/0.01, Dwell = 0.12(sec), Max-I = 4751, Anode = CU Date: 02-20-96@10:58

Search Parameters: Filter = 7(pts), Threshold = 0.5(esd), Peak-Cutoff = 4.0%, 2-Theta Zero Offset = 0.0(deg)

Note: Intensity data from raw counts, Centroid peak location, Wavelength for computing d-spacing = 1.540562<CU, K-alpha1>

| # | 2-Theta | d(A) | BG | Int | I% | Area | A% | FWHM | | Phase-ID | d(A) | I% | h | k | l | 2-Theta | Delta-2T | # |
|---|---|---|---|---|---|---|---|---|---|---|---|---|---|---|---|---|---|---|
| 1 | 30.175 | 2.9592 | 4 | 44 | 0.9 | 5 | 0.6 | 0.102 | <> | Ni3P | 2.9600 | 3 | 1 | 2 | 1 | 30.167 | -0.008 | 1 |
| 2 | 31.603 | 2.8287 | 6 | 22 | 0.5 | 2 | 0.2 | 0.082 | <> | Ni3P | 2.8300 | 2 | 1 | 3 | 0 | 31.589 | -0.015 | 2 |
| 3 | 36.383 | 2.4673 | 7 | 216 | 4.6 | 60 | 7.5 | 0.250 | <> | Ni5P2 | 2.4670 | 4 | 2 | 0 | 9 | 36.388 | 0.004 | 3 |
| 4 | 40.290 | 2.2366 | 10 | 47 | 1.0 | 6 | 0.7 | 0.115 | <> | Ni3P | 2.2390 | 3 | 0 | 4 | 0 | 40.245 | -0.045 | 4 |
| 5 | 41.790 | 2.1597 | 13 | 1102 | 23.4 | 299 | 37.3 | 0.244 | <> | Ni5P2 | 2.1600 | 35 | 4 | 2 | 0 | 41.784 | -0.005 | 5 |
| 6 | 42.857 | 2.1084 | 32 | 275 | 5.8 | 58 | 7.2 | 0.190 | <> | Ni3P | 2.1100 | 30 | 3 | 3 | 0 | 42.823 | -0.034 | 6 |
| 7 | 43.642 | 2.0723 | 45 | 596 | 12.7 | 140 | 17.5 | 0.211 | <> | Ni3P | 2.0730 | 60 | 1 | 1 | 2 | 43.626 | -0.016 | 7 |
| 8 | 44.489 | 2.0348 | 59 | 2883 | 61.2 | 465 | 58.0 | 0.145 | <> | Nickel, syn | 2.0340 | 100 | 1 | 1 | 1 | 44.507 | 0.017 | 8 |
| 9 | 45.290 | 2.0006 | 52 | 420 | 8.9 | 94 | 11.7 | 0.201 | <> | Ni5P2 | 2.0010 | 16 | 5 | 0 | 6 | 45.281 | -0.009 | 9 |
| 10 | 46.051 | 1.9693 | 34 | 123 | 2.6 | 28 | 3.5 | 0.205 | <> | Ni3P | 1.9710 | 16 | 2 | 0 | 2 | 46.009 | -0.042 | 10 |
| 11 | 46.651 | 1.9454 | 14 | 933 | 19.8 | 303 | 37.8 | 0.292 | <> | Ni5P2 | 1.9470 | 25 | 3 | 1 | 10 | 46.610 | -0.042 | 11 |
| 12 | 50.706 | 1.7989 | 18 | 136 | 2.9 | 29 | 3.6 | 0.192 | <> | Ni5P2 | 1.8030 | 8 | 4 | 3 | 4 | 50.583 | -0.123 | 12 |
| 13 | 51.843 | 1.7621 | 22 | 4709 | 100.0 | 802 | 100.0 | 0.153 | <> | Nickel, syn | 1.7620 | 42 | 2 | 0 | 0 | 51.846 | 0.003 | 13 |
| 14 | 51.971 | 1.7581 | 24 | 2895 | 61.5 | 561 | 70.0 | 0.174 | <> | Ni5P2 | 1.7560 | 4 | 5 | 0 | 9 | 52.036 | 0.066 | 14 |
| 15 | 52.769 | 1.7333 | 11 | 341 | 7.2 | 96 | 12.0 | 0.253 | <> | Ni5P2 | 1.7340 | 8 | 2 | 1 | 13 | 52.747 | -0.022 | 15 |
| 16 | 55.382 | 1.6576 | 9 | 95 | 2.0 | 38 | 4.7 | 0.360 | <> | Ni5P2 | 1.6580 | 4 | 4 | 3 | 7 | 55.367 | -0.016 | 16 |
| 17 | 58.931 | 1.5659 | 6 | 38 | 0.8 | 21 | 2.6 | 0.497 | <> | Ni3P | 1.5680 | 5 | 0 | 4 | 2 | 58.846 | -0.086 | 17 |
| 18 | 60.263 | 1.5345 | 9 | 33 | 0.7 | 5 | 0.6 | 0.136 | <> | Ni5P2 | 1.5330 | 4 | 4 | 4 | 6 | 60.327 | 0.064 | 18 |
| 19 | 66.057 | 1.4132 | 6 | 22 | 0.5 | 8 | 1.0 | 0.327 | <> | Ni2P | 1.4100 | 40 | 3 | 1 | 0 | 66.227 | 0.170 | 19 |
| 20 | 67.097 | 1.3938 | 7 | 56 | 1.2 | 14 | 1.7 | 0.225 | <> | Ni5P2 | 1.3960 | 4 | 7 | 2 | 1 | 66.978 | -0.119 | 20 |
| 21 | 74.260 | 1.2761 | 14 | 49 | 1.0 | 9 | 1.1 | 0.165 | <> | Ni5P2 | 1.2780 | 16 | 5 | 0 | 16 | 74.130 | -0.130 | 21 |
| 22 | 75.549 | 1.2575 | 26 | 101 | 2.1 | 45 | 5.6 | 0.401 | <> | Ni5P2 | 1.2580 | 16 | 5 | 5 | 6 | 75.513 | -0.036 | 22 |
| 23 | 76.370 | 1.2460 | 25 | 461 | 9.8 | 62 | 7.7 | 0.121 | <> | Nickel, syn | 1.2460 | 21 | 2 | 2 | 0 | 76.370 | 0.000 | 23 |
| 24 | 76.605 | 1.2428 | 24 | 268 | 5.7 | 41 | 5.1 | 0.138 | <> | Ni5P2 | 1.2430 | 16 | 8 | 2 | 2 | 76.588 | -0.017 | 24 |
| 25 | 77.851 | 1.2260 | 15 | 24 | 0.5 | 2 | 0.2 | 0.075 | <> | Ni3P | 1.2290 | 6 | 7 | 0 | 1 | 77.622 | -0.229 | 25 |
| 26 | 78.920 | 1.2120 | 10 | 58 | 1.2 | 24 | 3.0 | 0.372 | <> | | | | | | | | | 26 |
| 27 | 81.090 | 1.1850 | 8 | 40 | 0.8 | 31 | 3.9 | 0.697 | <> | Ni2P | 1.1870 | 60 | 4 | 0 | 1 | 80.922 | -0.168 | 27 |
| 28 | 85.770 | 1.1319 | 6 | 36 | 0.8 | 16 | 2.0 | 0.400 | <> | | | | | | | | | 28 |
| 29 | 87.972 | 1.1091 | 11 | 28 | 0.6 | 5 | 0.6 | 0.161 | <> | | | | | | | | | 29 |
| 30 | 89.289 | 1.0962 | 13 | 96 | 2.0 | 43 | 5.4 | 0.403 | <> | | | | | | | | | 30 |
| 31 | 91.282 | 1.0774 | 16 | 51 | 1.1 | 35 | 4.4 | 0.618 | <> | Ni2P | 1.0800 | 40 | 3 | 1 | 2 | 90.995 | -0.287 | 31 |
| 32 | 92.937 | 1.0625 | 10 | 540 | 11.5 | 94 | 11.7 | 0.157 | <> | Nickel, syn | 1.0624 | 20 | 3 | 1 | 1 | 92.944 | 0.007 | 32 |
| 33 | 95.997 | 1.0365 | 7 | 19 | 0.4 | 3 | 0.4 | 0.142 | <> | Ni3P | 1.3320 | 2 | 5 | 4 | 1 | 70.661 | -25.337 | 33 |
| 34 | 98.413 | 1.0175 | 10 | 178 | 3.8 | 41 | 5.1 | 0.207 | <> | Nickel, syn | 1.0172 | 7 | 2 | 2 | 2 | 98.446 | 0.033 | 34 |
| 35 | 106.589 | 0.9608 | 7 | 30 | 0.6 | 19 | 2.4 | 0.570 | <> | | | | | | | | | 35 |
| @ | End-of-List | | | | | | | | | | | | | | | Average Delta 2-Theta = 0.905 | | |

> PDF#04-0850 ———— Nickel, syn - Ni

> PDF#34-0501 ———— Ni3P - Nickel Phosphide

> PDF#17-0225 ———— Ni5P2 - Nickel Phosphide

> PDF#03-0953 ———— Ni2P - Nickel Phosphide

that of the nickel phosphides. Table 4-2 and Table 4-3 give the x-ray diffraction data from 400° C/1hr and 600°C/1hr heat treated coatings respectively.

It was also noted that some extra peaks appeared after XRD. These peaks do not belong to nickel and nickel phosphide ($Ni_3P$). It means that there may be other phases present in the coatings. The possible matching phases may be $Ni_5P_2$ and/or $Ni_2P$. These phases, however, are hard to find during TEM observations. Table 4-2 and Table 4-3 give the detailed x-ray diffraction data and matching phases.

From the SEM, TEM and x-ray analyses, it can be concluded that the as-deposited electroless nickel-phosphorus coatings with 10-12 wt% P content are mainly composed of the amorphous phase with tiny nickel crystallites. After heat treatment, the coatings are composed of nickel and nickel phosphides $Ni_3P$, with minor $Ni_5P_2$ and/or $Ni_2P$ phases. The nickel phase content is more than the $Ni_3P$ content in the heat treated coatings. The amount of nickel phase increases with the heat treating temperature, while the amount of $Ni_3P$ does not increase significantly with the heat treating temperature.

## 4.3 THE HARDNESS OF THE COATINGS

The hardness value of the coatings was obtained by a microhardness tester at a load of 200 g. Fig.4-15 shows the hardness of the coatings after different heat treatments. The coating after 400° C/1hr heat treatment has the highest hardness with 917DPH. The coating after 600°C/1hr heat treatment has medium high hardness. The as-deposited coating has the lowest hardness of the three kinds of coatings. The hardness is determined by the microstructure of the coatings. The as-deposited coating is mainly composed of the amorphous phase with tiny nickel crystallites in it. The hardness value of this coating is pretty low. The coating after 400°C/1hr heat treatment is crystallized with a small size of nickel crystallites and precipitates of $Ni_3P$. The size of both Ni

and $Ni_3P$ is very small, so this coating gives the highest hardness value. The nickel and nickel phosphide particles in the coating have grown after 600°C/1hr heat treatment, hence this coating has a lower hardness value than that after 400°C/1hr heat treatment.

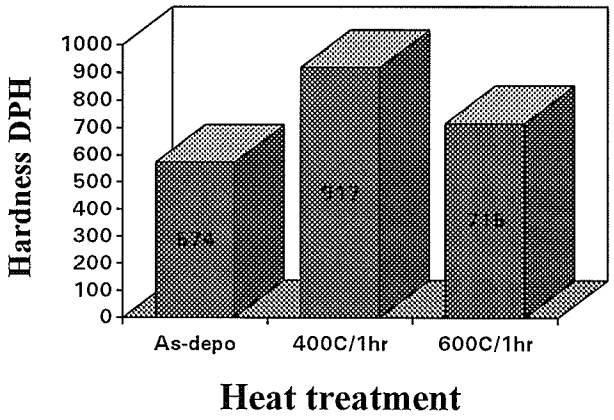


Fig.4-15 Hardness of the coatings versus the heat treatment

## 4.4 WEAR TESTING RESULTS UNDER LUBRICATION CONDITIONS

### 4.4.1 THE WEIGHT LOSS OF THE COATING VERSUS THE TEMPERATURE

Fig.4-16 shows the results obtained from the wear test of the electroless nickel-phosphorus coatings under two different loads (4kg and 8kg) and at three levels of temperatures. The tests for the coatings after heat treatment were only done at room temperature and 100°C. It is evident that the wear resistance of the coatings increases with the increase in temperature under both testing loads. For as-deposited coating, the weight loss under 8kg is almost four times higher than that under 4kg load at room temperature. As the test temperature is increased, weight loss of the coating decreases for both loads, and the results for 8kg are more dramatic. At 100°C, the weight loss under 8kg is almost equal to that under 4kg. These results indicate that at high contact stresses, an increase in temperature is very effective in reducing the weight loss in the coating under lubricated conditions. For an 8kg load, weight loss is reduced almost ten times. For the coating after 400°C/1hr heat treatment, the weight loss slightly decreases with increase of testing temperature under 8kg load. The coating after 600°C/1hr heat treatment does not give any weight loss even after the test at 8kg load. The coating after 600°C/1hr heat treatment shows excellent wear resistance. The results also show that the hardness is not proportional to the wear property although the hardness of a material is an important factor in wear resistance. The coating after 400°C/1hr gives higher hardness value than that of coatings after 600°C/1hr heat treatment, but the weight loss and the surface damage after wear test is higher and more severe than those of 600°C/1hr heat treatment coatings at room temperature. The weight loss at 100°C test for both the heat treated coatings is insignificant, indicating that the temperature does improve the wear resistance of coatings under lubricated conditions. In order to find out how temperature affects the wear of the 600°C/1hr heat treated coatings, tests were carried out at 8kg load with 335,000 cycles for both room temperature and 100°C. The result is shown in Fig.4-17. The weight loss decreases from 0.0078 g tested at room temperature to 0 tested at 100°C.

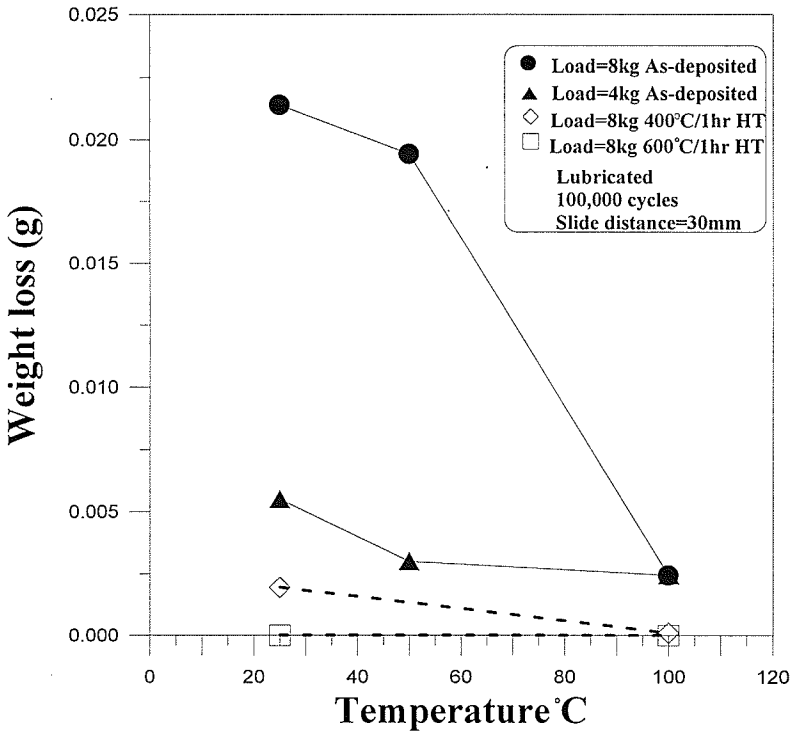


Fig.4-16 The weight loss versus testing temperature

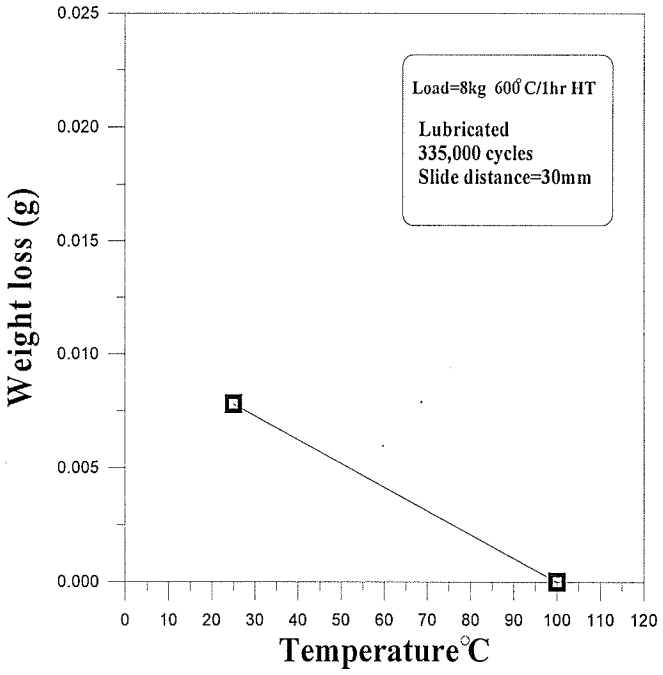


Fig.4-17 The weight loss versus temperature after the wear tests on 600°C/1hr

### 4.4.2 MORPHOLOGY OF THE WEAR TRACK AFTER THE TESTS

#### 4.4.2.1 As-deposited coatings.

For the wear track under 4kg load ( at 100,000 cycles) at room temperature, it was noted that at the beginning of the sliding, polishing and scuffing of the coating takes place. The coating starts to delaminate after 50,000 cycles, mainly in the middle part of the wear track as this part experienced the highest sliding speed. Fig.4-18 shows the SEM micrograph of the wear track with delaminations. It can also be seen in Fig.4-18 that there are several cracks running perpendicular to the sliding direction. There are also some cracks along the sliding direction under the delaminated surface. The clear brittle failure bands on the delaminated surface, which are similar to fatigue bands in metals, can be observed in Fig.4-18 as well. Fig.4-19 shows the closer look of the fatigue-like failure bands. Close to the track ends, however, a smooth wear surface is observed (Fig.4-20).

The wear track under 4kg at 100°C, in contrast to that at room temperature, is very smooth throughout the whole wear track (Fig.4-21). It is observed that there are only few places with small delamination. Some small cracks along the wear direction are present. Most of the wear track, however, is smooth as in Fig.4-21. Scuffing and polishing occurs on the coating surface and there are a few spots where adhesion is observed.

The wear track under 8kg load at room temperature is shown in Fig.4-22. The coating layer is noted to be significantly worn off after testing for 100,000 cycles. It is noted that during the test initially, scuffing and polishing of the coating occurs. Delamination and spalling occurs after certain cycles. At the edge of the wear scar (point A), brittle fracture/spalling of the coating is evident (Fig.4-22). In the middle of the wear track, the delaminated or spalled pieces becomes the debris, and causes severe abrasion. This process leads to significant coating weight loss. Fig.4-23

shows the bottom of the wear track. Deformation of the substrate and the coating can be clearly seen in the Figure.

At 100°C and under the 8kg load, the wear track becomes quite smooth. There are very few delaminations, and the coating is nearly intact (Fig.4-24). Several cracks in the track are, however, present because of the high normal stress applied on the coating. The direction of the cracks is mainly along the wear track and directly under the sliding contact area. The surface looks polished after the test with only a few scuffing spots. The weight loss at 100°C is significantly low compared to that at room temperature.

The weight loss and the morphology of the wear tracks clearly show that the temperature has a significant effect on the wear resistance of the as-deposited coating under lubricated conditions, especially at 8kg load. The coatings tested at room temperature were either delaminated (at 4kg) or completely wore off (at 8kg), while the coatings tested at 100°C were not delaminated and wore off except for some cracks presented in the coating. For further exploration of the mechanisms of the temperature effect, the SEM/EDS analysis and X-ray mapping analysis of the wear track were carried out.

Table 4-4 lists the complete SEM/EDS quantitative analysis results from the points identified on the wear track in the related figures. The important trend that can be obtained from the analysis of results is that, for both 4kg and 8kg load tests, the Ni content decreased and P content increased on the wear track after 100°C tests; there is also high S content on the wear tracks. After the 4kg and room temperature test, the Ni and P content are almost the same on the non-wear surface and the wear track.

After the 4kg at 100°C test, there is 81 at% Ni on the non-wear place and the lowest content of 68 at% Ni on the wear track. The P content, on the other hand, increases from the 18 at% on the

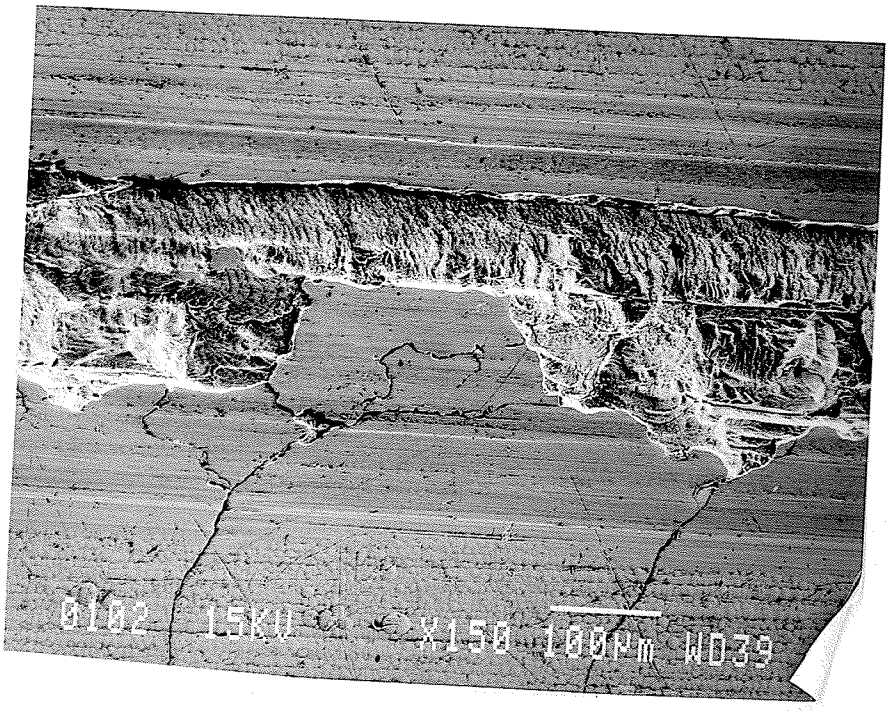


Fig.4-18 SEM micrograph of the wear track with delamination after 4kg, room temperature test (as-deposited coating)

Fig.4-19 SEM micrograph of the wear track with fatigue bands on the delaminated place after 4kg, room temperature test (as-deposited coating)

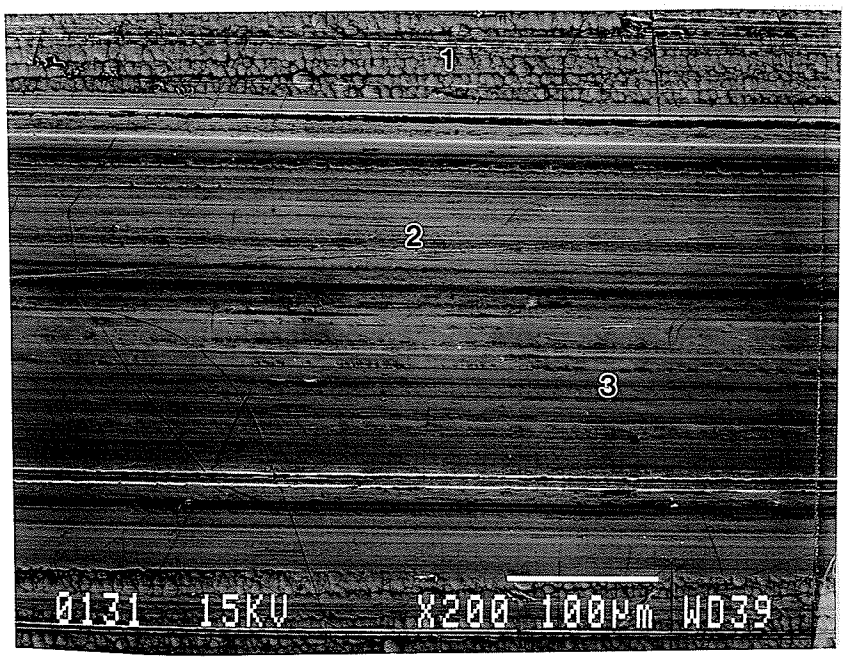


Fig.4-20 The smooth wear track at position close to the track ends after 4kg room temperature test

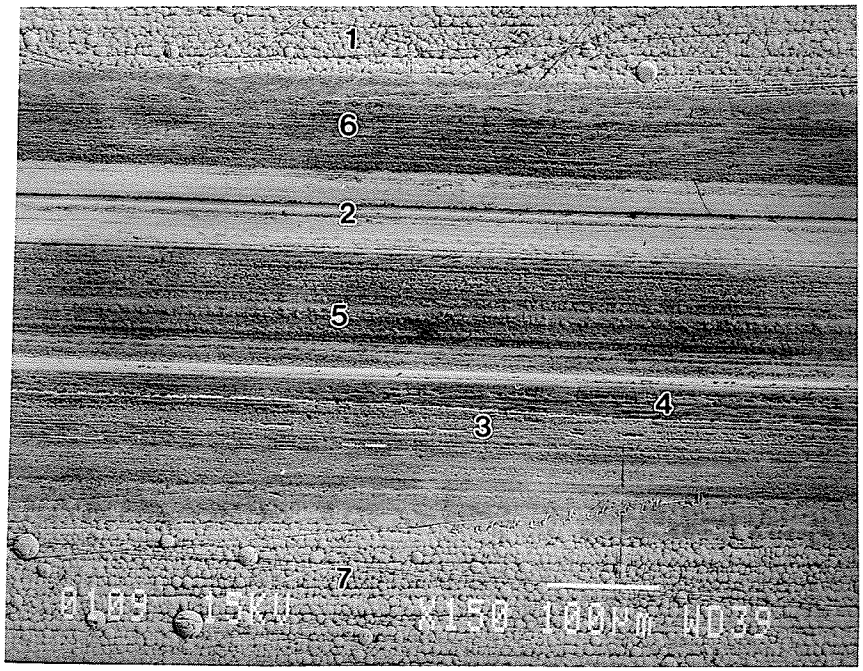


Fig.4-21 SEM morphology of wear track after 4kg, 100°C test

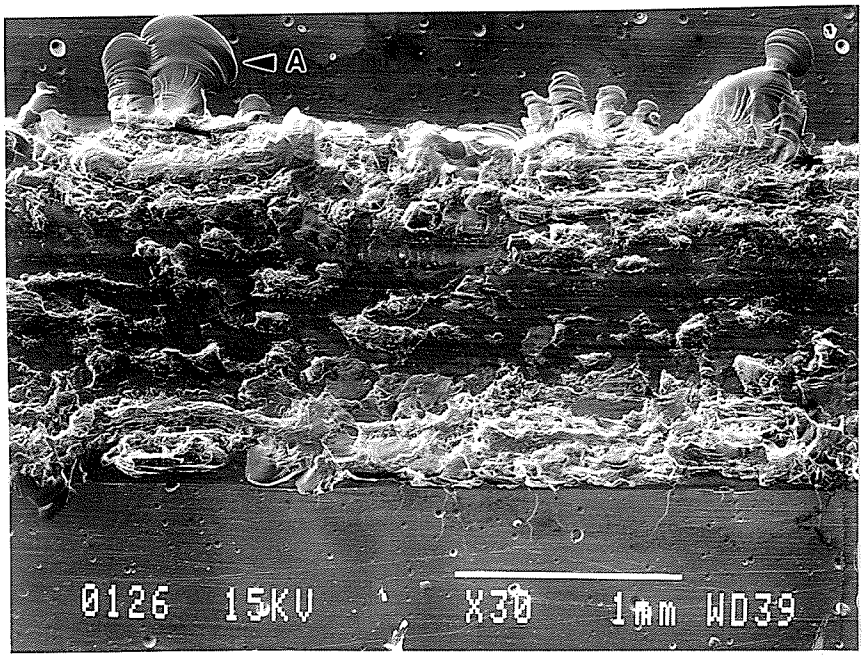


Fig.4-22 SEM morphology of wear track after 8kg, room temperature test

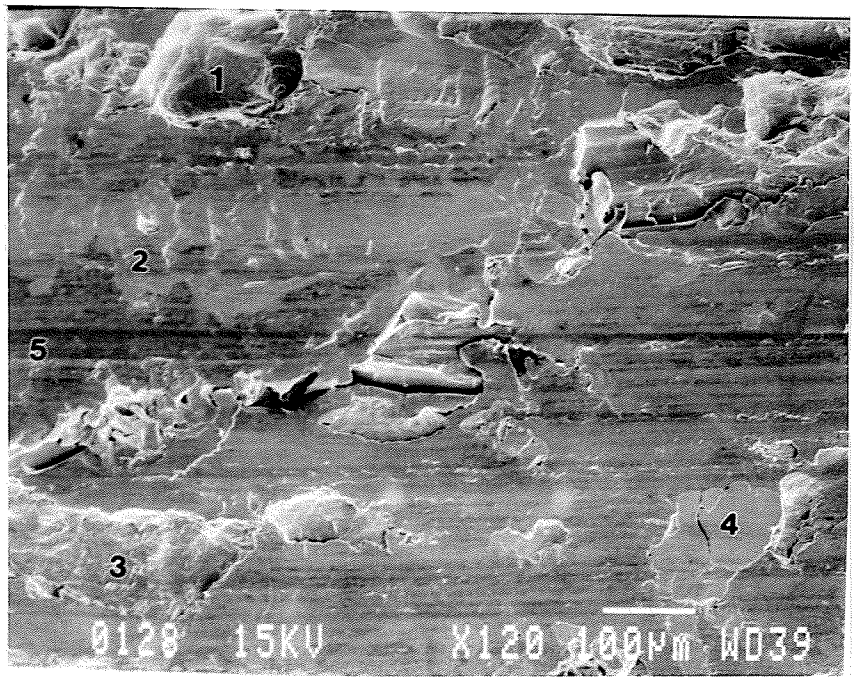


Fig.4-23 Enlarged part of Fig. 4-22 shows the bottom morphology of the wear track

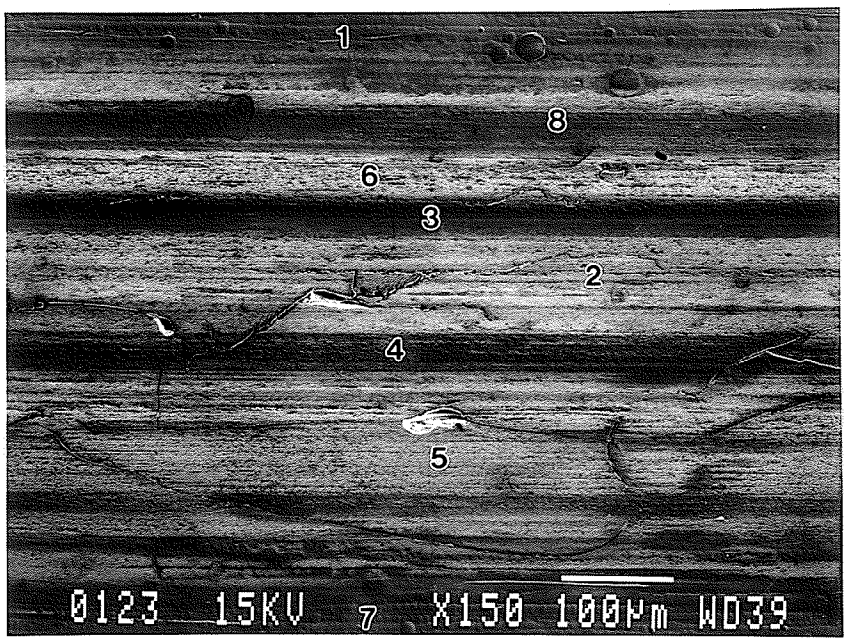

Fig.4-24 SEM morphology of wear track after 8kg, 100°C test

non-wear surface to 24 at% on the wear track. The wear track after 8kg, 100°C test shows a low Ni content of 63 at% and a high of P content of 19 at%, compared to the non-wear surface with 80 at% Ni and 20 at% P. The results show that the coating is worn off after the 8kg, room temperature test, since the mild steel substrate shows up an Fe. Sulfur appears in the wear track after all tests, but with a higher content after the 100°C test than what shows up at a room temperature test for both loads.

The X-ray mapping results give a clearer picture of elements' distribution on the wear track. Fig.4-25 shows an x-ray map of the wear track after the 4kg, room temperature test. Except for the S content showing up, there is less change in the Ni & P content from the non-wear place to the wear track. The difference of Ni & P content between non-wear place and the wear track, however, is obvious after the 4kg, 100°C test (Fig.4-26). The same results are shown in Fig.4-27 and Fig.4-28 for the 8kg tests at two different temperatures.

Table 4-4 The energy dispersive spectrum quantitative analysis results (corresponding to the points in Figures)

| | | | Ni | | P | | S | | Fe | | Si | | Mn | |
|---|---|---|---|---|---|---|---|---|---|---|---|---|---|---|
| Load | Temperature | Point | at% | wt% | at% | wt% | at% | wt% | at% | wt% | at% | wt% | at% | wt% |
| 4kg | Room temp. (Fig. 4-20) | 1 | 81.75 | 89.47 | 18.25 | 10.53 | 0.00 | 0.00 | 0.00 | 0.00. | ---- | ---- | ---- | ---- |
| | | 2 | 77.58 | 86.62 | 17.38 | 10.24 | 4.89 | 2.98 | 0.15 | 0.16 | ---- | ---- | ---- | ---- |
| | | 3 | 78.79 | 87.50 | 17.70 | 10.37 | 3.51 | 2.13 | 0.00 | 0.00 | ---- | ---- | ---- | ---- |
| | 100°C (Fig. 4-21) | 1 | 81.42 | 89.26 | 18.58 | 10.74 | 0.00 | 0.00 | 0.00 | 0.00 | ---- | ---- | ---- | ---- |
| | | 2 | 77.64 | 86.76 | 19.54 | 11.52 | 2.82 | 1.72 | 0.00 | 0.00 | ---- | ---- | ---- | ---- |
| | | 3 | 74.19 | 84.42 | 22.18 | 13.32 | 3.63 | 2.26 | 0.00 | 0.00 | ---- | ---- | ---- | ---- |
| | | 4 | 71.49 | 82.49 | 20.92 | 12.73 | 7.59 | 4.78 | 0.00 | 0.00 | ---- | ---- | ---- | ---- |
| | | 5* | 68.64 | 80.46 | 24.40 | 15.09 | 6.96 | 4.46 | 0.00 | 0.00 | ---- | ---- | ---- | ---- |
| | | 6* | 68.91 | 80.58 | 24.74 | 15.26 | 6.12 | 3.91 | 0.23 | 0.25 | ---- | ---- | ---- | ---- |
| | | 7 | 80.77 | 88.80 | 19.13 | 11.09 | 0.00 | 0.00 | 0.00 | 0.00 | ---- | ---- | ---- | ---- |
| 8kg | Room temp (Fig. 4-23) | 1 | 0.24 | 0.26 | 0.19 | 0.11 | 0.55 | 0.32 | 97.18 | 97.92 | 0.87 | 0.44 | 0.96 | 0.95 |
| | | 2 | 78.24 | 86.09 | 18.86 | 10.95 | 0.00 | 0.00 | 2.75 | 5.88 | 0.15 | 0.08 | 0.00 | 0.00 |
| | | 3 | 0.17 | 0.18 | 0.14 | 0.08 | 0.23 | 0.13 | 97.44 | 98.02 | 0.84 | 0.43 | 1.18 | 1.16 |
| | | 4 | 78.37 | 86.89 | 20.14 | 11.78 | 0.36 | 0.22 | 0.97 | 1.02 | 0.16 | 0.09 | 0.00 | 0.00 |
| | | 5 | 0.21 | 0.22 | 0.00 | 0.00 | 0.00 | 0.00 | 98.26 | 98.62 | 0.72 | 0.36 | 0.81 | 0.80 |
| | 100°C (Fig. 4-24) | 1 | 79.80 | 88.22 | 20.20 | 11.78 | 0.00 | 0.00 | 0.00 | 0.00 | ---- | ---- | ---- | ---- |
| | | 2 | 66.23 | 78.72 | 28.81 | 18.06 | 4.96 | 3.22 | 0.00 | 0.00 | ---- | ---- | ---- | ---- |
| | | 3* | 76.87 | 86.30 | 23.13 | 13.70 | 0.00 | 0.00 | 0.00 | 0.00 | ---- | ---- | ---- | ---- |
| | | 4* | 64.60 | 77.42 | 30.26 | 19.13 | 4.96 | 3.25 | 0.17 | 0.20 | ---- | ---- | ---- | ---- |
| | | 5 | 66.36 | 78.80 | 28.09 | 17.60 | 5.55 | 3.60 | 0.00 | 0.00 | ---- | ---- | ---- | ---- |
| | | 6 | 63.15 | 76.25 | 24.86 | 15.83 | 12.00 | 7.91 | 0.00 | 0.00 | ---- | ---- | ---- | ---- |
| | | 7 | 79.66 | 88.13 | 20.34 | 11.87 | 0.00 | 0.00 | 0.00 | 0.00 | ---- | ---- | ---- | ---- |
| | | 8* | 66.85 | 79.16 | 27.14 | 16.95 | 6.01 | 3.89 | 0.00 | 0.00 | ---- | ---- | ---- | ---- |
| | | | | | | | | | | | | | | |

* With high carbon peak in EDS spectrum

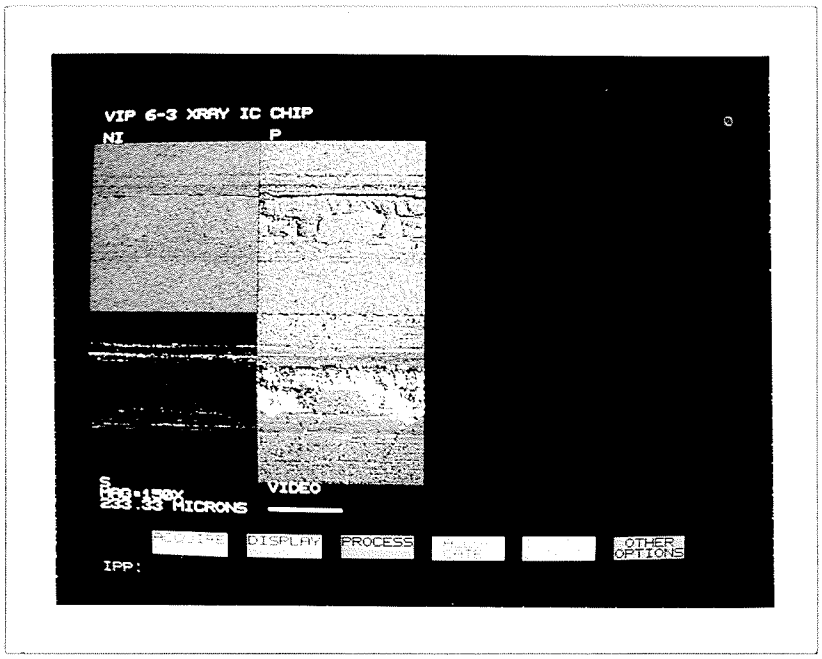


Fig.4-25 X-ray map of the wear track after 4kg, room temperature test

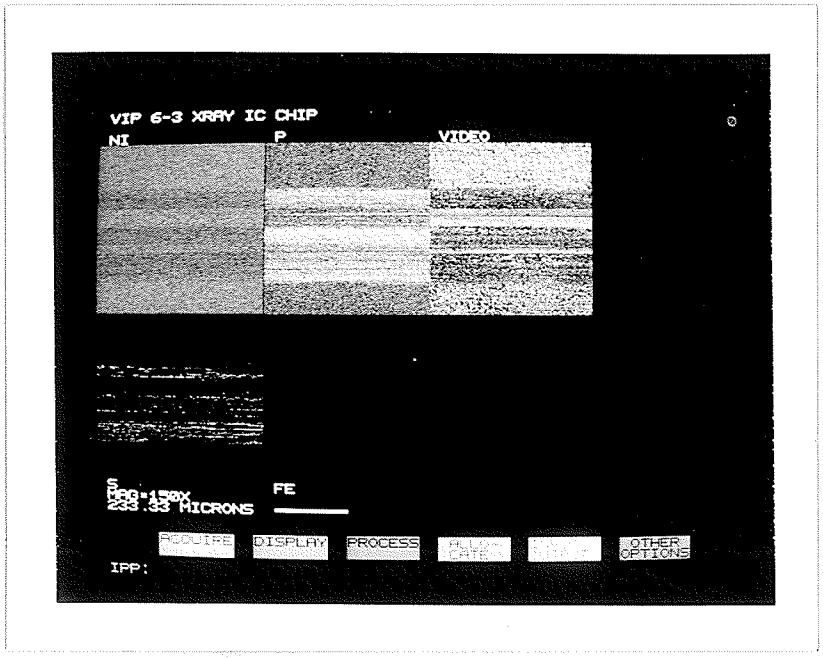


Fig.4-26 X-ray map of the wear track after 4kg, 100°C test

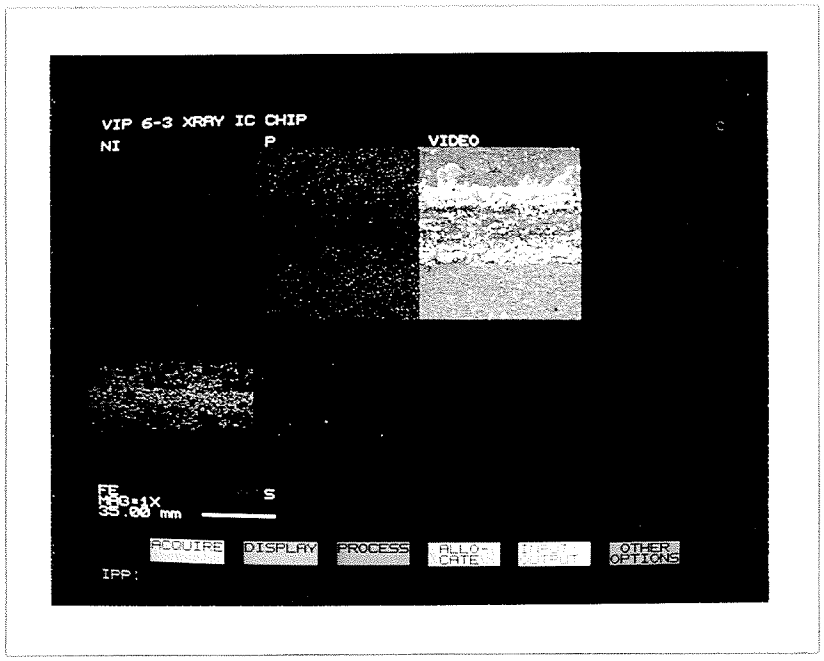


Fig.4-27 X-ray map of the wear track after 8kg, room temperature test

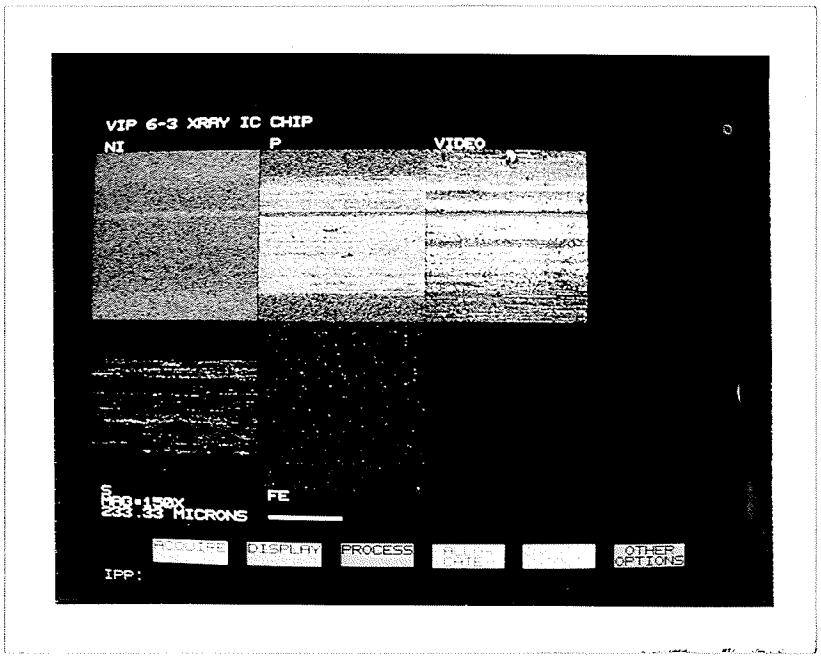


Fig.4-28 X-ray map of the wear track after 8kg, 100°C test

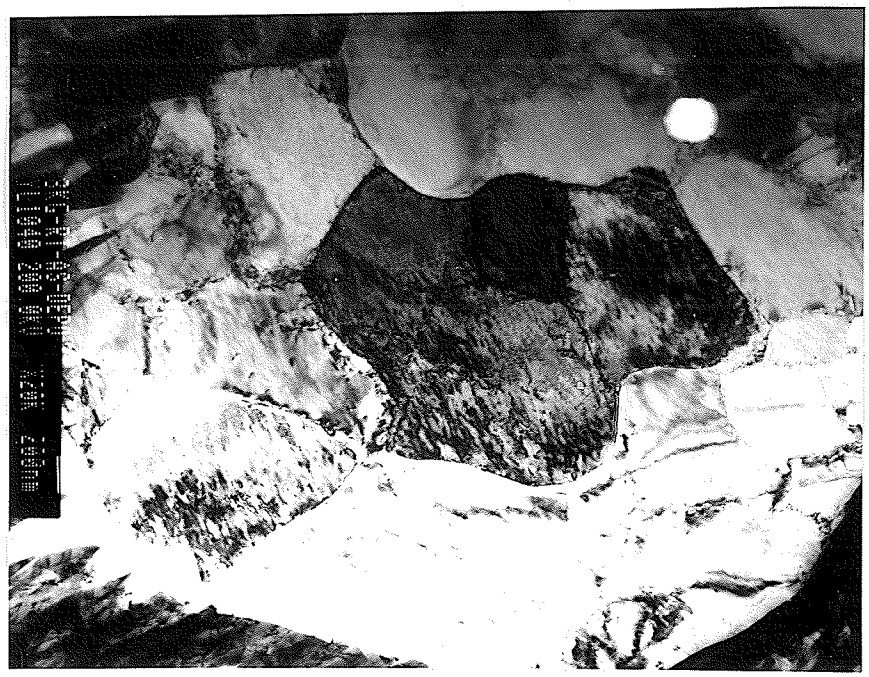

a

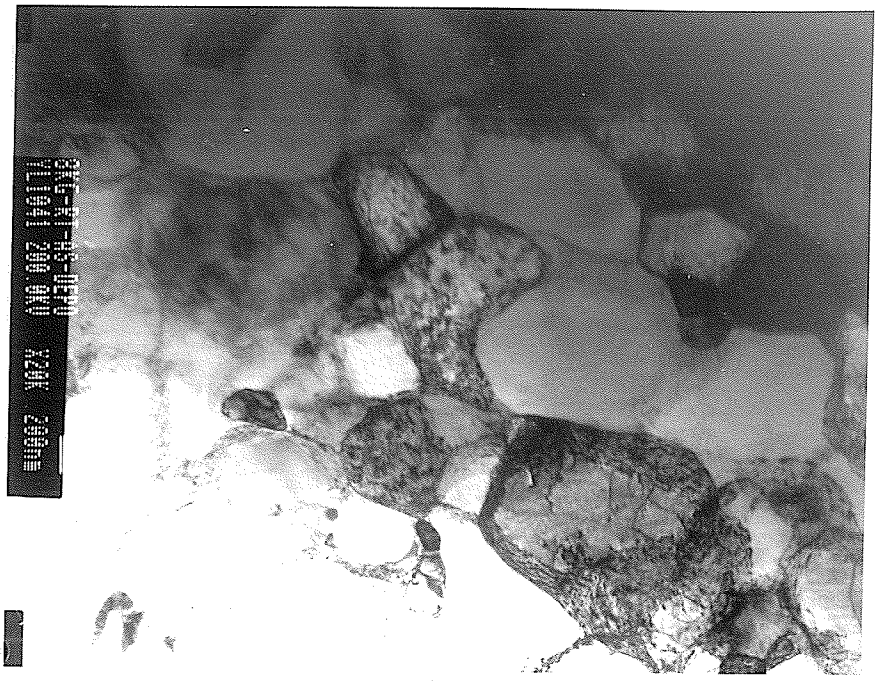

b

Fig.4-29 TEM morphology of crystallized precipitates of $Ni_3P$ and Ni after 8kg, room temperature test

Fig.4-30a The TEM image of the crystallized precipitates from as-deposited Ni-P coatings after 8kg 100°C test

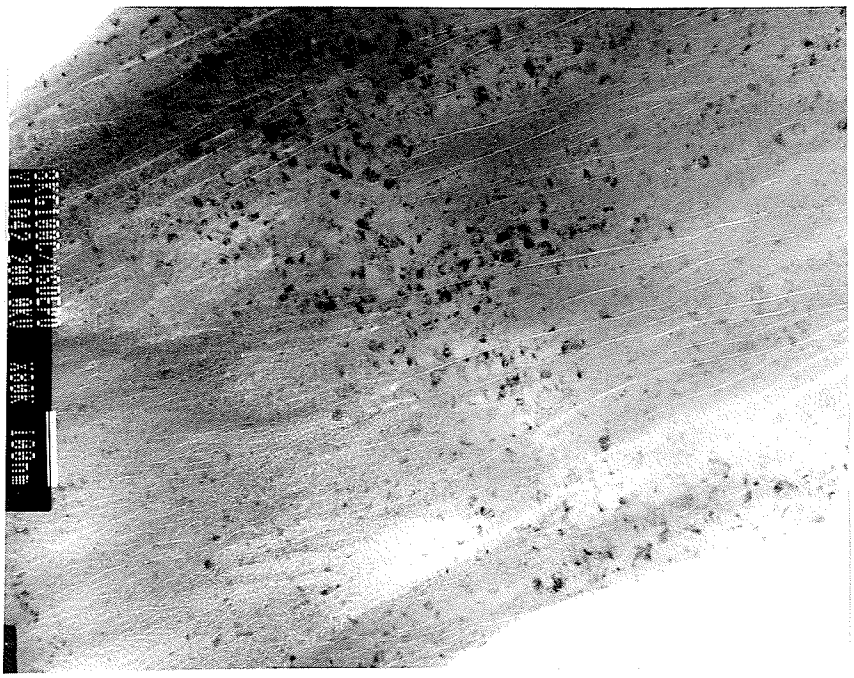

Fig.4-30b Amorphous phase with tiny nickel crystallites still exists at the side of the wear track after 8kg 100°C test

Fig.4-31 Large crystallized particles are also found on the wear track of as-deposited coatings after 8kg 100°C test

Under the high stress reciprocating sliding, the heat generated on the interface is very high so that the as-deposited coating is subjected to crystallization from the amorphous phase to crystallized precipitates. Fig.4-29a and b show the TEM images of crystallized precipitates of $Ni_3P$ and Ni after the 8kg, room temperature test. The size of the crystallites is larger than those in the coating after 600°C/1hr heat treatment. This is caused by either high temperature or the long crystallization time (the reciprocating cycles are 100,000 times at 160/min frequency, which gives about ten and half hours testing period). Two phenomena should be noted in these pictures. One is the dislocation lines existing in the precipitates, which may be caused by the high stress sliding. Another is the small particles existing on the grain boundaries of precipitates. What those phases are is not clear. Fig.4-30a is the TEM image of the wear track after the 8kg, 100°C test. The crystallization of amorphous is clear but the size of the particles is smaller than those after the room temperature test. Lots of twin boundaries exist in the precipitates. Fig.4-30b shows the coating close to the wear track center. It is still amorphous structure with tiny nickel crystallites, but the amorphous structure shows the orientation preference along the sliding direction. Large

size of precipitates were also found in some areas of the 8kg, 100°C test wear track center (Fig.4-31).

#### 4.4.2.2 400°C/1hr heat treated coating

The wear track after the 8kg, room temperature test was found delaminated on the center of the wear track (Fig.4-32a). Cracks along the sliding direction were also noted on the track. Brittle spalling of the coating can be seen from Fig.4-32b. The coating was lost from the substrate and some debris was pressed into the substrate.

The X-ray mapping shows the appearance of the substrate (Fig.4-33a and b). A few places of the wear track were not delaminated but were severe cracked (Fig.4-34). The X-ray map shows little changes of the Ni and P content on the wear track but with S appears on the wear track (Fig.4-35). The wear track after 8kg, 100°C test were cracked with few places of delamination (Fig.4-36). Most of the wear track seen were almost intact. The weight loss can not be weighed and hence does not give the value of the weight loss. X-ray mapping analysis gives the same changes of Ni and P content on the wear track as those on as-deposited coatings. The Ni content decreased and P content increased on the wear track compared with the content of Ni, P on the non-wear place (Fig.4-37). S content was also increased as well. Table 4-5 lists the SEM/EDS results from the both room temperature and 100°C test. It is obvious that the Ni content decreased and P content increased on the wear track and S appeared on the wear track as well.

#### 4.4.2.3 600°C/1hr heat treated coating

The wear track after 8kg, room temperature test has only one small delamination of the coating from the substrate (Fig.4-38). The rest of the coating on the wear track has only cracks along the sliding direction. The asperities on the surface of the coating can be clearly seen from the figure.

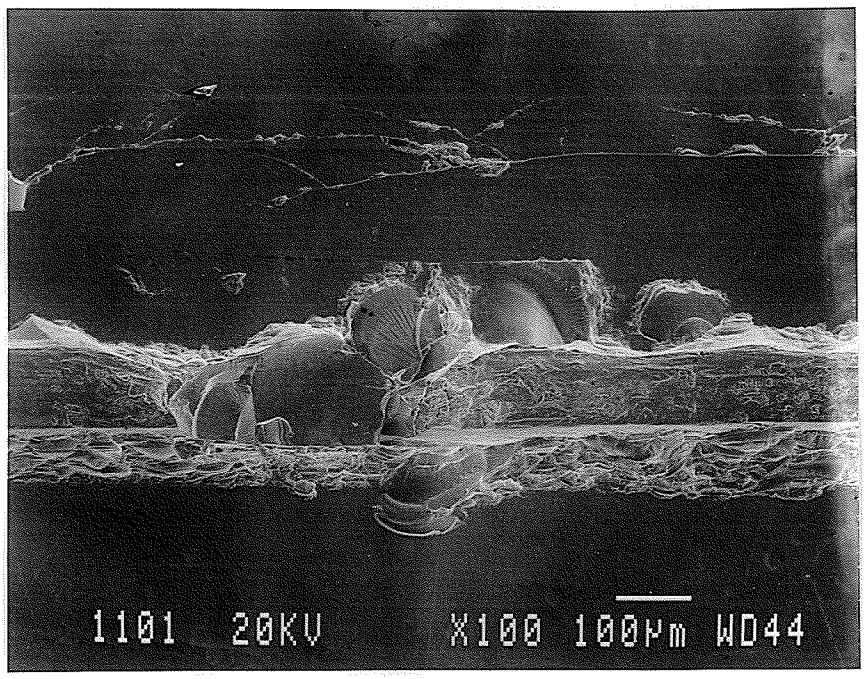


Fig.4-32a SEM morphology of the wear track after 8kg room temperature test (400°C/1hr heat treated coating)

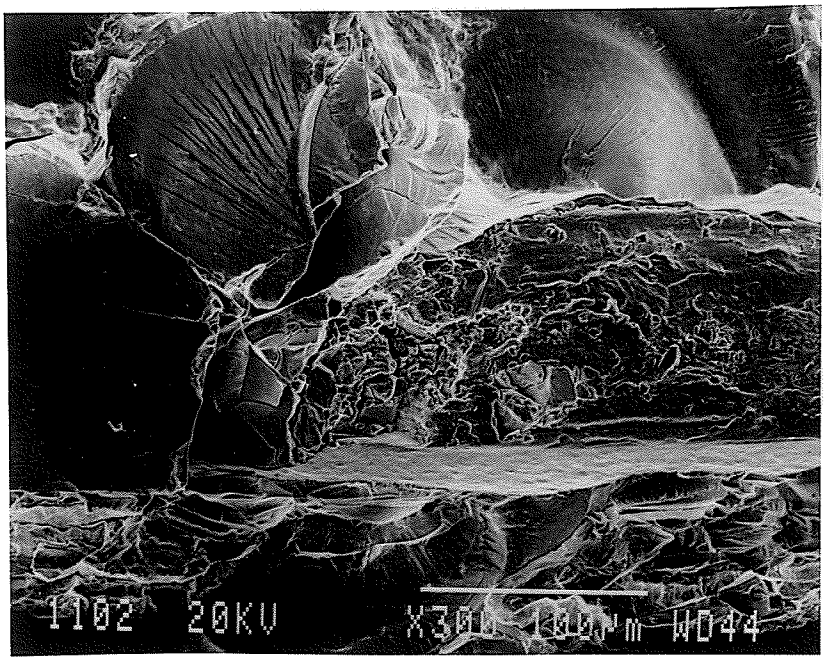


Fig.4-32b SEM image of the delaminated coating surface (enlarged from Fig4-32a)

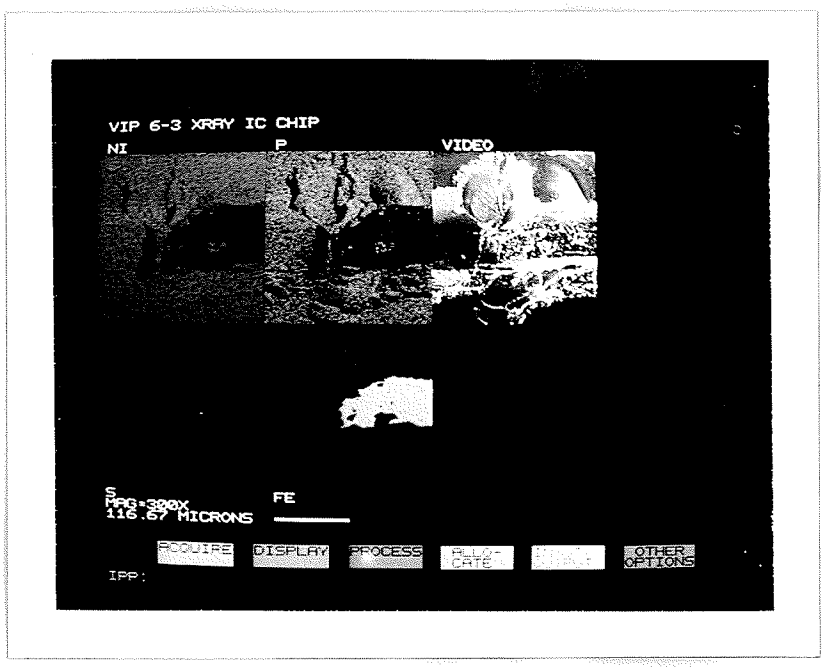


Fig.4-33a X-ray map of the wear track after 8kg room temperature test (400°C/1hr heat treated coating)

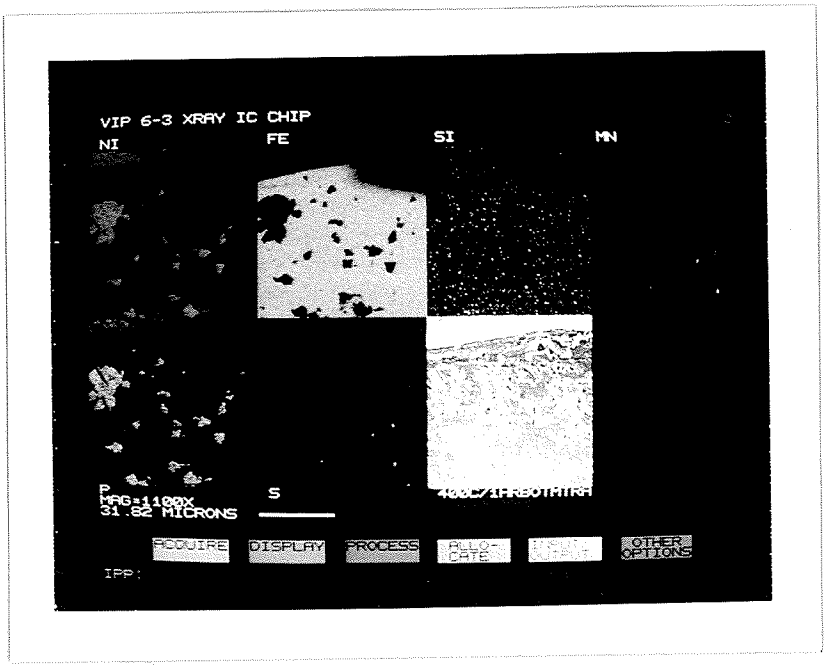


Fig.4-33b X-ray map of the wear track after 8kg room temperature test (400°C/1hr heat treated coating)

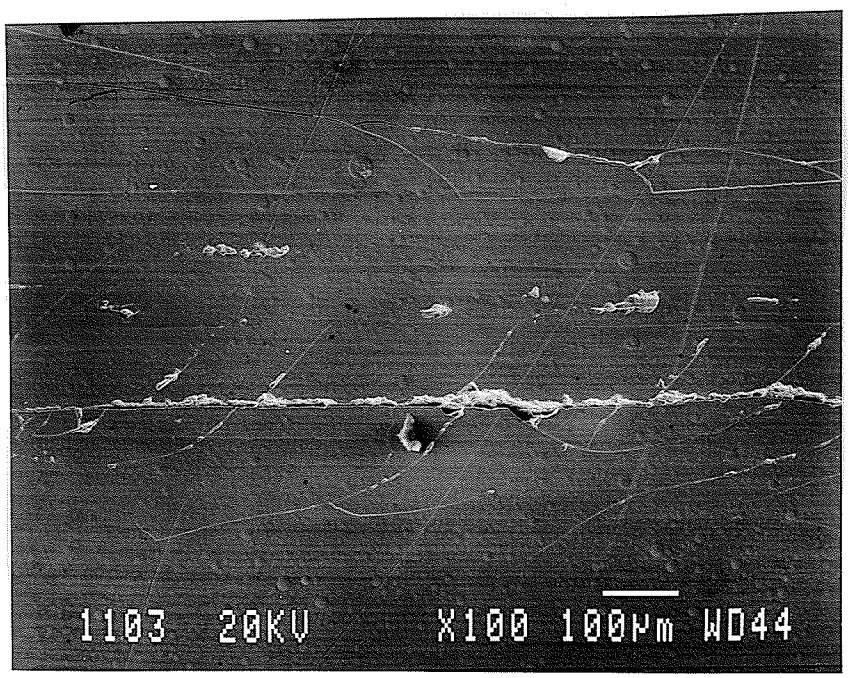


Fig.4-34 Wear track without severe delamination after room temperature test (400°C/1hr heat treated coating)

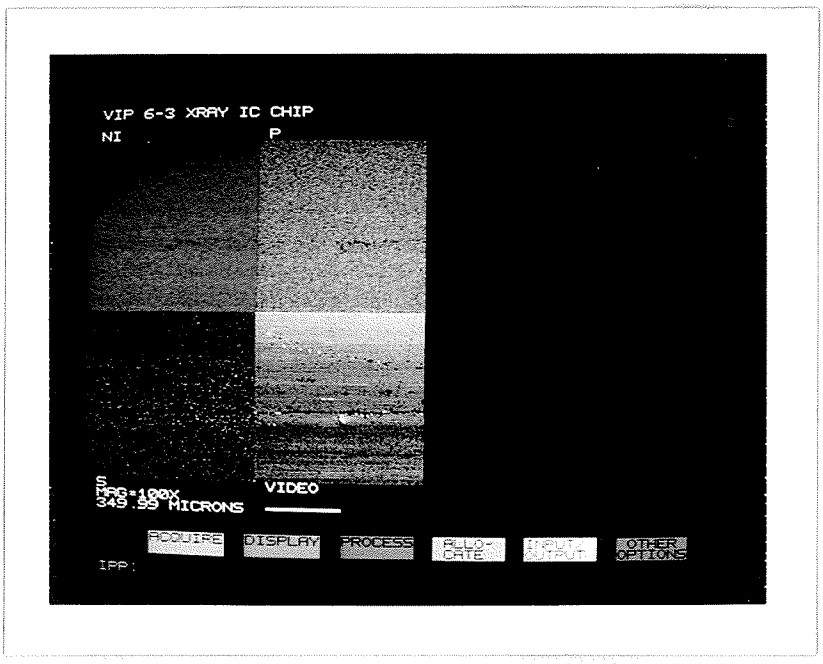


Fig.4-35 X-ray map of the wear track of Fig.4-34


Fig.4-36 SEM morphology of the wear track after 8kg 100°C Test (400°C/1hr heat treated coating)

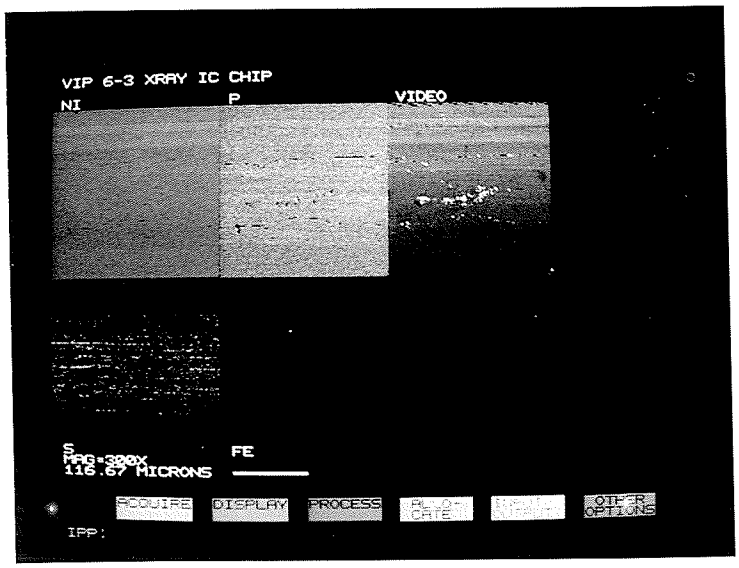


Fig.4-37 X-ray map of the wear track shown in Fig. 4-36

Table 4-5 The energy dispersive spectrum quantitative analysis results
(400°C/1hr heat treated coating)

| | | | Ni | | P | | S | | Fe | |
|---|---|---|---|---|---|---|---|---|---|---|
| | Place | Point | at% | wt% | at% | wt% | at% | wt% | at% | wt% |
| 8kg Room temp (Fig.4-34) | Non wear | 1 | 81.07 | 89.04 | 18.93 | 10.96 | 0.00 | 0.00 | 0.00 | 0.00 |
| | | 2 | 80.91 | 88.93 | 19.09 | 11.07 | 0.00 | 0.00 | 0.00 | 0.00 |
| | Wear track | 3 | 81.25 | 89.14 | 18.55 | 10.74 | 0.20 | 0.12 | 0.00 | 0.00 |
| | | 4 | 80.79 | 88.85 | 19.13 | 11.10 | 0.09 | 0.05 | 0.00 | 0.00 |
| | | 5 | 80.52 | 88.68 | 19.48 | 11.32 | 0.00 | 0.00 | 0.00 | 0.00 |
| 8kg 100°C (Fig.4-36) | Non wear | 1 | 80.71 | 88.80 | 19.29 | 11.20 | 0.00 | 0.00 | 0.00 | 0.00 |
| | | 2 | 81.45 | 89.27 | 18.55 | 10.73 | 0.00 | 0.00 | 0.00 | 0.00 |
| | | 3 | 81.82 | 89.47 | 18.10 | 10.44 | 0.00 | 0.00 | 0.00 | 0.00 |
| | Wear track | 4 | 79.55 | 88.04 | 19.58 | 11.43 | 0.88 | 0.53 | 0.00 | 0.00 |
| | | 5 | 79.43 | 87.94 | 19.63 | 11.46 | 0.87 | 0.53 | 0.07 | 0.07 |
| | | 6 | 78.8. | 87.48 | 20.40 | 11.95 | 0.61 | 0.37 | 0.19 | 0.20 |

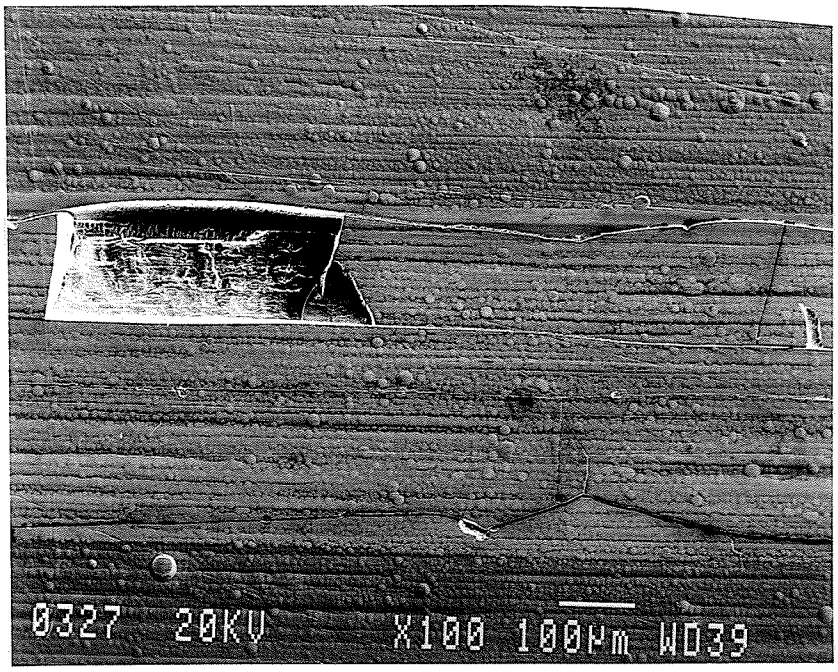


Fig.4-38 SEM morphology of the wear track after 8kg room temperature test
(600°C heat treated coatings)

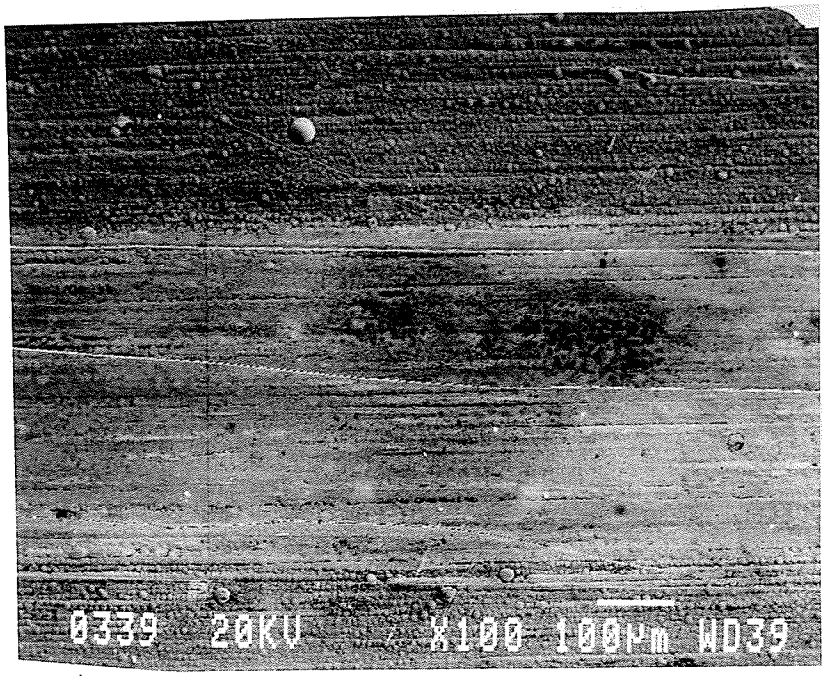


Fig.4-39 SEM morphology of the wear track after 8kg 100°C test
(600°C heat treated coatings)

Table 4-6 The energy dispersive spectrum quantitative analysis results
(600°C heat treated coatings)

| | Place | Point | Ni | | P | | S | | Fe | |
|---|---|---|---|---|---|---|---|---|---|---|
| | | | at% | wt% | at% | wt% | at% | wt% | at% | wt% |
| 8kg Room Temp | Non wear | 1 | 81.96 | 89.60 | 18.04 | 10.40 | 0.00 | 0.00 | 0.00 | 0.00 |
| (Fig.4-38) | Wear track | 2 | 81.32 | 89.19 | 18.57 | 10.74 | 0.11 | 0.07 | 0.00 | 0.00 |
| 8kg 100°C (Fig.4-39) | Non wear | 1 | 81.06 | 89.03 | 18.94 | 10.97 | 0.00 | 0.00 | 0.00 | 0.00 |
| | | 2 | 81.03 | 89.01 | 18.97 | 10.99 | 0.00 | 0.00 | 0.00 | 0.00 |
| | Wear track | 3 | 75.73 | 85.48 | 20.71 | 12.33 | 3.56 | 2.19 | 0.00 | 0.00 |
| | | 4 | 72.73 | 83.41 | 22.79 | 13.79 | 4.48 | 2.81 | 0.00 | 0.00 |

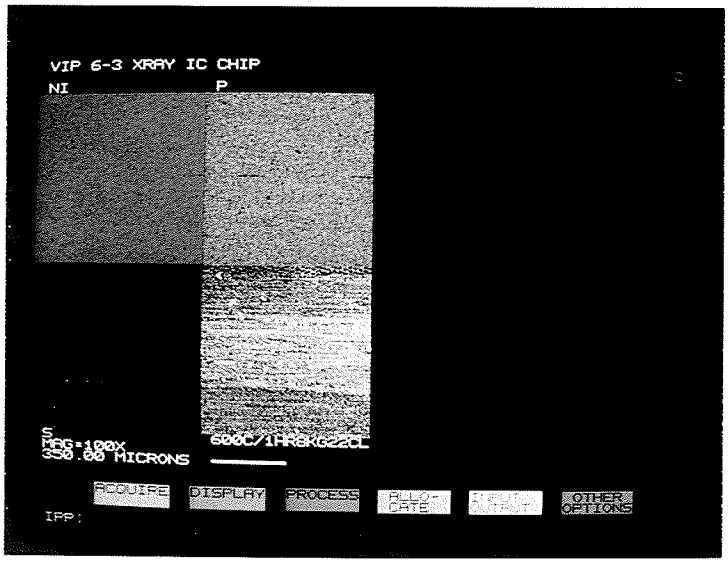


Fig.4-40a X-ray map of the wear track after 8kg room temperature test (600°C heat treated coatings)

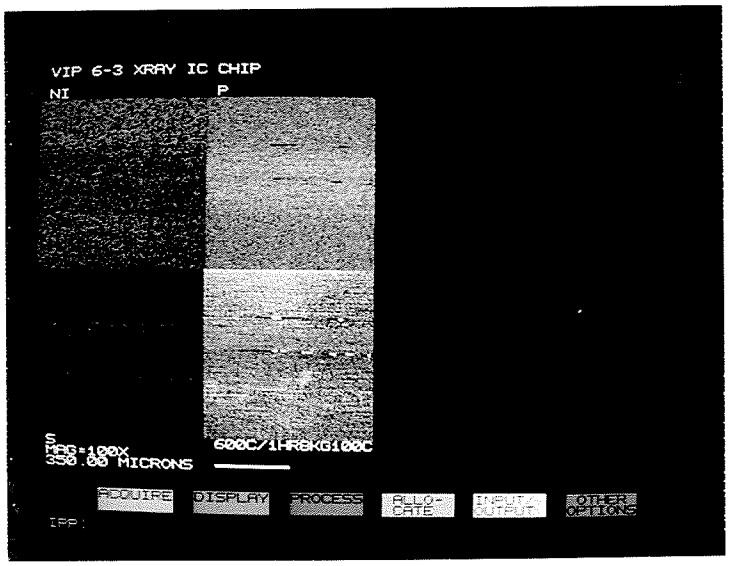


Fig.4-40b X-ray map of the wear track after 8kg 100°C test (600°C heat treated coatings)

The coating surface is not even severely scratched except for some small polished tracks. The wear track after the 8kg, 100°C test is very smooth with cracks along the sliding direction (Fig.4-39). The surface of the coating is polished compared with the room temperature test. No delamination is found on the wear track. The X-ray mapping results give the same trend as those obtained from the test on as-deposited and as-deposited + 400°C/1hr heat treated coatings. The Ni content decreases and P content increases after 100°C test (Fig.4-40a and b), with S on the wear track as well. Table 4-6 lists the results from the SEM/EDS quantitative analysis. The results support the X-ray mapping results.

#### 4.4.2.4 600°C/1hr heat treated coating after 335,000 cycles, lubricated test

The coating was severely damaged at the place close to the track ends after the 8kg, room temperature test with 335,000 lubricated reciprocating sliding cycles. Fig.4-41 is the SEM image of the wear track with coating damage. The ellipse-shaped bands can be seen in the figure, indicating the fatigue failure of the coating at this position due to the cyclic load conditions. A large crack can be seen at the bottom center of the wear track, along the sliding direction. On the track bottom, severe abrasive wear occurred (Fig.4-42). Some hard coating particles were also pressed into the substrate. The rest of the wear track, however, remained smooth with a few cracks in the center of the sliding track (Fig.4-43). The wear track after the 8kg, 100°C test with the same cycles as the room temperature test is shown in Fig.4-44. A small delamination occurred in the coating close to one track end. The rest parts of the coating remained smooth with cracks in the track center. The weight loss is too small to be weighed. The weight loss versus temperature has been already shown in Fig.4-18. The morphology of the wear track shows apparently that the temperature has significant effect on the wear of the coating. The increase in temperature decreases the wear of the coating. The quantitative analysis results of the Ni, P, S elements on the wear track by SEM/EDS is given in Table 4-7. The data were obtained from the non-damaged

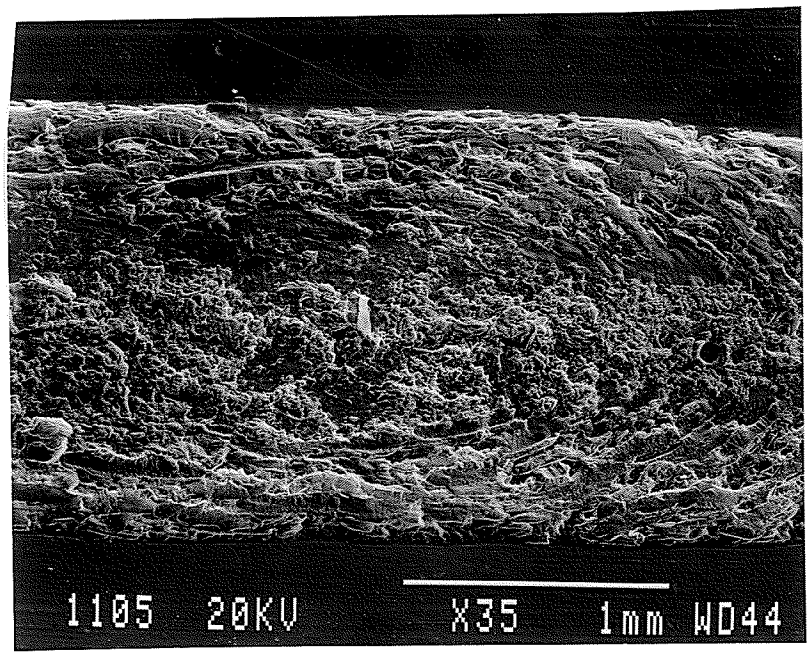


Fig.4-41 SEM morphology of the wear track after 8kg, room temperature with 335,000 cycles test (600°C heat treated coating)

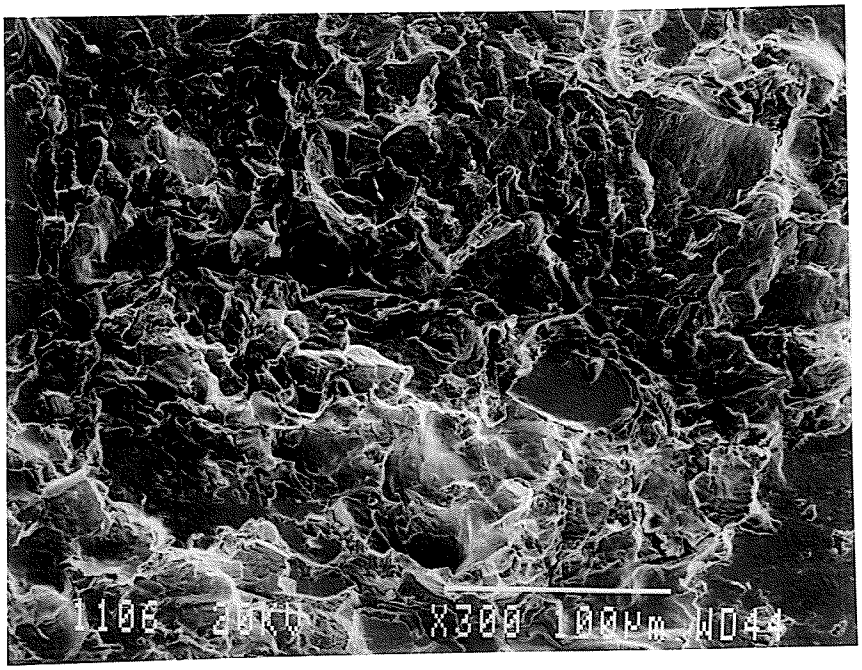

Fig.4-42 The SEM image of the wear track bottom in Fig.4-41

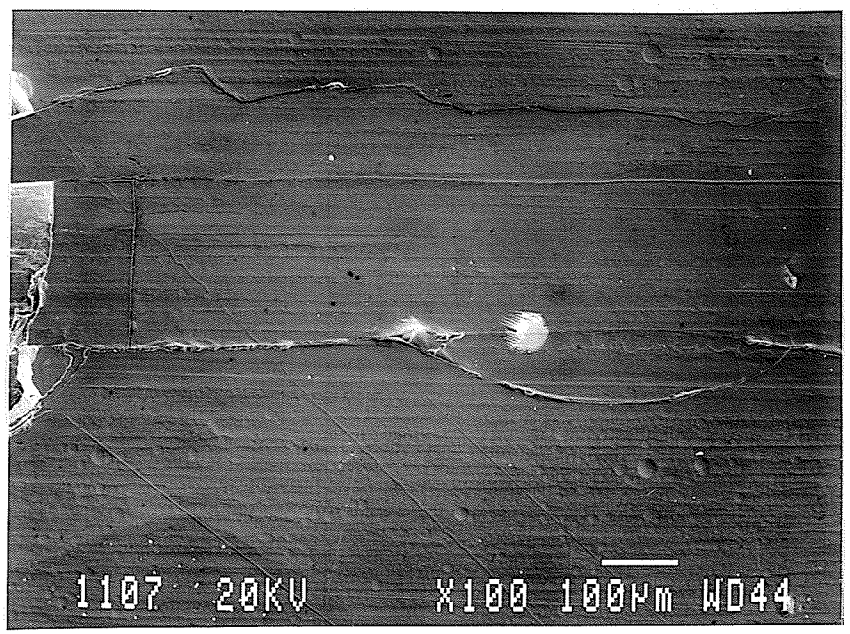


Fig.4-43 SEM morphology of the smooth part of the wear track after 8kg, room temperature with 335,000 cycles test (600°C heat treated coating)

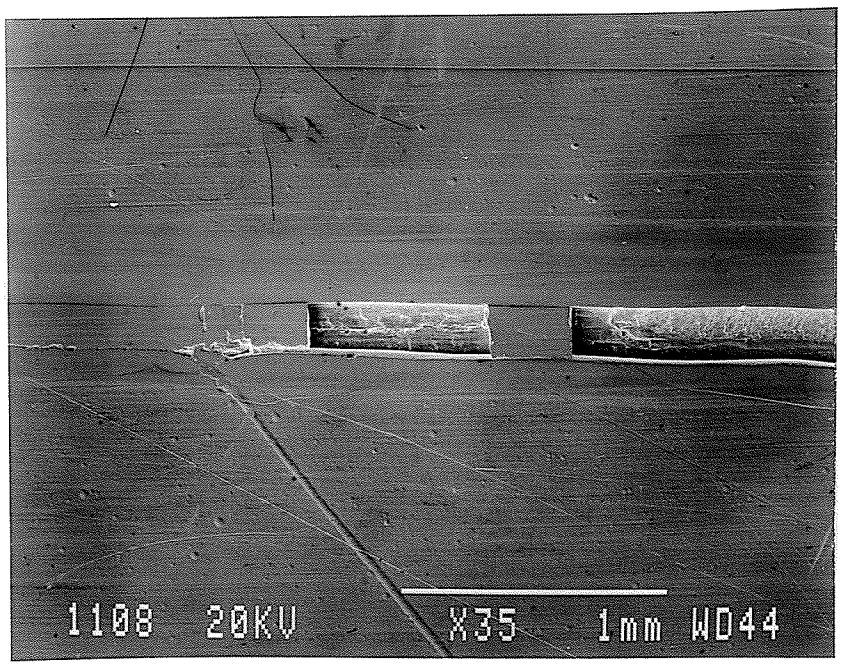


Fig.4-44 SEM morphology of the wear track after 8kg, 100°C with 335,000 cycles test (600°C heat treated coating)

area on the wear track. The results also indicate that the Ni content decreased and P, S content increased on the wear track after 100°C test.

Table 4-7 The energy dispersive spectrum quantitative analysis results (600C/1hr heat treated coatings after 335,000 cycles test)

| | | | Ni | | P | | S | |
|---|---|---|---|---|---|---|---|---|
| | Place | Point | at% | wt% | at% | wt% | at% | wt% |
| 8kg Room Temp (Fig. 4-43) | Non wear | 1 | 82.05 | 89.65 | 17.95 | 10.35 | 0.00 | 0.00 |
| | Wear track | 1 | 79.83 | 88.21 | 18.83 | 10.98 | 1.34 | 0.81 |
| 8kg 100°C (Fig.4-44) | Non wear | 1 | 80.95 | 88.96 | 19.05 | 11.04 | 0.00 | 0.00 |
| | Wear track | 1 | 74.80 | 84.85 | 21.80 | 13.05 | 3.40 | 2.11 |

The above results obtained from the tests under lubrication have clearly shown that the temperature has a significant effect on the wear of the electroless nickel-phosphorus coatings under reciprocating sliding conditions. An increase in temperature decreases the weight loss of the coatings. The wear mechanism of the coatings changes when load changes from low to high load and when temperature changes from room temperature to 100°C. The wear mechanism and the temperature effect will be discussed in detail in the "Discussion" Chapter.

## 4.5 THE WEAR TEST RESULTS UNDER DRY CONDITIONS

The wear tests without lubrication have been carried out on two kinds of coatings: as-deposited and as-deposited+600°C/1hr heat treated coatings. The test temperature was set at room temperature, 50°C and 100°C. The testing cycle was chosen as 500 cycles with frequency of 160/min. The load was 4kg and sliding distance was kept at 30mm. Weight loss at 500 cycles was not significant for both coatings.

### 4.5.1 MORPHOLOGY OF THE WEAR TRACK OF AS-DEPOSITED COATING

Fig.4-45 shows the SEM image of the wear track after a room temperature test. The deformation and shear of the coating, and abrasive scratching by the tiny debris can be seen in Fig.4-46. This indicates that the adhesive and abrasive wear occurs during reciprocating sliding. There is no delamination and spalling observed on the wear track. At the end of the wear track, the accumulation of the debris, the deformation and shear of the coating layers can be found (Fig.4-47). The wear tracks after the 50°C and 100°C tests have similar morphology as that of the room temperature test (Fig.4-48 and Fig.4-49). It is, however, noted that the wear track after 100°C test shows more smooth characteristics than those at lower test temperatures. This can be observed from Fig.4-50.

### 4.5.2 MORPHOLOGY OF THE WEAR TRACK OF 600°C/1HR HEAT TREATED COATING

Fig.4-51 to Fig.4-53 show the three wear tracks after three testing temperatures. The wear track becomes smoother as the temperature increases. Severe adhesion occurs at the track center during the room temperature test (Fig.4-54). The coating surface gets polished on the sides of the wear track. The adhesion, however, decreases when temperature increases so that the wear track becomes smoother at the high temperature test. Fig.4-55 and Fig.4-56 show the wear track ends with the accumulation of the wear debris. The wear debris after the 100°C test are more tiny than those after the room temperature test, indicating the polishing wear dominating mechanism at the 100°C test.

The X-ray mapping of the wear track gives very interesting results. Fig.4-57 and Fig. 4-58 show the X-ray maps for Ni and P obtained from the wear track after the room temperature test and

after the 100°C test. Both show that the Ni content slightly decreases and P content increases on the wear track, the same results as those obtained from the lubricated test at high temperature conditions. SEM/EDS quantitative analysis of the same spots fully supports the X-ray mapping results (Table 4-8).

Table 4-8 The energy dispersive spectrum quantitative analysis results

| | | | Ni | | P | | O | |
|---|---|---|---|---|---|---|---|---|
| | Place | Point | at% | wt% | at% | wt% | at% | wt% |
| Room temp | Non wear | 1 | 81.90 | 89.58 | 18.03 | 10.40 | ---- | ---- |
| | | 2 | 81.77 | 89.48 | 18.23 | 10.52 | ---- | ---- |
| | Wear track | 1 | 79.54 | 88.27 | 19.57 | 11.46 | 0.89 | 0.27 |
| | | 2 | 79.39 | 87.95 | 20.61 | 12.05 | not counted | not-counted |
| 50°C | Wear track | 1 | 75.57 | 86.01 | 22.08 | 13.26 | 2.35 | 0.73 |
| | | 2 | 77.38 | 86.64 | 22.62 | 13.36 | not counted | not counted |
| 100°C | Wear track | 1 | 77.47 | 86.89 | 21.77 | 12.88 | 0.76 | 0.23 |
| | | 2 | 79.72 | 88.17 | 20.28 | 11.83 | not counted | not counted |

The SEM/EDS spectrum shows the oxygen peak on all wear tracks (Fig.4-59), which indicates that the oxidation during the test must have occurred. Although the oxygen content is analyzed at few points, the data are not very accurate due to the limitation of the SEM/EDS and therefore is not quantitatively analyzed at all points. The results, however, do not change the trend of Ni and P content.

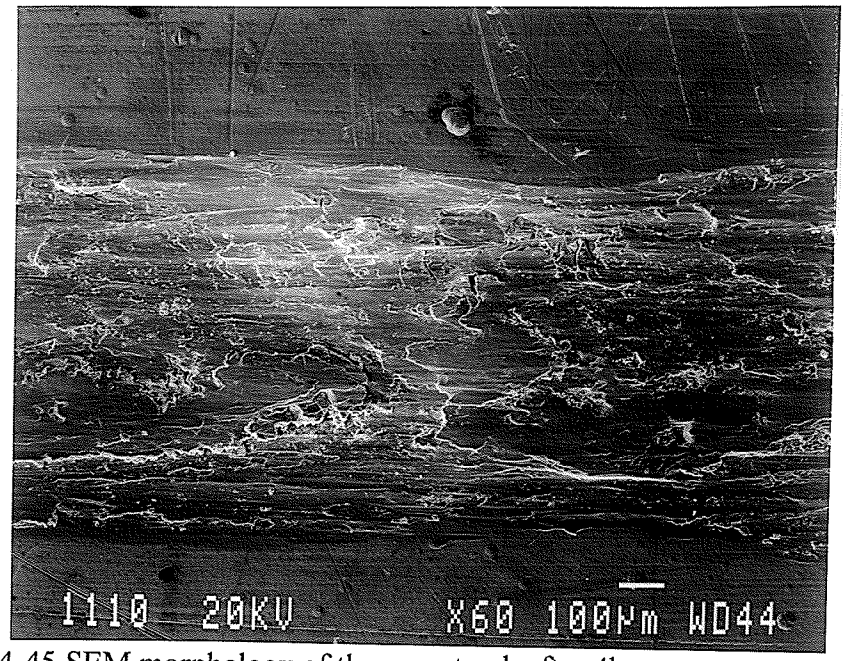


Fig.4-45 SEM morphology of the wear track after 4kg room temperature dry wear test (as-deposited coating)

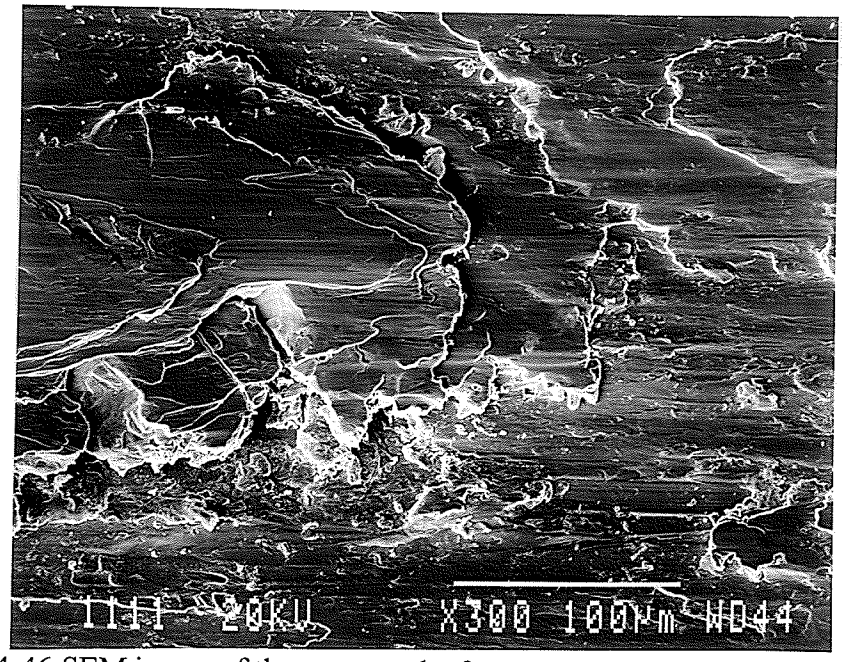


Fig.4-46 SEM image of the wear track after room temperature dry wear test under high magnification (as-deposited coating)

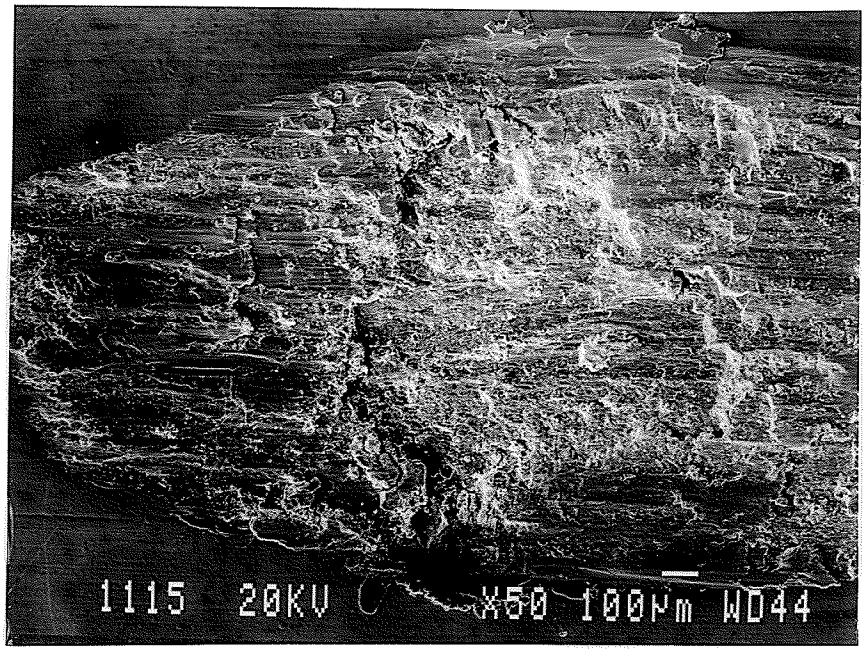


Fig.4-47 The wear track end of as-deposited coating after dry wear room temperature test

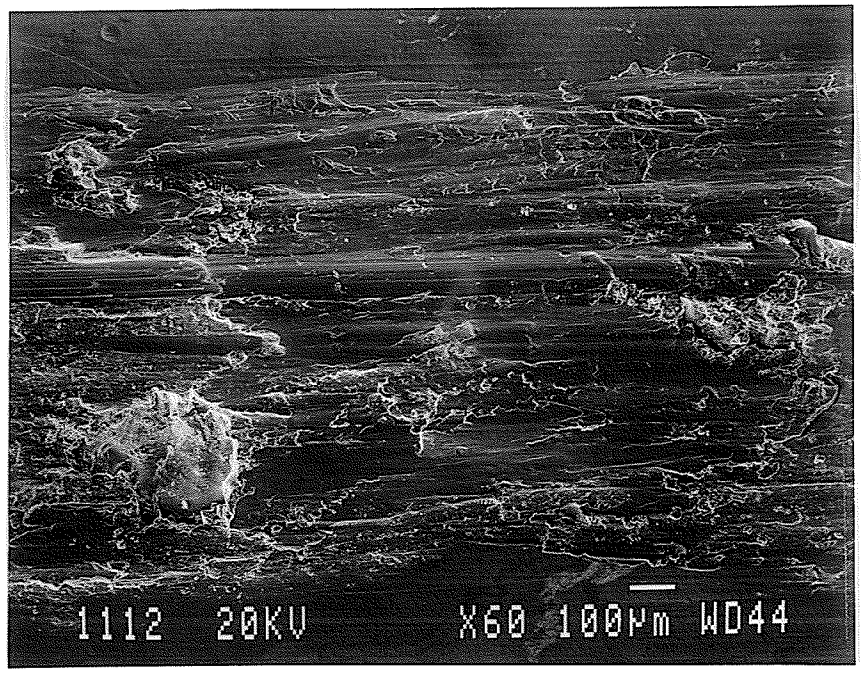


Fig.4-48 SEM image of the wear track after 50°C dry wear test

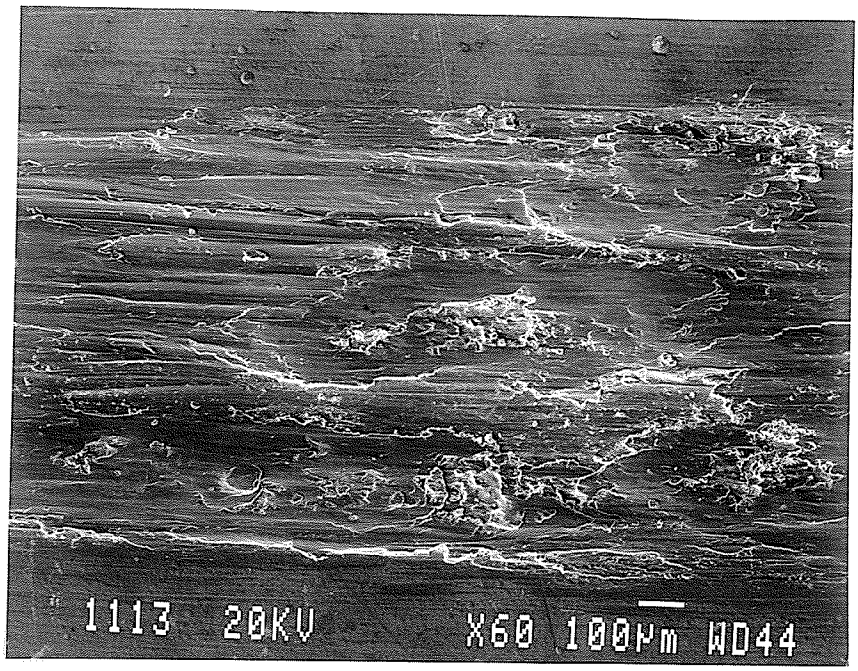


Fig.4-49 SEM image of the wear track after 100°C dry wear test

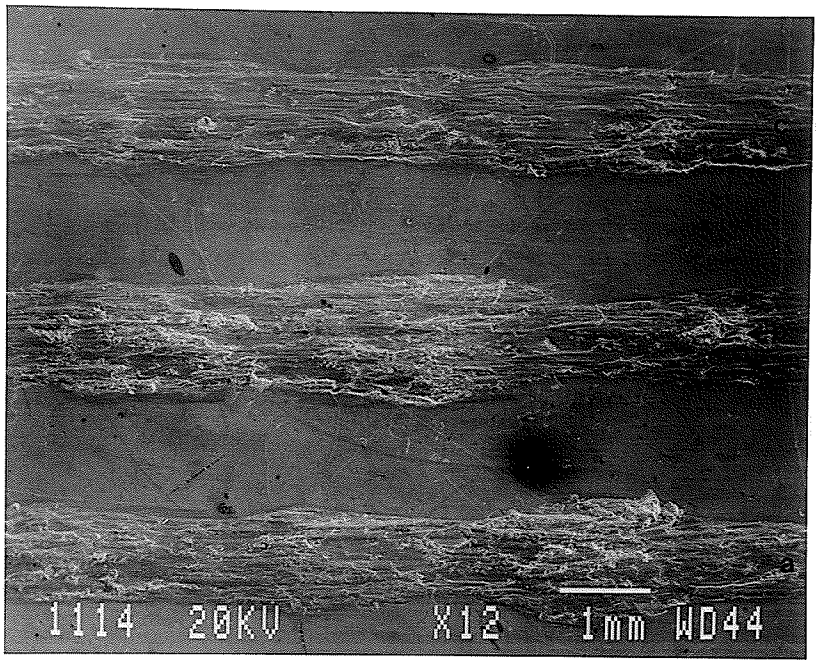


Fig.4-50 SEM image of the wear tracks at three test temperatures
a. room temperature; b. 50°C; c. 100°C

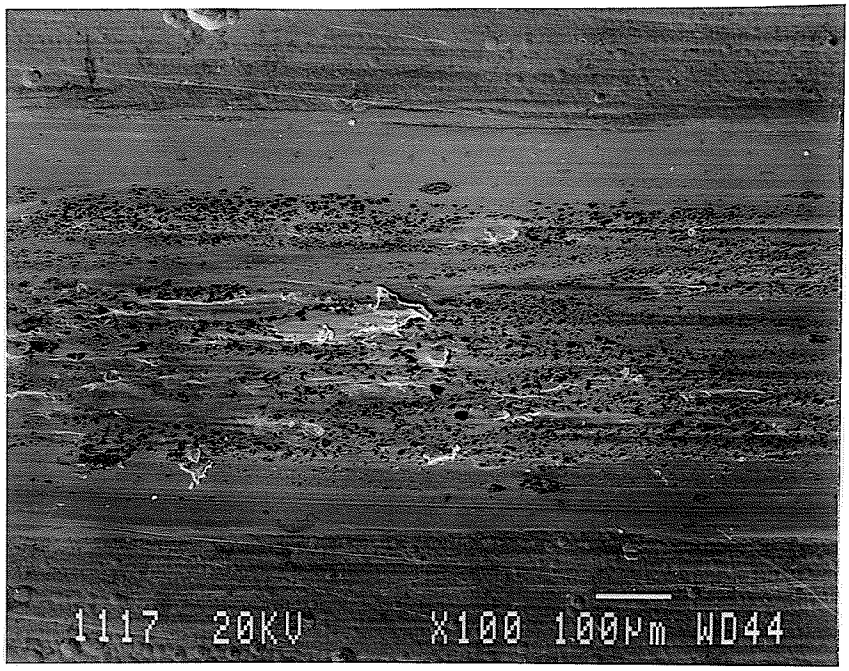


Fig.4-51 SEM morphology of the wear track after dry wear room temperature test (600°C/1hr heat treated coating)

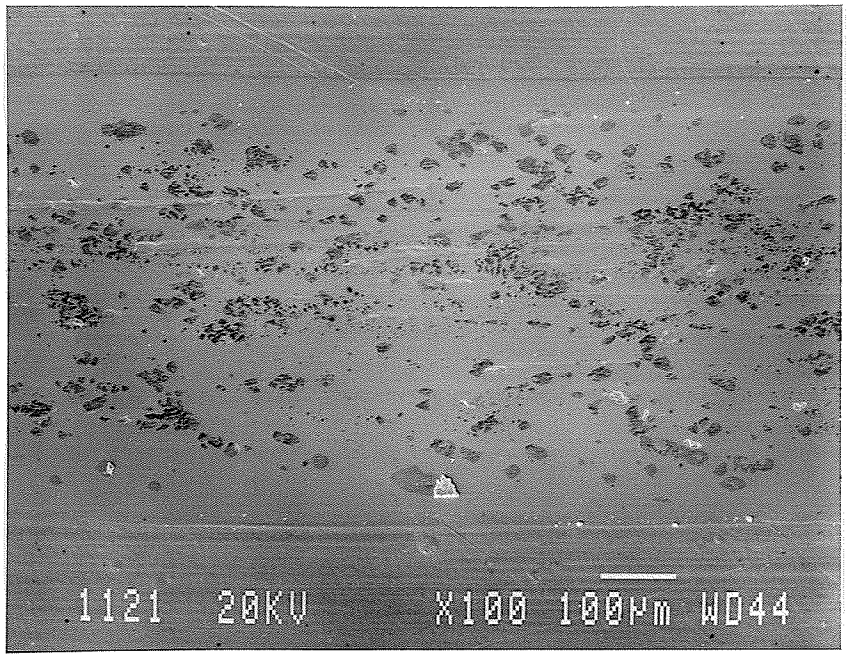


Fig.4-52 SEM morphology of the wear track after dry wear 50°C test (600°C/1hr heat treated coating)

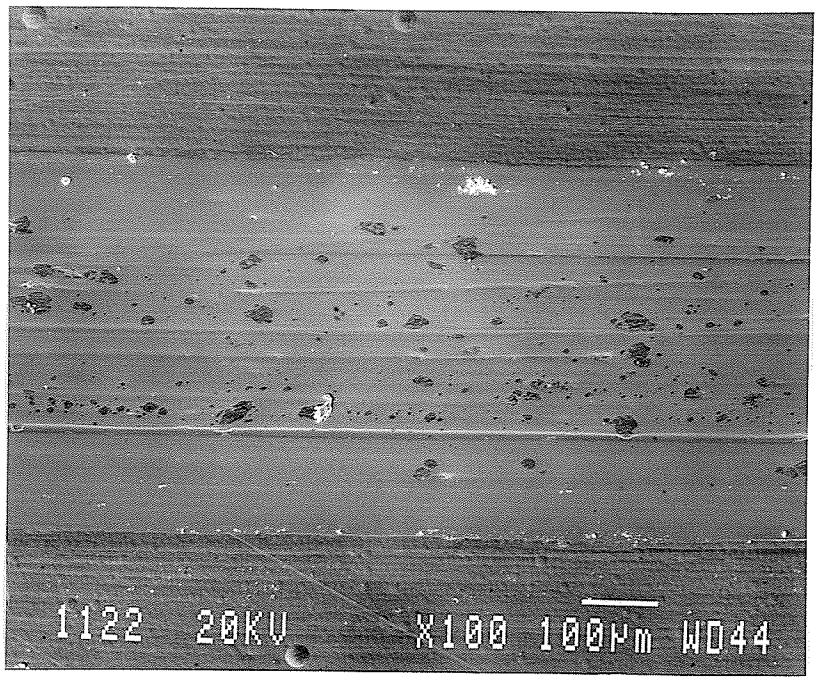


Fig.4-53 SEM morphology of the wear track after dry wear 100°C test (600°C/1hr heat treated coating)

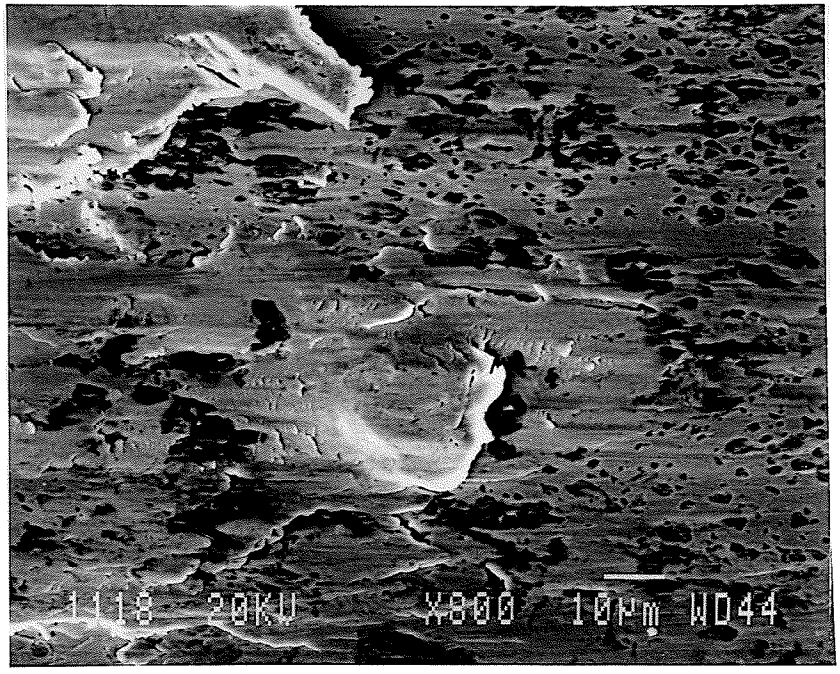


Fig.4-54 SEM morphology of the wear track after dry wear room temperature test. Enlarged track center (600°C/1hr heat treated coating)

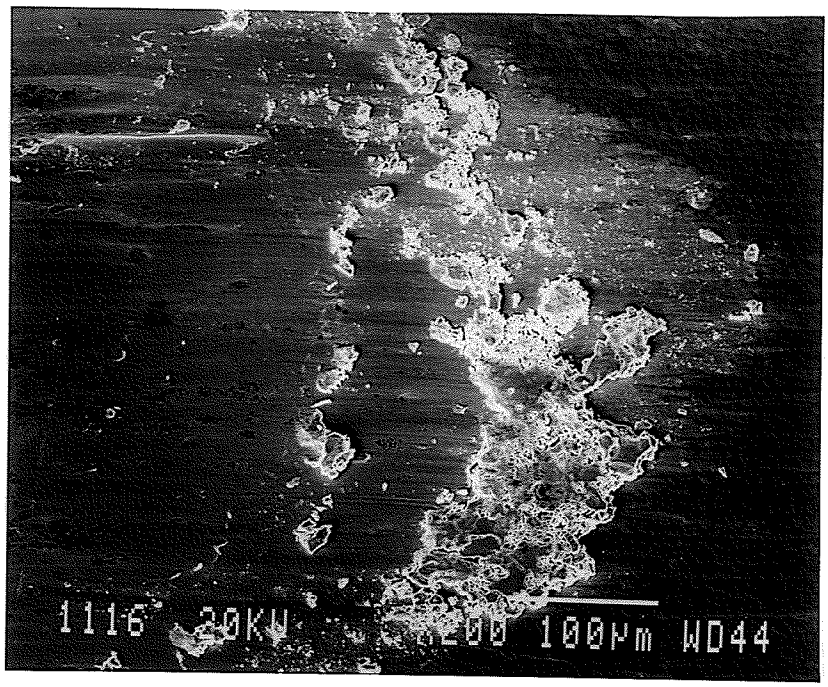


Fig.4-55 SEM morphology of the wear track end after dry wear room temperature test (600°C/1hr heat treated coating)

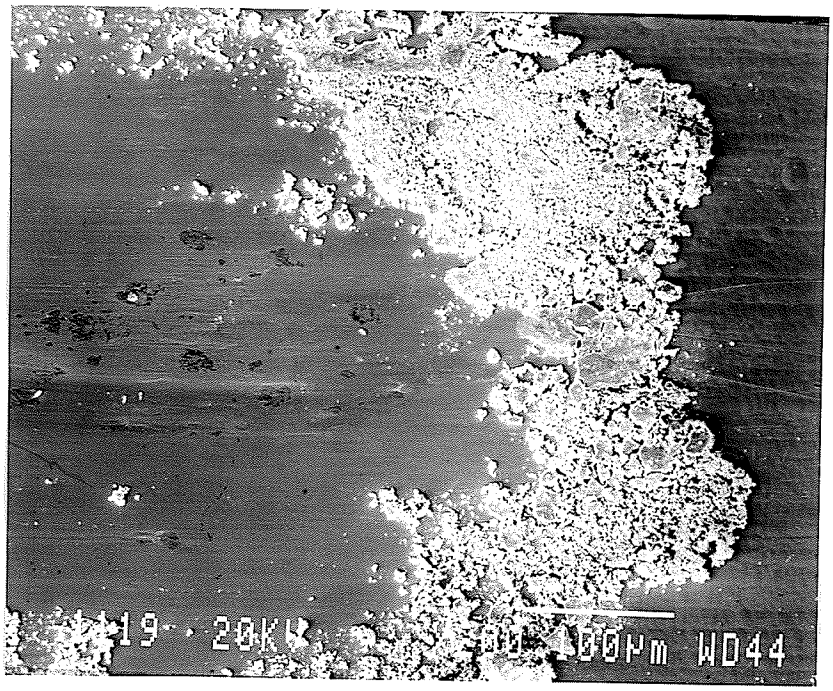


Fig.4-56 SEM morphology of the wear track end after dry wear 100°C test (600°C/1hr heat treated coating)

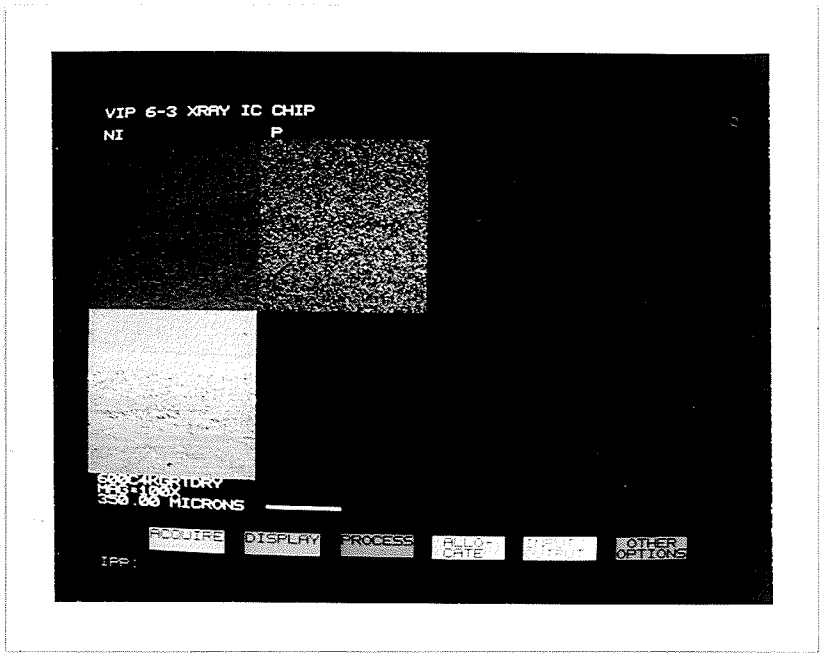


Fig.4-57 X-ray map of the wear track after dry wear room temperature test (600°C/1hr heat treated coating)

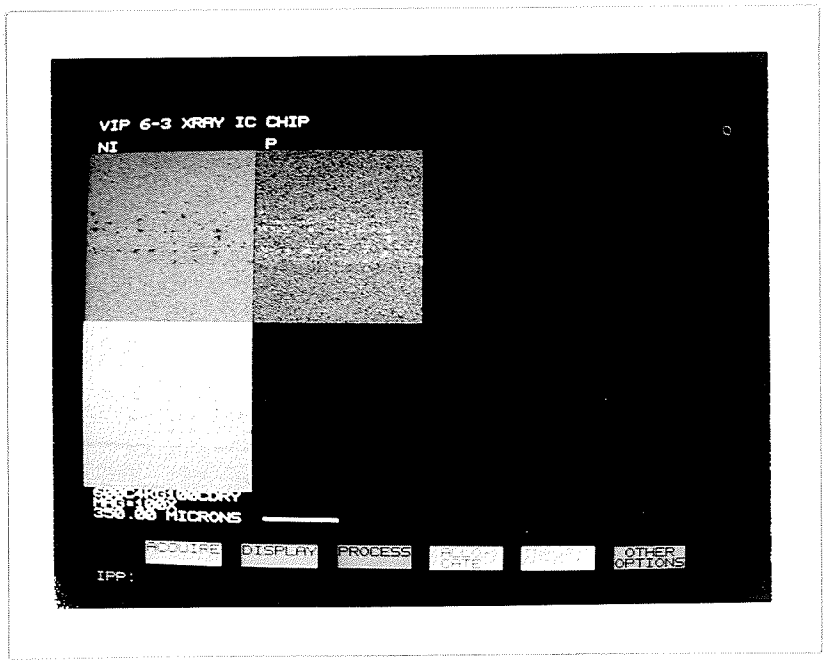


Fig.4-58 X-ray map of the wear track after dry wear 100°C test (600°C/1hr heat treated coating)

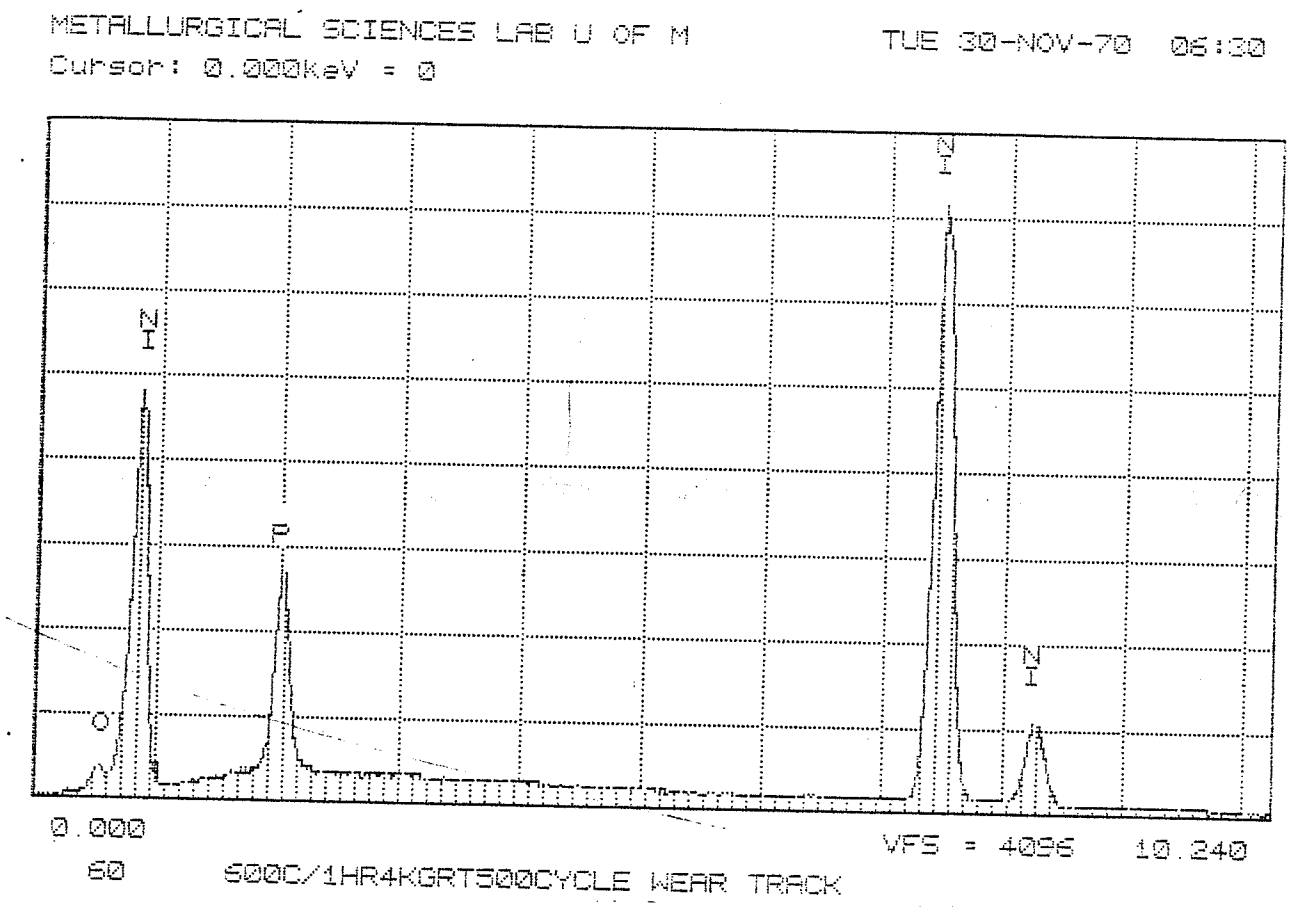


Fig.4-59 SEM/EDS spectrum of an analyzed point on the wear track after dry wear room temperature test. Note the oxygen peak

# CHAPTER 5

# DISCUSSION

## 5.1 THE MICROSTRUCTURE OF THE NICKEL PHOSPHORUS COATINGS

The structure of the electroless nickel phosphorus coatings has been investigated by several investigators [39-43, 52-53]. Different phosphorus content coatings can be obtained by using appropriate solutions [34, 43]. For low P content coatings, the microstructure of the as-deposited coating is composed of supersaturated nickel solid solution [39, 54], which after heating to 400°C transforms into many small coherent precipitates forming in the matrix, resulting in significant dispersion hardening [54]. At 600°C, incoherent $Ni_3P$ precipitates develop in the nickel matrix, together with a precipitous drop in hardness. Coatings with medium and high phosphorus contents show amorphous phase structure as examined by X-ray diffraction, but the TEM reveals that small tiny nickel crystallites present in the amorphous matrix, like the results obtained in this study [39-43, 52-53]. This has even raised arguments about where to draw the line for the presence of an amorphous structure with respect to P content. It is noted that even at a higher P content, the as-deposited coating has tiny Ni crystallites in it [52]. Bredael et al [52] stated that the border between microcrystalline and amorphous electrodeposited Ni-P coatings can be shown between 11.6 and 13.1 wt % P.

The Ni-P binary phase diagram shows that in the range 0-15 wt% phosphorus content, the equilibrium structure is $Ni+Ni_3P$ [56]. In addition, the solid solubility of phosphorus in nickel is negligible at room temperature. The as-deposited electroless nickel phosphorus coating obtained by Shipley formula NIPOSIT Electroless Nickel NL-63, in this study, gives 10-12 wt% P content (Table 4-1). The X-ray diffraction (Fig.4-11) shows the existence of an amorphous state of the coating, but TEM observation reveals the coating is composed of amorphous phase with tiny

nickel crystallites in it (Fig.4-3). Selected area diffraction patterns in Fig.4-4 show clearly the ring diffraction of amorphous and nickel crystallites. The size of the nickel crystallites is very small so that it is even hard to reveal them under TEM (Note the magnification of the TEM image Fig. 4-3 is 150k). This microstructure is in conformance with the previous results [43, 52].

The structure of the electroless nickel-phosphorus coating varied with P content is due to the electroless plating process and the fact that the atomic radius of phosphorus is smaller than that of nickel, according to Lambert and Duquette [54]. The atomic radius of phosphorus is 0.109nm and nickel is 0.125nm. This difference allows the nickel lattice to accommodate small amounts of phosphorus with only small increases in lattice stress and misfit. Electroless coating process is a rapid, low temperature process for forming alloys. The electroless plating process does not provide the time or temperature necessary for atomic diffusion and nucleation. Therefore the coating cannot reach its equilibrium state or relieve stresses. The transition from a microcrystalline to an amorphous structure around 7-10 wt% phosphorus can be expected since the level of lattice misfit and stress steadily increases with the addition of more phosphorus solute atoms. In addition, the Ni-P system has an Ni-$Ni_3P$ eutectic point, which is a feature found in the glass-forming region of most glass-forming systems, thus promoting supersaturated and/or amorphous microstructures [54].

The as-deposited nickel-phosphorus coatings will crystallize or transform into nickel crystallites and nickel phosphides. The major or final nickel phosphide after transformation is $Ni_3P$ after several investigations [39-43]. After heat treatment at 400°C, the as-deposited coating with 10-12 wt% P in this study has crystallized into nickel and nickel phosphides. X-ray diffraction reveals the major nickel phosphide is $Ni_3P$ (Fig.4-12). The size of the nickel crystallites and nickel phosphides are very small. This has been clearly shown in Fig. 4-5. Note that the magnification of this TEM image has already been 100K. SADP gives the nickel rings and diffraction streaks of $Ni_3P$. After heat treatment at 600°C, the coating has crystallized into large size of nickel

crystallites and nickel phosphides, mainly $Ni_3P$ (Fig. 4-7). The SADP can be obtained from single particles in the coating. The content of the nickel crystallites increases with the increase of the heat treatment temperature. X-ray diffraction pattern of 600°C heat treated coating gives higher intensity of nickel peaks than the 400°C heat treated coating (Fig. 4-14).

It is clear now that the Ni-P coating is mainly composed of Ni and $Ni_3P$ after heat treatment. The amorphous phase is changed finally into $Ni_3P$ and Ni phases. Few investigators, however, indicated the existence of $Ni_5P_2$ or other nickel phosphides in the heat-treated Ni-P coatings, although most of them did the X-ray diffraction analysis. Hur et al noted that the $Ni_5P_2$ appeared in the high P content coatings after heat treatment [43]. The X-ray diffraction results in this study, however, clearly show that there are some other phases present in the heat-treated coatings. The X-ray diffraction patterns from both 400°C/1hr and 600°C/1hr heat treated coatings give apparent peaks that do not belong to nickel or $Ni_3P$ (Fig.4-12, 4-13). The obvious peaks, after search and match, indicate most possibility the existence of $Ni_5P_2$ phase (peak no. 21 and 25 in Fig. 4-12 and 21 and 26 in Fig.4-13). The other peaks (15, 29 and 30 in Fig. 4-12 and 16, 30 and 31 in Fig. 4-13) are a good match with $Ni_2P$ phase. Unfortunately, these two phases are not identified by TEM due to the limitation of the time and the possible small size of the particles. Vafaei-Makhsoos [40] in his studies has stated the possible formation of $Ni_5P_2$ and similar kinds of nickel phosphides when the amorphous coating was heated up. The formation of $Ni_xP_y$ form of nickel phosphides depends on several factors. It is not clear now in which situation there will be the formation of $Ni_5P_2$ kinds of phases after heat treatment of Ni-P coating. It is believed that the coatings with high content of P are likely to form $Ni_xP_y$ phase after heat treatment [43]. The present results in this research has clear shown by X-ray the existence of $Ni_5P_2$ and/or $Ni_2P$ nickel phosphides in the 10-12 wt% electroless nickel-phosphorus coatings after 400°C and 600°C heat treatment. Therefore, it is believed that the coating with high P content is not only composed of nickel crystallites and $Ni_3P$ after heat treatment, but also includes other nickel phosphides like $Ni_5P_2$ and $Ni_2P$.

## 5.2. THE HARDNESS OF THE COATINGS

The microhardness values of the coatings (Fig. 4-15) indicate that the coating after 400°C/1hr heat treatment has the highest hardness with 917DPH. The coating after 600°C/1hr heat treatment has medium high hardness. The as-deposited coating has the lowest hardness of the three kinds of coatings. The same trend about the hardness has been obtained by several investigators and the highest hardness value of the coating is achieved when heat treating the coating at around 400°C [37-38, 49, 57]. The hardness of the coating is mainly determined by the microstructure of the coatings. The as-deposited coating is mainly composed of the amorphous phase with tiny nickel crystallites. The hardness value of this coating is very low. The coating after 400°C/1hr heat treatment is crystallized with a small size of nickel crystallites and precipitates of $Ni_3P$. The size of both Ni and $Ni_3P$ is very small, so this coating gives the highest hardness value. The nickel and nickel phosphide particles in the coating have grown after 600°C/1hr heat treatment, hence this coating has a lower hardness value than that after 400°C/1hr heat treatment.

## 5.3 WEAR MECHANISMS OF AS-DEPOSITED NI-P COATINGS AT DIFFERENT TEMPERATURES UNDER LUBRICATION CONDITIONS.

As mentioned in Chapter 4, the wear track after the 4kg room temperature test shows clearly the delamination phenomenon (Fig.4-18). Polishing and scuffing takes place at the beginning of sliding. The delamination occurs after 50,000 sliding cycles. Fatigue type bands show on the delaminated spots (Fig. 4-19). The wear track after the 8kg room temperature test is different from the one after the 4kg room temperature test. Delamination also takes place here after the initial polishing and scuffing, but severe spalling occurs afterwards due to the high load or high stress levels (Point A in Fig 4-22). The debris from spalling and delamination causes severe abrasive wear in the sliding track (Fig. 4-22) and the substrate shows up (Fig. 4-23). The weight

loss value under 8kg load is thus almost four times higher than that under 4 kg load at room temperature because of the severe abrasive wear occurred under high load condition (Fig. 4-16).

The wear tracks after the 4kg and 8kg, 100°C test have similar morphology. Both were smooth, showing the obvious polishing and scuffing wear morphology, except severe cracking occurred on the wear track after the 8kg 100°C test (Fig. 4-21 and Fig. 4-24). The cracking may be due to high normal load (stress) on the coating. The weight loss under both loads at 100°C test gives the similar value which shows in Fig. 4-16.

It is known that when a solid is subjected to load, stresses are produced in the solid which increase as the load is increased [2]. These stresses will cause deformation and if the load keeps increasing, the elastic behavior is replaced by plastic behavior, in which the material is permanently deformed. The contact stress between the two contact bodies depends upon the contact types. For the contact of a sphere on a plane body, the actual size of the contact zone increases due to increased flattening of the curved surfaces. This can be described by Hertzian values. For a sphere on a plane, the actual relationship for the contact size is given by

$$a = \left| \frac{3WR(1-\nu^2)}{E} \right|^{\frac{1}{3}}$$

where a is the contact size, W is the load, R is the radius of the sphere, $\nu$ is the Poisson ratio and E the young's modulus of the material. The pressure distribution is given by

$$p = \frac{3W}{2\pi a^2}(1-\frac{R^2}{a^2})^{\frac{1}{2}}$$

where p is the pressure. For tribological consideration, the stress distribution is important. For spherical contact, the maximum stress occurs at a small distance below the surface and this is different from the uniform pressure contact (Fig. 5-1) [2]

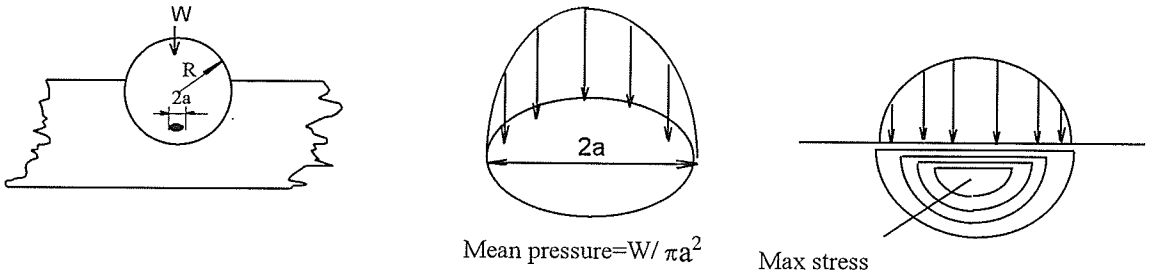


Fig. 5-1 The contact of a sphere and the resulting pressure and stress distribution [2]

Suh [9], who established the delamination theory, states that the delamination wear follows sequential events which lead to loose wear sheet formation:

1) the deformation of asperities generates a relatively smooth surface.
2) the surface traction induces incremental plastic deformation per cycle of loading which accumulates with repeated loading.
3) cracks are nucleated below the surface. Crack nucleation cannot occur very near the surface because of the triaxial state of compressive loading which exists just below the contact region.
4) further loading and deformation causes the cracks to extend and propagate, eventually joining with neighboring cracks. The cracks tend to propagate parallel to the surface at a depth governed by material properties and the state of loading.
5) long and thin wear sheets delaminate when the cracks finally shear to the surface.

Suh also indicated that the crack nucleation is related to the inclusions or hard second-phase particles. The crack nucleation in single-phase material without any inclusions is not clearly understood up to now.

Under the lubrication condition, the contact surfaces are separated by a lubricant film and adhesive or abrasive wear is eliminated. The applied load is still transmitted to the solid surfaces through a lubricant film, and can still cause stresses in the surface, so that fatigue-type failures are not excluded.

For the ball-on-block wear test, the maximum stress is located below the contact surface. The tiny nickel crystallites in the amorphous as-plated coatings and the hard nickel phosphides in the heat treated coatings may be the source of crack nucleations. Therefore, wear at room temperature for the as-plated coating under low loadings exhibites the obvious delamination mechanism of wear (Fig. 4-18). Clear fatigue bands are obvious in Fig. 4-19, which indicates the crack generated and propagated under the surface. The wear at high loading exhibits the delamination also at low cycles following the severe wear of spalling and abrasion (Fig. 4-22).

## 5.4 WEAR MECHANISMS OF HEAT TREATED NI-P COATINGS AT DIFFERENT TEMPERATURES UNDER LUBRICATION CONDITIONS.

The coatings after heat treatment become crystallized and hard nickel phosphides are formed (Fig. 4-5 and Fig. 4-7). Nickel crystallites and $Ni_3P$, $Ni_5P_2$ or $Ni_2P$ nickel phosphides are formed in the coatings after heat treatment. The size of the nickel crystallites and nickel phosphides in the coating after 400°C/1hr heat treatment are very small (Fig. 4-5) while the size of the particles in 600°C/1hr heat treated coating becomes very large (Fig. 4-7) compared to that in 400°C/1hr heat treated coating. Similar results have been reported by several other investigators [43, 52]. The hardness increases as compared to the as-plated coating. The coating after 600°C/1hr heat treating, has shown a diffusion layer at the substrate (Fig. 4-2c) which increases the adhesion between the coating and the substrate. The wear resistance is increased, although the hardness of the coating is lower than the coating after 400°C/1hr heat treatment

[49]. The coating after 400°C/1hr heat treatment has more severe delamination (Fig. 4-32) than that after 600°C/1hr heat treatment (Fig. 4-38). Parker [38] also indicated that the hardness and wear resistance are not synonymous and sometimes a softer coating will provide longer wear life. In his study, the coating after 600°C heat treatment gives the better wear resistance under a rotating steel ball. It is noted that the coating after 400°C/1hr heat treatment is more brittle than that after 600°C/1hr heat treatment and this has been reported by Yu and Zhang [49] as well. Compared with the as-deposited coating, the wear resistance of the coatings after heat treatment has improved significantly at 8kg load, room temperature test. The weight loss of the as-deposited coating is higher than that of the heat treated coatings after wear test (Fig. 4-16). The morphology of the wear track shows delamination wear mechanism for the as-plated coating under low loading condition. The difference is that the severe cracking appears on the wear track because of the high loading condition for both heat-treated coatings. It is, therefore, believed that the delamination wear mechanism is the dominated one in the reciprocating sliding wear of heat-treated coatings. Spalling also occurs after delamination for the 400°C/1hr heat treated coatings (Fig.5-32). The Little abrasive wear is also displayed due to the little debris being trapped during the sliding wear.

The wear track of both heat treated coatings is almost intact after a 100°C test (Fig. 4-36, Fig. 4-39). There are only a few cracks along the sliding direction. The morphology of the wear track is smooth with little delamination on the 400°C/1hr heat treated coating. No delamination occurred on the 600°C/1hr heat treated coating. Polishing wear is a dominating wear mechanism for both coatings at 100°C test. The weight loss decreases compared to that for room temperature tests. The high cycle test results of the 600°C/1hr heat treated coating gives strong support for the temperature effect. The coating surface has delaminated and spalled after room temperature test. Abrasive wear has occurred on certain areas as well after the room temperature tests (Fig. 4-42}. The coating surface after 100°C test, however, has only a few delaminations (Fig. 4-44).

Therefore, temperature has improved the wear resistance of the Ni-P coatings under the lubricating condition.

## 5.5. EFFECT OF TEMPERATURE ON WEAR BEHAVIORS OF NI-P COATINGS UNDER LUBRICATION CONDITION

It is obvious that the wear mechanism has changed for the coatings during high temperature tests compared to the room temperature test under lubrication sliding. Few delaminations, spalling and abrasions occur at 100°C test. The wear tracks for all the test on all the coatings at 100°C show the polishing, and scuffing wear appears to dominate on the coating surface. Cracking on the coatings appears at the high loading condition. Compared to the wear at room temperature, the wear resistance is increased at 100°C. High wear resistance at high temperature test could be attributed to the following aspects:

**1) The self-lubricity of P and S reduce the friction coefficient**

The SEM/EDS and X-ray mapping reveals that the content of Ni and P changes in the wear track. The Ni content decreases and the P content increases after the 100°C test on the wear track. Meanwhile, some sulfur shows up on the wear track as well. It is known that the P and S themselves are good lubricants [32]. The P and S present on the wear track would therefore reduce the wear because of the reduced friction between the contact surface. The chemical analysis of the oil has shown that there is 0.485 mass% S in the oil, and 1011 μg/g phosphorus. The extra P exhibited on the surface of the wear track most likely comes from the oil. The high temperature and the induced frictional heat promote the diffusion of the P and S from the oil into the surface of the coating.

**2) The formation of the film of S or P compounds decreases the wear**

Usually, a small quantity of additive is dissolved in a lubricating oil [58]. Nugold 10W30 motor oil also includes several kinds of additives [59]. The most commen additives used for this purpose contain phosphorus, chlorine and sulfur. In general, these materials function by reacting with the surface to form a surface film which prevents metal-to-metal contact. If the surface film formed has a low shear strength, it will not only protect the surface, it will also give a low coefficient of friction. Sulphide films are generally more stable, are unaffected by moisture and retain their lubricating properties up to high temperatures [55]. The chemical analysis results, however, revealed the presence of S and P in the oil. Therefore, the formation of sulfur or phosphorous compounds film on the surface is possible. Effectiveness of sulfide films in reducing friction has been shown to be a function of film thickness [55]. The formation of sulfur film reduces the friction of coefficient because of the low shear stress needed for the films [55]. It is thus believable that the high temperature promotes the formation of the films during the test as the supply of the oil is constant. Therefore, the wear mechanism in the high temperature test is dominated by polishing and scuffing.

## 5.6 THE WEAR MECHANISMS OF ELECTROLESS NI-P COATINGS UNDER DRY CONDITION

When tested under the dry condition (without lubrication), the surface of the ball directly contacts the surface of the coating. There is no oil film to separate this metal-to-metal contact. The friction coefficient is large and the deformation of the asperities on both mating parts is severe. Therefore, adhesion (cold joining) and seizure are likely to occur. Tsuji et al [17, 18] also found that an adhesive wear mechanism is dominated one when carbon steels are tested at dry

condition. As the temperature increases, an oxidation film forms on the surface of the testing material [20, 21]. For the Ni-base alloy, NiO is likely to form at high temperature. The thickness of the NiO film determines the wear of the materials [21, 55]. As sliding continues, frictional heating increases at the points of contact, thus increasing the amount of transient oxidation. Although oxide is removed on each traverse, more is formed due to the high localized temperature. If the temperature becomes high enough, a stable, thermally softened, or even molten, layer is formed [21]. When this happens, a drop-off in the coefficient of friction is observed and only very limited further wear takes place. As the ambient temperature is increased, the formation of the oxide layer becomes easier, due to a higher overall temperature, caused by a combination of ambient and frictional heating in the immediate surfaces during sliding. For the electroless Ni-P coatings, apart from the formation of the oxide film NiO, the self-lubricity of P and the possible formation of the Ni-P compound decreases the wear of the coating as well.

The SEM morphology of the wear tracks indicates that the severe adhesive wear is involved in the reciprocating sliding of Ni-P as-deposited coatings for all three testing temperatures (Fig. 4-46 - Fig. 4-53). The formed debris also causes the abrasive scratches afterwards. The SEM/EDS results show that the content of Ni and P changes and the O content increases. Therefore, it is definite that the formation of the Ni-P compound or oxide film occurrs during sliding. Seizing occurrs at first for the test at room temperature when observing the sliding to start. The initial sliding for the test at 100°C iss much smoother than that at the room temperature test, although adhesive and abrasive wear still occurrs. This may contribute to the formation of the oxide film. The increase of the temperature promotes the formation of oxide film up to a certain thickness so that the wear of the coatings is decreased.

# CHAPTER 6

# CONCLUSIONS

The following conclusions have been reached:

1. The microstructure of as-deposited electroless nickel phosphorus coating with 10-12 wt% P is mainly amorphous phase with tiny nickel crystallites present in it.

2. The microstructure of the coatings with 400°C/1hr and 600°C/1hr heat treatment is composed of nickel crystallites and nickel phosphides $Ni_3P$, and possibly $Ni_5P_2$ phase. The size of the nickel crystallites and nickel phosphides increases with the increase of heat treatment temperature.

3. The average hardness of the as-deposited coating is 574 DPH. The hardness increases to 917 DPH after 400°C/1hr heat treatment, but the value decrease to 715 DPH after 600° C/1hr heat treatment.

4. Under lubrication conditions, a temperature rise from 25°C to 100°C reduces the lubricated wear of as-deposited electroless nickel-phosphorus coatings, especially at high loads. An increase in temperature also reduces the lubricated wear of coatings after 400° C/1hr and 600°C/1hr heat treatment.

5. For as-deposited coatings under lubrication conditions, the wear mechanism is mainly delamination for the 4 kg, room temperature test and delamination/spalling and abrasive wear for the 8 kg room temperature test. The wear mechanism becomes polishing wear at 100°C, for both loads. The X-ray mapping results indicate that the Ni-P coating has undergone phase changes. The high temperature and the frictional heat induced by

reciprocating sliding may have caused the S transfer from the oil into the surface of the coating which reduces the friction as well. The formation of the sulphide films may also contribute to the decrease in wear at the high testing temperatures.

6. Increase in temperature reduces the wear of heat treated electroless nickel-phosphorus coatings. Delamination wear dominates the reciprocating sliding wear for the coatings after 400°C and 600°C heat treatment at room temperature tests. The polishing wear mechanism dominates the wear at 100°C tests.

7. The hardness of the coatings is not proportional to the wear resistance of the coatings under lubrication condition. Coatings after 400°C/1hr heat treatment have more weight loss and delamination than the coatings after 600°C/1hr heat treatment. The hardness value, however, is higher for the coatings after 400°C/1hr heat treatment.

8. For as-deposited coatings under dry condition (without lubrication), the adhesive wear mechanism dominates the reciprocating sliding wear. Abrasion caused by debris takes part in the sliding process at later stage. For the heat treated coatings, light adhesion occurs at the room temperature test. Polishing wear is the main mechanism for the tests at 100°C.

# REFERENCES


1. R. M. Bentley and D. J. Duquette: Environmental considerations in wear processes, in "Fundamentals of friction and wear of materials", American Society for Metals, Metals Park, Ohio 44073, 1981

2. J. Halling: "Introduction to Tribology", Wykeham publications (London) Ltd., 1976

3. H. Czichos: "Tribology, a systems approach to the science and technology of friction, lubrication and wear", Elsevier, 1978

4, Kenneth G, Budinski: "Surface engineering for wear resistance", Prentice Hall, Englewood Cliffs, New Jersey, 1988

5. D.A. Rigney: Introduction, in "Fundamentals of friction and wear of materials", American Society for Metals, Metal Park, Ohio 44073, 1981

6. D. Kuhlmann-Wilsdorf: Dislocation concepts in friction and wear, in "Fundamentals of friction and wear of materials", American Society for Metals, Metal Park, Ohio 44073, 1981

7. R.C. Tucker: Wear failures, Metals Handbook, 9th edition, Vol.11, 1986, pp145-162

8, Z.C. Feng: "The reciprocal sliding wear behavior of SiC particulate reinforced aluminum composite", M. Sc. thesis, Univ. of Manitoba, 1995

9. N.P. Suh: Update on the delamination theory of wear, in "Fundamentals of friction and wear of materials", American Society for Metals, Metal Park, Ohio 44073, 1981

10. L.E. Samuels: E.D. Doyle and D.M. Turley, Sliding wear mechanisms, in "Fundamentals of friction and wear of materials", American Society for Metals, Metal Park, Ohio 44073, 1981

11. A.T. Alpas and J. Zhang: Metallurgical and Materials Transactions A, Vol. 25A, May 1994 p969

12. Y. Kimura: The role of fatigue in sliding wear, in "Fundamentals of friction and wear of materials", American Society for Metals, Metal Park, Ohio 44073, 1981

13. S.C. Lim and M.F. Ashby: Acta Metall. Vol. 35, No.1, pp1-24, 1987

14. H.Czichos: Presentation of Friction and Wear Data, in" ASM Handbook, Vol. 18, Oct. 1992, p490

15. H. S.Cheng: Lubrication Regimes, in "ASM Handbook", Vol. 18, Oct., 1992, pp89-97

16. E.P. Dahlberg: Trans. ASM Quart. 58(1956), p46

17. E. Tsuji and Y. Ando: Effects of air temperature and air humidity on speed dependency of sliding wear of steels, Preprint of JSLE-ASLE International lubrication conference, Tokyo, June 10, 1975, pp1-8

18. E.Tsuji and Y. Ando: "Wear of Mat.", Conf. Proc., St. Louis, MO, 1977, p95

19. N. A. Tuan, N. Doan Y and P.V. Hung: Wear 162-164(1993) pp1066-1067

20. M.B. Peterson and J.J. Florek: Sliding characteristics of metals at high temperature, in Handbook of Mechanical Wear, ed. by C. Lipson and L.V. Colwell, Ann arbor, The Univ. of Michigan Press,

21. D.S. Lin, F.H. Stott, and G.C. Wood: ASLE Transactions, Vol.17, 4,1973, pp251-262

22. D.K. Chaudhuri, A.J. Slifka and J. D. Siegwarth: Wear, 160(1993) pp37-50

23. A.J. Slifka, T.J. Morgan and R. Compos: Wear, 162-164 (1993) pp614-618

24. M.G.Gee and D. Butterfield: Wear, 162-164 (1993) pp234-245

25. T.H.C. Childs and A. Mimaroglu: Wear, 162-164 (1993), pp890-896

26. W.Scott, P. Suntiwattana: Wear 181-183(1995) pp850-855

27. B.A. Baldwin: Lubr. Engg, 32(1976) p125

28. Y. Wang, Y. Jin and S. Wen: Wear, 128(1988) pp265-276

29. M.C. Jeng and L. Y. Yan: Wear, 161 (1993) pp111-119

30. J.C. Bell and K.M. Delargy: Lubrication influences on the wear of piston-ring coatings, Vol.17 Mechanics of coatings, ed. by D.Dowson, C.M. Taylor and M.Godet, Elsevier, 1990, p371

31. M. Thoma: Wear 162-164 (1993) pp1045-1047

32. W. D. Fields: Electroless Nickel Plating, in Metal Handbook, Ninth edition, Vol. 5, 1990

33. R. Tracy: Mater. Engg. Vol. 106 n11 Nov. 1989, p38

34. G.G. Gawrilov: Chemical(Electroless) Nickel-Plating, Portcullis Press Ltd., 1979

35. R. Duncan: Properties and applications of electroless nickel deposits, Finishers Management, April, 1981

36. T. Bleeks, G. Shawhan: Metal Finishing, Oct., 1989 Vol. 87 n10 p21

37. K. Parker: Plating, Vol.61(no.9) 1974, p834

38. K. Parker: Plating and Surface Finishing, Dec. 1981, pp71-76

39. E. Vafaei-Makhsoos, E. Thomas, and L. Toth: Metall. trans. A, Vol. 9A, Oct. 1978 pp1449-1460

40. E. Vafaei-Makhsoos: J. Appl. Phys., 51(12), Dec. 1980 pp6366-6376

41. E. Vafaei-Makhsoos: J. of Mater. Sci., 16(1981) pp2103-2108

42. S. H. Park, D. N. Lee: J. of Mater. Sci., 23(1988) pp1643-1654

43. K-H Hur, J-H Jeong, D. N. Lee: J. of Materials Science, 25 (1990) pp2573-2584

44. J. Campbell, J. Materials Methods, 27 (1953) 5, p96

45. E. Gostin, Iron Age, 171 (1953) 24, p115

46. J.P. Randin and H.E. Hintermann, Plating 54 (1967) 5, p523

47. H. Wiegand, G. Heinke and K. Schwitzgebel, Metalloberfl. 22 (1968) 10, p304

48. U. Ma, D. T. Gawne: Trans IMF Vol. 64, 1986, p129

49. L. Yu, X. Zhang: Thin Solid films, 229(1993) pp76-82

50. C.M. Li, K.N. Tandon: J. of Mater, Sci, 29(1994) pp1462-1470,

51. K.H.Z. Gahr: Tribology Series, 10, 1987

52. E. Bredael, B. Blanpain and J.P. Celis: J. of the electrochemical society, Jan. 01, 1994 Vol. 141 n1, pp294-299

53. N.M. Martyak: Metal Finishing, Vol. 92, n6, Jun 01, 1994, pp111-116

54. M.R. Lambert and D.J. Duquette: Thin solid Films, 177 (1989) pp207-223

55. E. E. Bisson, R. L. Johnson M.A. Swikert and D. Godfrey: Friction, wear, and surface damage of metals as affected by solid surface films, Report 1254, National Advisory Committee for Aeronautics.

56. T.B. Massalski(ed.): Binary Alloy Phase Diagrams, American Society for Metals, Metals Park, OH, 1986

57. H. Gao, H. Gu and H. Zhou: Wear, 142 (1991) 291-301

58.F.P. Bowden and D. Tabor: Friction, An Introduction to Tribology, Anchor Press, New York, 1973.

59. Motomaster Nugold Engine Oil data sheet, provided by Imperial Oil Ltd., Fab. 1996